SC

THE DEVELOPMENT OF A CURVED CENTRE CRACKED SPECIMEN FOR FRACTURE TOUGHNESS TESTING OF CANDU REACTOR PRESSURE TUBES

A Thesis

Prepared in partial fulfillment of requirements for degree of

M.A.Sc.

A.C. Wallace

Department of Mechanical Engineering

University of Ottawa

November 1987

ACKNOWLEDGEMENTS

The author wishes to acknowledge the support of both Atomic Energy of Canada Limited and Ontario Hydro for financial support and for freely making available the resources that permitted this work to be completed. In particular, the use of the computing facilities at AECL's Chalk River Nuclear Laboratories proved invaluable. Special thanks is due to Mr. R.R. Hosbons for acting as my on-site advisor at CRNL, and to Dr. A.S. Krausz for his extreme patience. The technical assistance of John Smeltzer at CRNL and Paul Stearns and Dave Carpenter at OHRD is also gratefully acknowledged. Finally, special recognition is due to my wife, Denise, for her patience, and providing the motivation to finally finish this Thesis.

TABLE OF CONTENTS

ABSTRACT

The curved centre-cracked specimen is a newly designed specimen specifically intended for fracture toughness testing of CANDU reactor pressure tubes. It offers two main advantages over other types of specimens currently in use. First, its curved shape avoids any need to flatten material that may be embrittled by irradiation or hydrogen ingress. Second, its centre-cracked geometry permits testing of defects similar to those likely to be encountered in reactor, and thus any effects of specimen geometry on the test results are eliminated.

The key to using the specimen is a specially designed set of grips that constrain the specimen to deform in a manner approximately that of a similar section of the wall of a tube under internal pressure. Axial loads and the effects of bulging around a crack cannot be duplicated, but the circumferential and radial strains are similar to those in an internally pressurized tube.

The stress intensity factor calibration for the specimen has been determined by both a three-dimensional elastic-plastic finite element analysis and from an experimental compliance calibration. The finite element results show close agreement with the theoretical relationship for an equivalent-sized flat plate. The stress intensity factor predicted from compliance results also agrees closely with theory for intermediate crack lengths. However, at shorter crack lengths the experimental results predict higher than theoretical K values while the reverse is true at higher crack lengths. This information is sufficient to permit use of the specimen for various testing applications in the linear-elastic regime.

The specimen is currently undergoing further development to qualify its use for elastic-plastic fracture toughness testing, as part of a $6M+ fracture research program supported jointly by Ontario Hydro and Atomic Energy of Canada. It has provided new options for testing surface cracks and is expected to be a useful experimental tool for fracture toughness testing in the future.

LIST OF SYMBOLS

B – specimen wall thickness

C – compliance (displacement/load)

CCL – critical crack length

CCT – centre–cracked–tension (specimen)

CT – compact–tension

E – Young's modulus

G – elastic strain energy release rate

J – J–integral

K, K_I – opening mode stress intensity factor

K_{IC} – plane strain fracture toughness

K_C – toughness in non–plane strain conditions

LBB – leak–before–break

M – Folias factor to correct for bulging around an axial crack in a tube

R_i – tube internal radius

R – tube mean radius

SENT – single edge notched tension (specimen)

T – tearing modulus

TPB – three point bend (specimen)

W – specimen width

a – half crack length

r_i – tube internal radius

t – tube wall thickness

σ – stress

$\bar{\sigma}$ – flow stress = $(\sigma_{ys} + \sigma_{uts})/2$

σ_{ys} – yield stress

σ_{uts} – ultimate tensile strength

σ_H – hoop stress

ε – strain

ε_{cir} – circumferential strain in a tube

ν – Poisson's Ratio

μ – shear modulus = $E/2(1 + \nu)$

LIST OF FIGURES

LIST OF TABLES

LIST OF APPENDICES

1.0 INTRODUCTION

The history of fracture toughness testing of CANDU reactor pressure tubes reflects progress in the development of fracture mechanics theory and test techniques in general, particularly in the area of elastic–plastic fracture mechanics (EPFM). While there has been a great deal of progress in understanding the fracture properties of pressure tubes, further research is still required before the fracture toughness of a tube operating in–reactor can be reliably predicted from the results of small specimen tests. Specifically, problems remain in understanding the geometry and size dependence of fracture toughness test results and also the use of non–standard specimens for testing brittle, irradiated material removed from reactors. It was mainly for these reasons that the decision was made to develop a small, centre–notched fracture toughness specimen that would maintain the cylindrical curvature of the pressure tube.

While this document provides some of the background to fracture toughness testing of pressure tubes, its main purpose is to give details of the design and development of the curved centre–cracked specimen and the associated testing grips.

Basically there are three areas to be considered. First the design concept and details of operation are to be explained. Second, the results of finite element analysis to determine the load–displacement characteristics of the test configuration and the specimen stress–intensity factor calibration are described in detail. Finally, the results of the experimental compliance calibration and testing experience using this specimen will be presented, thereby covering the full state of development up to the present time.

It is hoped that this information will prove useful to those interested in continued fracture studies of CANDU pressure tubes, as well as to experimentalists concerned with the fracture properties of tubular and piping materials in general.

2.0 STATEMENT OF OBJECTIVE

The objective of this project was to develop a small fracture toughness specimen having a centre-cracked geometry that would also retain the curvature of the CANDU reactor pressure tube. The purpose of developing such a specimen is to provide a small specimen test technique for obtaining accurate predictions of fracture toughness in tubular or piping materials.

3.0 BACKGROUND I - REACTOR AND PRESSURE TUBE FUNDAMENTALS

3.1 The CANDU Reactor Fuel Channel

The core of a typical CANDU nuclear reactor consists of up to 480 horizontal fuel channels passing through a calandria vessel containing the heavy water moderator. The system is shown schematically in Figure 1. Figure 2 shows a more detailed view of the fuel channel assembly. The innermost component of the fuel channel is a cold-worked Zr-2.5wt% Nb alloy pressure tube which contains the fuel bundles and provides containment for the heavy water coolant circulating over the fuel. The ends of the pressure tube are rolled into type 403 stainless steel end fittings to produce a leak-tight joint. Coolant enters and exits the end fittings through small diameter feeder pipes connecting to the inlet and outlet headers. These lead to the pumps and the steam generators respectively, thereby completing the primary heat transport circuit. Surrounding the pressure tube is a thin-walled Zircaloy-2 calandria tube, the main purpose of which is to provide thermal insulation between the hot pressure tube and the colder moderator. The annulus between the pressure tube and calandria tube contains carbon dioxide or nitrogen gas which is circulated and sampled to detect any coolant leaks from the pressure tubes. Either 2 or 4 coiled spring spacers surround the pressure tube in the annulus space, and provide physical separation of the two tubes.

Pressure tubes are nominally 6.3 m in length, with a mean diameter of 107 mm and a 4.1 mm wall thickness. Normal operating pressure is from 9.6 - 11.2 MPa producing an operating hoop stress of between 120 and 140 MPa, depending on the reactor unit. The operating temperature at the pressure tube inlet is about 520 K, rising to 570 K at the outlet.

3.2 Delayed Hydride Cracking (DHC)

Zirconium alloys are susceptible to an unusual cracking mechanism referred to as delayed hydride cracking (DHC). This phenomenon involves the fracture of a brittle zirconium hydride phase that forms perferentially in regions of hydrostatic tensile stress, such as that existing at the tip of a crack. The basic mechanism has been well documented elsewhere [1–6] and will be reviewed only briefly here.

Hydrogen is virtually insoluble in zirconium below 150^{o}C although the solubility limit increases rapidly with further temperature increases (Figure 3). On installation, pressure tubes nominally contain from 5–15 ppm by weight of hydrogen, and this amount will be entirely in solid solution at normal operating temperatures. However, during operation, deuterium, the isotope of hydrogen in the heavy water coolant, is generated by the corrosion reaction

$$Zr + 2D_2O \rightarrow ZrO_2 + 2D_2 \qquad (1)$$

Some of this deuterium will then be absorbed by the pressure tube by a variety of mechanisms[7], and thus, the concentration of hydrogen in a pressure tube will increase during the reactor lifetime.

When the concentration of hydrogen in the metal exceeds the solubility limit for a given temperature, referred to as the terminal solid solubility or TSS, it will begin to precipitate as solid zirconium hydride, a non–stoichiometric compound with the approximate chemical composition $ZrH_{1.6}$. Normally, hydrides precipitate as platelets or needles and lie in the axial–circumferential plane of the pressure tube, that is with platelet normals in the radial direction. This orientation is determined by the strains generated during manufacture of the tubes. In the absence of these strains, the hydrides would precipitate in the radial–axial plane with platelet normals in the circumferential direction. Hydride orientation is also determined by the level of applied stress, since hydrides have a tendency to orient themselves in a plane perpendicular to the direction of maximum tensile stress. Thus, the operating hoop stress in a pressure tube would tend to encourage hydrides to orient themselves in the radial–axial plane. However, these stresses are not sufficiently high to overcome the effects of the cold–working manufacturing strains, and in the absence of other effects, hydrides will remain in the axial–circumferential plane.

Zirconium alloys are extremely strong and tough, even at room temperature after extensive irradiation. Zirconium hydrides, on the other hand, are inherently weak and brittle, and thus their presence in any significant quantities can severely reduce the fracture toughness of pressure tubes.

Apart from affecting the orientation of precipitated hydrides, stress can also affect the distribution of hydrogen. This is because hydrogen in solution increases the metal volume, and an applied stress makes this volume increase, and the dissolved hydrogen easier to accommodate[8]. Thus, hydrogen migrates up stress gradients and tends to precipitate in regions of high hydrostatic stress such as at the tips of notches or flaws. Precipitation of zirconium hydride results in about a 17% volume increase of the hydride phase over the matrix[9]. Thus hydrides will also be more easily accommodated at the tips of flaws. If the applied stress is sufficiently large, the crack tip hydride will eventually fracture, thereby extending the existing defect. Hydrides present in the metal matrix, but removed from the flaw will then preferentially dissolve in favour of those hydrides precipitating in the hydrostatically stressed region at the tip of the new flaw. At some critical condition this hydride will also crack. Thus, once cracking has initiated, provided the applied stress is maintained and TSS is exceeded, cracking will continue in this intermittent fashion known as delayed hydrogen cracking.

A minimum or threshold value of the mode I stress intensity factor, K_I, is required for hydride cracking to occur. This value is termed K_{IH} and is currently estimated at about 6 MPa $\sqrt{m}$. For applied stress intensity factor levels above K_{IH}, but low enough that the crack remains stable, the macroscopic crack growth rate, da/dt, is a constant for a given temperature, independent of K_I. The fact that the crack velocity increases with temperature indicates that DHC is a ther–

mally activated process. The crack velocity depends on the rate of accumulation of hydrogen at the crack tip and, to the first order, has the temperature dependence of the product of the diffusion rate and solubility limit. The Arrhenius relationship between the crack velocity and temperature has a slope close to the sum of the activation enthalpies for solution and diffusion of hydrogen in zirconium[5].

The dependence of the crack velocity on K_I is shown schematically in Figure 4. Provided the conditions are suitable, a crack will continue to grow by the DHC mechanism until it either grows through the pressure tube wall causing a leak and is detected, or it reaches a critical size and propagates in an unstable manner. In Figure 3 this happens as K_I approaches K_{IC}. The size of crack at which instability occurs, measured in the axial direction, is referred to as the critical crack length (CCL).

3.3 Summary – The Need for Fracture Toughness Testing

It is apparent from the preceding discussions that defects initiated in a pressure tube can grow to an unstable size by delayed hydride cracking. Thus, accurate knowledge of the critical crack length in a pressure tube is a necessity.

Cracks in pressure tubes have usually penetrated the wall, leaking coolant to the annulus space, prior to reaching a critical size. This phenomenon is known as leak-before-break (LBB) and is important since leak detection permits a reactor to be shut down safely prior to a rupture event. Knowledge of CCL permits an estimate of the likelihood of LBB and thus provides a measure of the ability to detect a leaking crack before it becomes unstable.

Unfortunately, leak before break cannot be guaranteed. In spite of this, fracture toughness testing at least provides some assurance that an adequate level of toughness exists. Periodic determination of critical crack length for operating tubes will provide early warnings of reductions in toughness with age and alert operators to potential problems in advance. There has thus been considerable emphasis placed on reliably determining the fracture toughness of CANDU pressure tubes.

4.0 BACKGROUND II - FRACTURE TOUGHNESS TEST TECHNIQUES AND DEVELOPMENT

4.1 Burst Tests

The traditional method of determining fracture toughness in pressure tubes has been to conduct a burst test. Sections of tube about 50 cm long containing artificial defects are pressurized to failure. Fracture toughness is calculated using the following expression for the stress intensity factor of an axial crack in a tube[10].

$$K_c = \left(\frac{8a\,\bar{\sigma}^2}{\pi} \cdot \ln\left(\sec \frac{\pi M \sigma_H}{2\bar{\sigma}}\right) \right)^{1/2} \qquad (2)$$

where: $2a$ = crack length

$\bar{\sigma}$ = flow stress = $(\sigma_{YS} + \sigma_{UTS})/2$

σ_{YS} = 0.2% yield stress

σ_{UTS} = ultimate tensile strength

σ_H = applied hoop stress at failure

M = correction factor

$$= 1 + 1.255\left(\frac{a^2}{Rt}\right) - 0.0135\left(\frac{a^4}{R^2t^2}\right)^{1/2}$$

R = tube mean radius = 53.5 mm

t = tube wall thickness = 4.1 mm

Equation (2) is a semi-empirical modification of the linear-elastic equation for a crack in a plate with an Irwin-type crack length correction to account for the effect of the plastic zone. The correction factor, M, often referred to as the Folias factor, accounts for the additional stresses produced at the crack tip due to the curvature of the tube and bulging around the crack during pressurization. Essentially the same equation was developed by Hahn et al[11] with the exception that the original form of the correction factor, M, developed by Folias[12] is used. This relation gives slightly more conservative (ie, higher) K values for the same conditions. In this case,

$$M = \left(1 + 1.61 \frac{a^2}{Rt}\right)^{1/2}$$

where a, R and t have the same meanings as in equation 2.

A large number of burst tests have been performed on pressure tubes[13–16] and the results analyzed to determine 95% confidence limits for critical crack length for a range of stress and temperature[17]. However, not all of the tests were performed on material containing radial–axial hydrides or on irradiated material. Thus there are some situations for which currently available burst test results do not permit confident predictions of fracture toughness.

There are other drawbacks to burst tests. Testing is cumbersome and expensive, and comparatively little information is obtained for the amount of material expended. There are also considerable difficulties associated with the need to seal test sections containing through–wall defects. For these reasons the majority of the fracture toughness tests performed on pressure tube material have been conducted using small specimen test techniques.

4.2 Small Specimen Tests

4.2.1 Advantages of Small Specimens

It has long been recognized that the use of small specimens to obtain critical crack length data for pressure tubes offers many advantages over the burst test technique. Small specimen tests are easier and less expensive to perform than burst tests and require considerably less material. Specimen and experimental characteristics can be changed more easily thus permitting a wider range of variables to be examined. In addition, data can be obtained from a larger materials base, thereby producing more statistically significant results[18].

However, the decision to use small specimens is not without its complications. Due to the small size of the specimens, and the ductility of pressure tubes in general, plane strain conditions cannot be obtained, and the theories and test techniques of elastic-plastic fracture mechanics (EPFM) must be used to obtain valid predictions of crack instability. Since EPFM is a relatively new field of research, a number of controversial issues remain to be resolved, and there are a variety of test methods and specimen types to choose from. As far as pressure tubes are concerned, the basic problem is that of deciding upon a fracture criterion that can be unambiguously defined for both a small specimen and a pressure tube. However, even armed with a suitable criterion, it is not necessarily a simple matter to relate the results of a small specimen test to a pressure tube in an operating reactor. This problem of relating small specimen test results to full-size component behaviour is common to all plane-stress situations.

4.2.2 Elastic-Plastic Resistance Curve (R-Curve) Techniques

Generally, cracks in pressure tubes subjected to monotonically increasing loads will extend stably for several millimetres before becoming unstable. If the material is severely embrittled due to irradiation and high concentrations of radial-axial hydrides, crack instability may occur without any prior stable crack extension. In this case, a failure criterion based on the initiation of crack extension, such as K_{IC} from linear-elastic fracture mechanics, might be a suitable failure parameter. However, for more ductile material, the use of analogous elastic-plastic initiation criteria, such as the J-integral at initiation, J_{IC}, or the crack opening displacement at initiation, δ_i, would be inappropriate. The use of these parameters as failure criteria would seriously underestimate the flaw tolerance of the material by neglecting its capacity to sustain stable crack extension[19]. This need to characterize the crack growth resistance properties of pressure tubes led to the selection of a crack growth resistance curve (R-curve) technique as the most promising method for predicting critical crack size in pressure tubes.

The technique is based on measurement of the J-integral of Rice[20], which was subsequently shown to uniquely define the elastic-plastic stress and strain fields at the crack tip in a strain hardening material[21,22]. It was then determined that this property made the J-integral ideally suited as a fracture criterion for elastic-plastic materials[23], in a similar fashion to which the stress intensity factor, K_I, serves by defining the stress field at the crack tip in linear elastic materials. The suggestion that J was also a valid characterizing parameter under conditions of stable crack growth received considerable attention[24,25] and was subsequently given more rigorous theoretical backing[26,27,28]. The techniques of J-integral based R curves (J_R-curves) were demonstrated to be suitable for application to the testing of pressure tube material[29], and the method has now gained sufficient acceptance to be the subject of an engineering handbook for elastic-plastic fracture analysis[30. An ASTM standard test method for determining J_R-curves is expected to be released this year.

A brief description of the method applied to CANDU pressure tubes is given in [19] and [31]. Basically, critical crack length is determined from the point of tangency of the experimentally derived J_R-curve and a theoretical crack driving force curve for the pressure tube[19,30]. The procedure is illustrated in Figure 5. The crack driving force curve is defined by equation (2) in section 3.1, with units of K converted to J using the plane stress relation

$$J = \frac{K^2}{E} \qquad (3)$$

Work is currently underway to determine a more accurate crack driving force curve using finite element methods[32] since the plastic zone correction of the stress intensity factor used in equation (2) is only approximate. However, the current approach seems to be adequate for the present time. The J_R-curve, determined from a small specimen test, is moved along the x-axis of the crack driving force plot until the two curves are just touching. The intersections of the J_R-curve with the x-axis at this point of tangency defines the critical crack length.

An alternative description of the same procedure is given by the definition of the tearing modulus, T, defined in[26] as

$$T = \frac{E}{\bar{\sigma}^2} \frac{dJ}{da} \qquad (4)$$

where E = Young's Modulus

$\bar{\sigma}$ = flow stress

$\frac{dJ}{da}$ = slope of the J_R curve at a given point

The tearing modulus is simply a measure of the slope of the J_R curve, expressed in a non-dimensional form by normalizing with respect to Young's Modulus and the flow stress. The tangency condition for crack instability is then defined by the equivalence of the tearing modulus and the slope of the crack driving force curve. That is, instability occurs when the specimen or material $T \leq T$ applied. This form of theoretical interpretation has been supported experimentally[33] and this so-called J-T approach is gaining popularity.

4.3 Geometry Effects in Resistance Curve Testing

It is now well understood that resistance curve shape is dependent upon specimen geometry[34,35]. Basically, resistance curves generated using specimens in which the crack tip is essentially loaded in tension, such as the centre-cracked- tension (CCT) or single-edge-notch-tension (SENT) specimens, are steeper than resistance curves generated using specimens in which the crack tip is primarily loaded in bending, such as the compact-tension (CT) or three-point-bend (TPB) specimens. This observation is generally attributed to a deviation from so- called "intrinsic" R-curve behaviour[36], brought about by the gradual loss of dominance of the HRR singularity in the crack-tip stress-strain field due to extensive deformation occurring along the 45^o shear bands emanating from the crack tip. The implication of this is that J-dominance of the crack-tip field is lost and single parameter (ie, J) characterization of the field under stable crack growth is not possible unless stringent specimen size requirements are met[37,38]. Currently, it is recommended that the ratio of the specimen ligament length to the ratio of J/σ_y, where σ_y is the yield stress, be at least 200 for a centre-cracked specimen but only 25 for a compact-tension specimen. Thus, a CCT specimen must be much larger than a CT specimen to generate an equivalent valid result.

Tests have been performed on pressure tube material using both CT and CCT specimens to generate resistance curves[39]. It was found, however, that although the tangency point with the crack driving force curve occurred beyond the validity limits for J, predictions of critical crack length based on R-curves from the CCT specimen were in excellent agreement with the results of burst tests. Predictions based on R-curves from CT specimens tended to underestimate CCL, reflecting the increased constraint and triaxiality for the bending geometry. It was agreed at the time that it was preferable to have conservative predictions of critical crack length and that estimates obtained from compact-tension specimens were not so conservative as to unduly penalize the material. For this reason, and because CCT specimens tend to be difficult to test, little attention has been given to testing with the CCT geometry over the last few years.

Recently, however, there has been renewed concern about the magnitude of effects of specimen geometry on predictions of critical crack length. The uncertainty is undesirable and it is felt that a small specimen with a crack geometry most similar to that in a tube may be better suited to providing an accurate prediction of CCL.

An additional complicating factor that has not yet been properly addressed, is the likelihood that a crack in a pressure tube may not be amenable to single-parameter J characterization.

Since an axial crack in a pressure tube is essentially loaded in tension by the hoop stress (the longitudinal stress has been shown to have no effect[40]) it is possible that the HRR singularity does not dominate the crack-tip stress-strain field beyond certain limits. In this case, the significance of the measured J value is not clear, but it may explain the observed good agreement between CCT specimen predictions of CCL and the burst test results.

4.4 Flattening - The Impetus for Curved Specimen Development

The vast majority of small specimen fracture toughness tests on pressure tube have been performed using compact tension specimens machined from flattened and stress-relieved material. The flattening operation reduces the wall-thickness of the specimen and introduces residual stresses that are not entirely removed by the stress relief operation, which is designed so as not to significantly alter the cold-worked microstructure of the pressure tube. These residual stresses probably have an effect on test results, and certainly make it difficult to prepare specimens having specific hydride structures.

In many instances flattening is simply not possible. Material removed from reactors, which may be embrittled due to irradiation or high hydrogen concentrations, would probably break if flattened. Even if flattening could be performed, subsequent stress relief operations would render further testing pointless by altering the hydride structure and annealing out irradiation damage. For these reasons, attention has turned to the development of small fracture toughness specimens that retain the curvature of the pressure tube.

Three different specimen designs have been proposed and have been reviewed in[41], which also gives some background to the development of the curved centre-cracked specimen. Results of testing experience with the curved double torsion specimen (Figure 6) are reported in [42] and [43]. A description of the use of the curved compact-tension specimen (Figure 7) in the failure investigation of a ruptured pressure tube is given in [44]. Each of these specimen types has its own merits and disadvantages. They are still being developed and it is likely that each will find application in the field of small specimen fracture toughness testing of pressure tube materials.

The problems associated with flattening material to obtain test specimens apply equally well to other tubular and piping components. In some cases the component thickness is sufficient for flat specimens to be obtained, but generally, the availability of a curved specimen would simplify fracture testing of many other materials.

4.5 Summary - The Need for a Curved Centre-Cracked Specimen

It is evident that there are a number of uncertainties remaining in the prediction of fracture toughness in CANDU pressure tubes. While the J-integral based crack growth resistance curve appears to offer the best technique for predicting fracture in pressure tubes, the effects of specimen geometry are not yet fully understood. Related to this is the question of whether or not the J-integral is really an appropriate parameter for characterizing the stress-stain field for a stable crack in a pressure tube. Given these uncertainties, it seems reasonable that a centre cracked specimen, having a geometry similar to that of an axial crack in a pressure tube, would give more realistic indications of how a real crack would behave. In addition, the curved centre cracked specimen also meets the requirements for testing embrittled material since flattening is not required. Thus is would appear that there are sufficient reasons for justify the development of a curved centre-cracked specimen.

5.0 CURVED CENTRE CRACKED SPECIMEN DESIGN

The curved centre cracked specimen (Figure 8) is simply one third of the circumference of a section of pressure tube 60 mm long. A radial-axial starter notch is spark machined in the centre of the specimen and sharpened by fatigue. The specimen is pin-mounted to specially designed grips, through four holes that are drilled with the aid of a rotating jig, (Figure 9). It is the grips that provide the key to testing the specimen by constraining it to deform radially and circumferentially in a manner approximating that of an internally pressurized tube.

5.1 Design and Analysis of the Testing Grips

Figure 10 shows an unnotched specimen mounted in the grips. Referring to the side view in Figure 11, the grips consist of two interlocking sections, a, connected to the side plates, b, by pins, c. The specimen, d, is fixed to the grips by four pins through the L-shaped plates at e. When a tensile load is applied from the clevis and pin assemblies, the two interlocking sections, a, will rotate slightly about their respective connecting pins, c, which act as pivot points. Because these pivot points are offset from the centre of curvature of the specimen, the curved surfaces of the grips, which initially follow the inside surface of the specimen exactly, push radially outwards on the inside of the specimen, constraining it to deform in a manner approximating that of a tube under increasing internal pressure.

The operation of the grips is demonstrated more clearly in Figures 12 and 13, which show the grips with the specimen removed. The curved surfaces of the mating grip halves consist of interlocking "fingers" that are initially closed (Figure 12) and open up as a load is applied (Figure 13). This motion effectively increases the length of the grip curved surface, although there are now some small gaps where the underside of the specimen is unsupported. This motion also increases the radius of curvature of the grip curved surface, and consequently that of the specimen. At this point, the radius of curvature is no longer uniform over the length of the specimen.

A computer analysis was performed to determine the precise shape of the curved surface for specified rotations of the grip halves. It was found that the variation in radius could nominally be restricted to only a few hundredths of a millimetre at the largest expected test displacements by optimizing the location of the pivot points (c in Figure 11).

Based on the average radius increase as determined by the computer analysis, circumferential strain was calculated from thin-walled pressure vessel theory as:

$$\varepsilon_{cir} = \frac{R_i - r_i}{r_i} \qquad (5)$$

where: ε_{cir} = circumferential strain

R_i = average deformed internal radius of specimen, determined by computer analysis

r_i = undeformed internal radius = 51.5 mm

Circumferential strain was also calculated as the difference between the deformed and undeformed arc lengths of the grip curved surface, as calculated numerically over the angle subtended by the specimen mounting pins. Comparisons of the strains determined by these two methods showed the two values to be in very close agreement (Table 1). This supports the contention that the grips produce radial and circumferential strains in the specimen that are in close approximation to those sustained in a tube under internal pressure. Note that the rotation angles given in Table 1 refer to one half of the grips only. The other half would rotate the same amount.

Figures 14 to 19 show computer generated plots of the displacement of the curved surface of one half of the grips for rotation angles of 0.4^o, 0.8^o, 2^o, 3^o, 4^o and 5^o. These plots were created as part of an analysis to optimize the position of the pivot points. In all these figures, the lower curve represents the undeformed position. The upper curve gives the location of the grip surface and thus the shape of the specimen inside surface after a counterclockwise rotation of the specified angle. The displacement of the other half of the grips could be shown by reflecting these curves about the line $x = 0$, which correspnds to the plane of the crack in the specimen. The 5^o rotation is probably the maximum that would ever be encountered in a test. Figure 19 shows that the radial strain at this rotation remains fairly uniform beneath the entire specimen, and thus the surface remains essentially a circular arc.

A two-dimensional finite element analysis was performed to gain an understanding of the behaviour of the grips under load. The analysis was performed using the mesh in Figure 20. The specimen was assumed to be unnotched and was rigidly connected to the grip mesh at nodes 66, 65, 38, 39 and 40. Thus the pin connections holding the specimen to the grips were not modelled. The pin connections at the load application point (node 11) and the pivot point (node 50) were also not modelled explicitly. Node 50 was fixed in both the x and y directions so that it would act as a pivot. Gap elements were used to separate the grip and specimen elements at nodes 71–84. Displacement increments of 0.1 mm were applied to node 11 in the positive x–direction to simulate loading. Loads, displacements and rotations were calculated at each increment and used to analyse the behaviour of the specimen.

It was determined that 97.5% of the applied load is transferred through the specimen. The remaining 2.5% is transferred through the connecting plates at the pivot pins (node 50). These proportions of load transfer were found to be constant up to and beyond specimen yield. Thus it can be assumed that the same load distribution will be obtained with cracked specimens having different values of compliance.

The grips themselves were found to be somewhat more compliant than had been anticipated, although this does not constitute a problem. As has been stated, the design of the grips is such that the application of a load will produce a rotation about the pivot points (node 50). However, it was found that the rotation at the load application point (node 11) was significantly greater than the rotation occurring along the region in contact with the specimen. This excess rotation is attributed to elastic bending of the grip lever arm (ie, the section between nodes 50 and 11). This is borne out by the fact that rotations along the grip curved surface (nodes 66 - 84) are essentially a constant fraction of the rotation at the load application point (node 11) for loads up to specimen yield. This is not really important since it would be impractical to monitor rotations during a test. The amount of rotation at a given load will also depend on the specimen compliance (ie, crack length). What is important here is that the analysis shows that the amount of rotation of the grips is essentially constant over the region in contact with the specimen. This insures that the specimen will be uniformly loaded.

5.2 Frictional Effects

An important factor to consider with this testing arrangement is the effect of friction between the grips and the specimen. If frictional forces are significant, they are likely to affect the strain distribution within the specimen, thereby affecting the results of a fracture toughness test. It is difficult to predict exactly what the nature of any frictional forces will be since they will vary directly with the contact force, which itself may vary substantially over the specimen inside surface. In addition, due to the interlocking design of the grips, the direction of the frictional forces will be different from one grip half to the other. Whatever, the direction, it is conceivable that the frictional forces could either restrict or enhance the crack opening in a test specimen and in this way alter the crack driving force at the crack tips, leading to an inaccurate test result. It is important, therefore, that any frictional forces be as small as possible.

By making a few assumptions as to the relationship between forces and stresses in the specimen, and those in an actual tube under internal pressure, it can be demonstrated that any stresses due to friction are likely to be extremely small compared to the other stresses in the specimen.

The first assumption to be made is that the main stress present in the specimen is a fairly uniform stress in the circumferential direction, analogous to the hoop stress in an operating pressure tube, σ_H. The second assumption to be made is that the contact stress of the grips on the specimen inside surface approximates a uniform internal pressure, P. Then, using thin-walled pressure vessel theory and the pressure tube geometry we can express the tube stress, σ_H, in terms of the contact stress, P, as follows:

$$\sigma_H = \frac{PD}{2t} = \frac{P \times 103 \text{ mm}}{2 \times 4.1 \text{ mm}} \simeq 12.5 \text{ P} \qquad (6)$$

The frictional force at any point is proportional to the normal or contact force at that point, the proportionality constant being the coefficient of friction, μ which has some value between 0 and 1. By considering a unit area on the contact surface, we can discuss stresses as opposed to forces. Assuming a coefficient of friction of 0.5, (typical of dry metals in contact[45]), we can estimate the frictional stress, σ_f = 0.5 P. Thus, referring to the previous equation, the stress within the specimen would be about 25 times greater than the frictional stress in the same region.

During a test, the grip surface is coated with graphite and a thin strip of teflon is sometimes placed directly under the crack in the specimen. Together, these lubricants probably reduce the coefficient of friction to 0.1 or less. In this case, the maximum sustainable frictional stress would be less than 1% of the comparable stress in the specimen. Thus it would appear that frictional effects may be safely neglected.

5.3 Summary - Specimen Design Concepts

The basic concept behind the design of the grips just described was to somehow constrain the specimen to deform in the same manner as it would if it were part of a complete internally pressurized tube. Although the axial stresses and the effects of bulging around the crack cannot be simulated, analysis suggests that the circumferential stresses and strains can be very closely approximated. The computer analyses may be somewhat simplistic in their modelling of the grips. This arises from necessity since it is basically impossible to model all pins and gaps in the assembly exactly. However, the analyses do provide a starting point for predicting specimen behaviour, and give information that can be compared with experimental results in the future. The indications are that the grips and specimen will function as originally conceived.

6.0 STRESS INTENSITY FACTOR CALIBRATION

In order to apply this specimen in practical research situations it is necessary to be able to calculate both linear-elastic (K) and elastic-plastic (J) stress intensity factors as a function of applied load and crack size. There are two techniques available to do this, both of which were employed in this project. The first is an analytical approach using finite element methods. This has the advantage of being useful in both the linear-elastic and elastic-plastic regimes although it is sensitive to simplifications in the model and to numerical problems. The other available method is to perform an experimental compliance calibration. This can be an accurate technique but is limited to use in the linear-elastic regime. The following sections describe in detail the appliction of both techniques to the stress intensity factor calibration of this specimen.

6.1 Finite Element Analysis

6.1.1 Analysis Technique and Program Description

The finite element analysis was performed using the MARC finite element code installed on the computer system at AECL's Chalk River Nuclear Laboratories.

Due to the necessity to model both the specimen curvature and a through-wall crack, a three-dimensional analysis was required. This proved to be many times more complicated than the two-dimensional analysis.

Initially, an attempt was made to model both the grips and the specimen precisely in their experimental arrangement. A three dimensional mesh was generated that modelled one half of the grips and specimen in a similar fashion to the two-dimensional mesh referred to earlier. In the 3-D case, the specimen connecting pin and both the pivot pin and clevis pin through the grips were modelled. This mesh is shown in Figure 21. However, due to the large number of gap elements used to separate the grip elements from the specimen elements, a convergent solution could not be obtained with the stiffness matrix. The MARC program requires a special node numbering scheme to be used with gap elements in an effort to minimize the stiffness matrix bandwidth. However, the use of gap elements was too extensive in this mesh to satisfy all the requirements. This, coupled with the need to constrain certain degres of freedom in the gap element nodes apparently made the stiffness matrix so complicated that the bandwidth could not be sufficiently optimized to obtain a solution. (The result was a class 1 system mode error). Thus, this approach was eventually abandoned.

A new (and eventually successful) approach was attempted that involved modelling only the specimen. Basically, the analysis was performed by applying displacement boundary conditions to the specimen mesh that were consistent with the deformation that would be imposed by the grips for a given applied load and rotation. It was necessary to perform the analysis in two stages, and to make extensive use of the user-written subroutines that can be utilized in the MARC program.

Initially the mesh to be used in the analysis was generated as that of a flat specimen having dimensions in the same proprtion as the curved specimen. Due to symmetry, only one quarter of the actual specimen was modelled. A sample listing of this mesh generation program, CSMESH, is given in Appendix A. A total of 5 different meshes were generated to provide specimen normalized crack length ratios, 2a/W, of 0.2, 0.4, 0.5, 0.6 and 0.8, where a is half the crack length and W is the specimen width (60 mm). These meshes are shown in Figures A1 to A5 in Appendix A.

To perform the actual analysis, the coordinates of the nodes in these flat meshes were mapped onto corresponding coordinates for the curved geometry of the actual specimen. This is demonstrated schematically in Figure 22. It will be useful to refer to this figure in conjunction with the explanation of the analysis procedure that follows. A 3 dimensional non-hidden line plot of the resulting curved specimen mesh for $2a/W = 0.5$ is shown in Figure 23.

As just mentioned, the analysis is based on prescribing the displacements of the specimen inside surface nodes, that is, those on the surface in contact with the grips. It must be assumed that for a given load and rotation, the elastic deformation of the grip curved surfaces in contact with the specimen is negligible. This assumption also applies to the mounting pins that hold the specimen to the grips. Since the grips are much more massive than the specimen, and made of a strong, hardened alloy steel, this would seem to be a reasonable assumption. Given this assumption, the position of the grip curved surface, (and therefore the specimen inside surface), can be calculated precisely from geometric considerations for any given rotation about the pivot point. It was also assumed that there was no friction between the grip and specimen along the contacting surface.

For a prescribed rotation, the specimen nodes directly in contact with the leading edge of the mounting pin will undergo exactly the same displacements as the mounting pin nodes. It is also apparent that the nodes in the uncracked ligament of the specimen will be constrained to motion in the plane $x = 0$. That is, the rotation of the grip curved surface forces these nodes to move radially outwards, but remaining in the same plane. The other nodes on the inside surface of the specimen will have positions located on the curved surface defined by the grips after the specified rotation. The problem becomes one of how to determine the displacements of these nodes more precisely for a given rotation increment. To do this the assumption is made that the specimen nodes will displace along the curved surface in the same relation to one another as will occur in a flat specimen of the same size loaded in tension.

Thus the first stage of the analysis was to apply a fixed displacement to the top edge of the pin-hole on the flat specimen mesh shown in Figure 22. The resultant displacements of the nodes on the surface corresponding to the specimen inside surface were stored in a file (DISPNOD) that could be read in a subsequent analysis. Note that the length of the flat specimen in Figure 22 is longer on one side than the other. This was done to preserve the volume of the specimen in the transformation from a flat to a curved geometry. This keeps all nodes in the same relative position in both the flat and curved meshes. This analysis was performed using a program known as NDISP. A sample listing is supplied in Appendix B. Displacement increments of 0.05 mm were applied to the pin hole.

It was now necessary to determine the applied rotation of the specimen grips that would result in an increase in the curved arc length measured along the grip surface between the crack plane and the specimen contacting edge of the loading pin that was equal to 0.05 mm. This was done using a small analytical program called LARC that calculated the increase in arc length between these two points for a range of rotations about the pivot points. Arc length calculations were performed using a trapezoidal approximation with 500 divisions. The calculation was done using a function representing a 10th degree polynomial fit to the equation of the curved surface. When checked against an exact arc length based on the initial circular position, this technique was found to be accurate within 0.0001 mm. A sample listing of program LARC is given in Appendix C.

All this data was combined for rotations up to 4.0 degrees, and an equation was fit to the data. It was found that the increase in arc length increased almost linearly with the rotation angle. This is shown in Figure C1. Thus, for a specified angular rotation of a grip half section about its pivot point, it was possible to analytically predict the corresponding increase in length of the specimen inside surface measured between the contacting edge of the mounting pin and the crack plane. Conversely, the grip rotation angle required to produce a given increase in arc length can be calculated. Once this rotation angle is known, it is a simple matter to calculate the equation of the curved surface from geometric considerations.

This was done using another small analytical program called DEFIT, a listing of which is given in Appendix D. DEFIT used the relation between rotation angle and length increase calculated by program LARC as input and determined equations of the curved surfaces for rotation angles corresponding to arc length increments of 0.05 mm. These equations were then used as input to the actual analysis program, CURK.

A sample listing of program CURK is provided in Appendix E. The analysis was performed in the following steps.

First, program CURK used the user subroutine UFXORD to transform the nodal coordinates in the CSMESH files to the curved specimen geometry.

Following this, user subrouting FORCDT was used to calculate the incremental and total displacements of the specimen inside surface nodes that were in contact with the grip surface and the leading edge of the connecting pin. The new displacements were applied as boundary conditions for the given analysis increment. To do this, FORCDT required as input the corresponding DISPNOD file created by the NDISP program, which contained inside surface nodal displacement data for the flat mesh for a displacement increment of 0.05 mm. The equation of the curved specimen inside surface for an incremental arc length increase of 0.05 mm was obtained from program DEFIT.

For a given increment, the distance measured along the inside surface between the crack plane and the mounting pin was the same for both the curved and flat geometry. Thus, the updated coordinates of the inside surface nodes for the curved geometry could be found by finding the point on the curved surface that was the same distance from the crack plane, measured on that surface, as the same node was on the flat specimen mesh.

The corresponding load through the specimen was found by summing the reaction forces for the ligament nodes in the crack plane. This was done with user subroutine IMPD.

The stress intensity factor, K_I, was calculated using the stiffness derivative technique of Parks[46]. This is also known as the virtual crack extension technique. This is a simple and widely accepted method of calculating elastic stress intensity factors by finite element methods, and a routine has been built into the MARC program for this purpose. Basically, this technique makes use the original definition of the J–integral by Rice[20] as the change in potential energy corresponding to an increment in crack length or

$$J = dU/da \tag{7}$$

In the linear–elastic case, J is equivalent to the strain energy release rate, G, and may thus be related to the stress intensity factor, K, by

$$G = K^2 \alpha/E \tag{8}$$

Where $\alpha = 1$ in plane stress and $1 - \nu^2$ in plane strain, ν being Poisson's ratio.

In the finite element case a potential energy change is determined by comparing the difference between the original solution and the solution where element stiffnesses within a user–defined contour are recalculated once the crack–tip element nodes are moved by a small increment, to model an infinitestimal increase in crack length. The change in potential energy for the given crack length change can be directly related to G and thus K.

Use of this approach requires that special crack tip elements of the type described by Barsoum[47] be used to correctly model the $1/\sqrt{r}$ singularity at the crack tip. These are quadrilateral elements that have been collapsed into triangles and have had the mid–side nodes in the sides adjacent to the crack tip shifted to a position one quarter of the distance from the crack tip measured along the element side. The crack tip elements used in this project were of this type.

Recently, it has become common to retain the nodes of the collapsed side rather than combine them into a single node, as was done here[48]. This has the advan–

tage of permitting crack tip blunting to be modelled once loading exceeds the linear elastic regime. For this reason, the results of this analysis are expected to be most accurate in the linear elastic regime, before significant crack tip blunting takes place.

Reference 48 also investigated different arrangements of elements around the crack tip. It was found that the use of collapsed quadrilateral elements with straight sides gave the highest accuracy. It can be seen from Figures A.1 to A.5 that the shape of the elements at the crack tip is unchanged as they are shifted to change the specimen crack length. The shapes of the elements in the surrounding rows become somewhat skewed as the position of the crack tip is shifted, but this is not thought to have any effect on the accuracy of the K solutions.

Stress contour plots were obtained at mid-thickness for both the flat and curved meshes at each load increment for different values of 2a/W. Some of these are shown for the curved geometry in Appendix F. The stress shown corresponds to that in the tube circumferential direction and gives an idea of the development of stresses and the plastic zone at the crack tip. Enlarged plots of the crack tip elements show the detailed contour patterns in this region.

Figure 24 shows the plot of applied load against load point displacement determined by the analysis for each crack size. Values obtained beyond displacements of 0.7 mm are not plotted since the shape of the load displacement curve would in reality be altered by the onset of stable crack extension. The finite element model cannot account for this. The load point displacement is determined as the change in the distance between the two pairs of loading pins as measured along the specimen inside curved surface.

6.1.2 Finite Element K Calibration Results

K values were calculated for two separate contour paths around the crack tip at each load/displacement increment in the analysis. A third contour path was specified but for reasons not presently understood, failed to return a logical number. The K values from the other two contours always agreed to within 10% at the very worst, and often much less. The best agreement was obtained for 2a/W values of 0.4 and the worst for 2a/W = 0.8. The average of the two K values are given in Table 2 for each load increment and crack length.

An independent determination of the accuracy of K determined by this method was made using the analytical expresions relating the stress intensity factor to the nodal displacements along rays emanating from the crack tip. The general expression is given[49] as:

$$K_I \begin{Bmatrix} (2k-1)\cos\frac{\theta}{2} - \cos\frac{3\theta}{2} \\ \\ (2k+1)\sin\frac{\theta}{2} - \sin\frac{3\theta}{2} \end{Bmatrix} = 4\mu\sqrt{\frac{2\pi}{r}} \begin{Bmatrix} u \\ v \end{Bmatrix} \qquad (9)$$

Where

$k = (3-\nu)(1+\nu)$ for plane stress

μ = the shear modulus = $E/2(1+\nu)$

ν = Poisson's ratio

r = the radial distance from the crack tip

u = displacement component in the global x direction

v = displacement component in the global y direction

This approach was applied to the second and fourth load increments for 2a/W = 0.5. Figures 25 and 26 show how the K values calculated at the nodes approach the value calculated by the stiffness derivative technique. The very large K_I values determined for the nodes closest to the crack tip are a result of the $1/\sqrt{r}$ singularity imposed by the 1/4 point position of the crack tip element mid-side nodes.

The Table 2 values of K vs. load for each crack length are plotted in Figure 27. It can be seen that for higher crack lengths and loads, the curves are non- linear, reflecting the increasing plasticity in the ligament ahead of the crack tip.

6.2 Experimental Compliance Calibration

6.2.1 Calibration Theory

Compliance is defined as the amount of displacement produced in a body for a given applied load. To see how this can be related to the crack size in a body refer to Figure 28 which shows the load–displacement curves for a body containing half crack lengths of a and a+ da.

Under a load P, a cracked plate of thickness B will undergo a displacement v. If the crack increases in size by an amount da, the displacement will increase by an amount dv, and the work done by the load will equal Pdv.

The total elastic energy, U_t, stored in the plate will then equal 1/2 Pv_2, change from the previous value, 1/2 Pv_1, of 1/2 $P(v_2-v_1)$ or 1/2 Pdv which is the area of the shaded region in Figure 28. The strain energy release rate, G, will equal the difference between the work done on the body and the increase in stored elastic energy for a given increase in crack length, da. This can be expressed as:

$$G = \frac{1}{B}\left(\frac{Pdv}{da} - \frac{dU_t}{da}\right) \tag{10}$$

since U_t = 1/2 Pv and compliance, C = v/P it follows that

$$U_t = 1/2\ CP^2 \tag{11}$$

Substituting into (10) gives

$$G = \frac{1}{B}\left(\frac{Pdv}{da} - \frac{d}{da}(1/2\ CP^2)\right) \tag{12}$$

$$G = \frac{1}{B}\left(\frac{Pdv}{da} - 1/2\ \frac{P^2dC}{da} - \frac{CPdP}{da}\right) \tag{13}$$

Substitute v = CP to get

$$G = \frac{1}{B}\,\frac{CPdP}{da} + \frac{P^2dC}{da} - \frac{1P^2}{2}\,\frac{dC}{da} - \frac{CPdP}{da} \tag{14}$$

$$G = \frac{P^2}{2B}\,\frac{dC}{da} \tag{15}$$

Further details of the preceding analysis can be found in most introductory textbooks on fracture mechanics, i.e. [53].

Since G is defined per crack tip a factor of 2 must be added to the left hand side of (15) to account for the two crack tips in the curved centre cracked specimen. If we substitute normalized values of compliance (EBC) and crack length (2a/W) into (15) we can now write

$$2G = \frac{P^2}{2B} \cdot \frac{1}{EB} \cdot \frac{2}{W} \cdot \frac{d(EBC)}{d(2a/W)} \tag{16}$$

or

$$G = \frac{P^2}{2WEB^2} \cdot \frac{d(ECB)}{d(2a/W)} \tag{17}$$

From equation (8) in section 6.1.1 we know that in plane stress, $K = \sqrt{EG}$ and therefore

$$K = \frac{P}{B}\sqrt{\frac{1}{2W} \cdot \frac{d(ECB)}{d(2a/W)}} \tag{18}$$

Thus the procedure used to experimentally determine the stress intensity factor K, was to measure compliance for a range of crack lengths and to analytically obtain a polynomial relationship for normalized compliance (EBC) as a function of the crack length ratio (2a/W). The derivative of this function was then substituted into (18), permitting K to be evaluated for any load or crack length.

6.2.2 Experimental Test Procedure

Compliance calibration tests were performed on 3 specimens with electron dis charge machined starter notches 10 mm long. The specimens were fatigue cycled at constant load amplitude of between 0 and 50 kN at 1 Hz. At regular intervals of crack extension, compliance unloadings were performed by unloading from 50 kN to 37.5 kN. The relatively high loads were used to get maximum displacements but still not exceed the maximum load used for fatigue cycling.

Compliance was measured with an MTS extensometer modified so that contact with the specimen surface was made with two compass points. The contact points were approximately 4 mm above and below the crack at its centre. The extensometer was held in position with a mounting bar and two springs as shown in Figure 29. The extensometer output signal was amplified such that 0.5% of the total 8 mm displacement range gave a 10 V signal. A computer was used to automatically sample the signal via a 12 bit analog to digital converter giving a theoretical resolution on displacement of about 2×10^{-5} mm, based on a resolution of 5 mV.

A total of 3 compliance unloadings were performed at each crack length, following which the specimen was heat tinted in a furnace for 10 minutes at 300°C to delineate the crack length at that point. The compliance was taken as the average of the 3 readings. Readings were obtained for about 6 or 7 different crack lengths on each specimen. Finally, the specimens were broken open and the crack length was measured for each heat tint band as the average of 7 readings taken through the thickness. Two typical specimens are shown in Figure 30 from which it can be seen that significant crack front curvature was present and that the crack fronts are quite symmetric.

For analysis purposes, the compliance, C, was normalized using the measured thickness, B, of 4.1 mm and a value of 10^5 MPa for the modulus, E. The crack length readings, 2a, were normalized with respect to the specimen width, W, nominally 60 mm.

6.2.3 Experimental Compliance Calibration Results

The normalized compliance data for the three specimens is given in Table 3 and plotted in Figure 31. Figure 32 shows the curve for the best 2nd degree poly nomial fit to the combined data. Although higher degree fits gave lower sums of squares of residuals, the quadratic form was used because higher order fits gave improbable shapes to the curve outside the range of the experimental data. The resulting equation relating normalized compliance to normalized crack length is:

$$EBC = 0.173922 + 0.370214\,(2a/W) + 2.24334\,(2a/W)^2 \qquad (19)$$

Differentiating this and substituting into (18) gives

$$K = \frac{P}{B}\sqrt{\frac{1}{2W}\,(0.370214 + 4.48668(2a/w))} \qquad (20)$$

Table 4 compares K values determined using (20) with the theoretical values obtained using the formula for a flat plate in tension[50].

$$K = \frac{P\sqrt{\ a}}{BW}\left(\sec \frac{\ a}{W}\right)^{1/2} \qquad (21)$$

Figures 33 to 37 plot K as a function of load according to: i) theory, by equation (21); ii) experimental compliance by equation (20), and; iii) the finite element results of Figure 27, for values of 2a/W of 0.2, 0./4, 0.5, 0.6 and 0.8,

Figure 38 shows the best fit curve from Figure 32 along with a theoretical compliance curve for a flat plate determined using equation 41 of reference[51]. It can be seen that the experimental curve lies somewhat below the theoretical curve at higher crack lengths. It is not clear whether or not this is a real effect or simply an experimental inaccuracy. However, both slopes are quite similar in the region of most interest from 2a/W = 0.4 to 2a/W = 0.6.

7.0 DISCUSSION ON THE STRESS INTENSITY FACTOR CALIBRATION

Referring to Figures 33 to 37, it can be seen that the finite element and theoretical results agree reasonably well for all values of 2a/W. The effects of crack tip plasticity can be seen in the finite element results, causing the curves to bend upwards at higher loads. This effect is more pronounced at larger crack lengths. In all cases, the K values predicted by the finite element analysis are slightly higher at equivalent loads, even when the effects of plasticity are negligible. This may be due in part to the curved geometry. In the analysis of axially cracked cylinders, a curvature correction is introduced to account for a slightly increase in crack tip stress intensity factor arising from curvature. This correction becomes larger at longer crack lengths due to bulging of the material adjacent to the crack. Since no bulging occurs with the curved specimen, this effect would not be expected to increase with crack length. It is also possible that the difference between the theoretical and finite element results is simply due to slight numerical inaccuracies in the analysis.

Compared to the finite element results, the K values obtained via the compliance calibration do not agree as well with the theoretical results. At lower crack lengths, the experimentally determined K values significantly exceed the theoretical values, while at larger crack lengths the theoretical values are underestimated. However, at intermediate crack lengths, with $0.5 < 2a/W < .65$, the agreement between the experimental and theoretical results is quite good.

At the longer crack lengths, part of the discrepancy is almost certainly due to error in the polynomial equation chosen to fit the experimental data. Figure 32 shows that beyond crack length ratio of 0.7 the compliance increases quite rapidly while the best fit curve has a shallower slope. Had more data points been obtained in this range, the fitted slope would have been steeper and equation (20) would probably have given better agreement with the flat plate theory.

At lower crack length ratios it is possible that some error has been introduced by the curvature of the crack fronts. It is quite likely that the compliance of a specimen with a straight crack front is less than that of a specimen with a skewed crack front of equivalent average length. This would explain the overestimates of the theoretical K values.

If this is the actual case, it is reasonable to presume that the results of the finite element analysis, for which the crack front was straight, give a fairly accurate description of the response of the specimen.

The uneven crack fronts observed in the experimental compliance specimens must be due to through wall stress variations. Although pressure tubes are usually treated as thin walled pressure vessels, application of the vigorous equations used for calculating the hoop stress in thick walled vessels shows that the hoop stress at the inside surface is 8% higher than at the outside surface. Since K varies linearly with stress, K at the inside surface will also be 8% higher than at the outside. Since in fatigue, the crack growth rate is proportional to ΔK raised to some power, n, a small increase in K can lead to a much greater increase in the crack growth rate. (i.e. if ΔK increases by 8%, da/dN increases by a factor of $(1.08)^n$). If the grips really do simulate the effects of internal pressure on the specimen, then the larger inside surface crack lengths could be explained on this basis alone. This effect is not normally seen in fatigue cycled pressure tube sections since the bulging that occurs with internal pressurization results in higher stresses at the outside surface.

However, a more likely cause of the skewed fatigue crack fronts is the imposition of a bending stress on the specimen due to slackness in the fitting of the specimen on the grips. Load–displacement traces with the extensometer attached indicated that the outside surface of the specimen actually goes into compression briefly before returning to tension as load increases and the grips open up in the way they were designed to. This behaviour is presumed to result from the necessary machining tolerances that must be incorporated into the grips to ensure they will fit together and the specimen can be easily mounted. Upon loading, the specimen bends out of its arc of curvature slightly as the slack from these tolerances is taken up. As a result of this the inside surface will go into tension before the outer surface and, in cyclic loading, will see a higher ΔK. Recent tests have shown that this behaviour can be reduced by inserting a narrow strip of teflon between the specimen and the grips, and straighter fatigue crack fronts can be produced[41].

Another possible cause for the shorter crack lengths on the specimen outside surface may be a small compressive residual stress resulting from the centreless grinding operation applied to the outside of the tubes during manufacture.

A further explanation for the difference between the experimental and theoretical K values may come from the method of loading of the curved specimen in the grips. It is presumed that all load through the specimen is transferred to it through the loading pins. However, if some of the load is transferred by frictional forces at points of contact with the grip curved surfaces, then the K vs crack length relationship could be significantly altered. This was shown in [52] where it was demonstrated that the K vs a relationship could be "customized" by varying the location of the load application points. However, this effect is unlikely since the graphite lubricant used in the tests would probably reduce any frictional forces to a minimum. The analysis of section 5.2 also suggests that any redistribution of applied load due to friction would be small.

To summarize, the potential user of this specimen has a choice of two expressions to calculate the linear-elastic stress intensity factor, K_I, from the applied load, P, and the crack length, a. For all values of 2a/W, the expression given in equation (20) should be used. A slight increase in accuracy may be obtained by fitting a higher degree polynomial to the experimental data given in Table 3 and substituting this for equation (19) in the derivation of 20. Such an expression would be valid for values of 2a/W between 0.15 and 0.76, the range of the experimental data.

For values of 2a/W between 0.5 and 0.65 the analysis has shown that the flat plate equation given in equation (21) is sufficiently accurate for most practical purposes. In either case, it should be noted that the finite element analysis indicates that the load transferred through the specimen is 97.5% of the total applied load. However, this has not been experimentally verified and will not lead to large errors if it is neglected.

8.0 CURVED SPECIMEN TESTING EXPERIENCE AND FUTURE PROSPECTS

Naturally, at the present time there is only limited testing experience to report for the curved centre cracked specimen. The toughness measured with a small curved compact tension specimen machined from one half of a fractured curved centre cracked specimen that had been hydrided was virtually identical to the centre cracked specimen result as evaluated using equation (21).

Tests performed on non-hydrided and unirradiated material have revealed a few minor problems with the design. Material in this condition is essentially not notch sensitive in the centre-cracked geometry, and failure occurs by collapse of the net section, or in some cases, shear at the pin holes. This is not totally surprising since many of the finite element stress contour plots in Appendix F show large stress concentrations at the pin holes. In some cases, fatigue cracks have initiated at the pin holes when trying to initiate fatigue cracks from short, shallow surface notches. The ASTM designation E338-81 on Sharp Notch Tension Testing of High-Strength Sheet Materials recognizes this problem and suggests the use of reinforcing plates around the pin hole. A similar approach is currently being applied to a new design for the gripping arrangement which will redistribute the load away from the pin holes. Another approach that has been applied to surface cracked specimens is simply to reduce the mid-section width of the specimen and thus increase the net section stress in the notch region. If this approach were to be used regularly, the grips would probably also be modified to insure that the specimen is supported equally by each grip half. This is currently only true for a specimen 60 mm wide.

Whatever technique is eventually chosen, it is felt that these problems can be overcome, and since most tests are likely to be performed on embrittled material, they may not be of much practical significance.

One of the main advantages of this specimen design is the opportunity to test surface cracks. The problem of assessing safety margins in the presence of surface cracks and irregularly shaped cracks exhibiting extensive tunnelling is becoming quite important. Currently this specimen is being used to perform calibrations to use the potential drop technique to monitor the depth of a part-through crack in a full sized burst-test specimen.

A remaining problem to be addressed with this specimen will be to determine resistance curves to characterize stable crack extension for the centre-cracked geometry. Traditionally, these resistance curves have been based on the J-integral. However, as mentioned in section 4.3, the significance of the J-integral in the centre-cracked geometry is questionable since J will only characterize the crack-tip stress strain field over a very small region. For this reason, it is likely that future work on resistance curves for the centre-cracked geometry will rely on crack opening displacement (COD) as a characterizing parameter.

9.0 CONCLUSIONS

1) There is a need for a small fracture toughness specimen that maintains the original curved geometry of the CANDU pressure tube. This will eliminate the need to flatten embrittled material, which would either cause breakage or introduce undesirable residual stresses.

2) There is also a need for a small specimen with a centre-cracked geometry. This will better simulate the situation of an axial crack in a pressure tube and will reduce uncertainties in fracture toughness results arising from geometry effects.

3) A set of testing grips have been designed that, to a reasonable degree, constrain the central portion of a 120^{o} circumferential tube section to undergo radial and circumferential deformations similar to those in an internally pressurized tube.

4) Finite element analysis indicates that the mode I linear elastic stress intensity factor (K_I) relation for the curved centre cracked specimen is very similar to that of a similar sized flat plate in tension.

5) The finite element results also show that non-linearity due to crack tip plasticity invalidates the use of the LEFM parameter K at higher loads and crack lengths.

6) An experimental compliance calibration has shown that the K relationship for the curved specimen is similar to that for a flat plate, at least for intermediate crack length ratios ($0.5 \leq 2a/W \leq 0.65$).

7) At lower and higher crack length ratios the K relations for curved and flat specimens do not agree very well. However, there are reasons to suspect that improved experimental data could show that the curved specimen obeys the flat plate relation in these regions as well.

8) The development of the curved centre cracked specimen offers a new alternative for small specimen fracture toughness testing of CANDU reactor pres sure tubes, and could be modified for testing of piping and tubular components in general.

REFERENCES

1. C.J. Simpson and C.E. Ells, "Delayed Hydrogen Embrittlement in Zr-2.5 wt% Nb", Journal of Nuclear Materials 52 (1974), 289-295.

2. C.E. Coleman, "Susceptibility of Cold-Worked Zirconium-2.5wt% Niobium Al loy to Delayed Hydrogen Cracking", Atomic Energy of Canada Ltd., Report AECL- 5260, Chalk River, January, 1976.

3. C.E. Ells, "Delayed Hydrogen Cracking in Zirconium Alloys", in Proceedings of 3rd Symposium on Engineering Applications of Solid Mechanics, Toronto, 1976, 445-458.

4. C.E. Ells, "Influence of Hydrogen on the Behaviour of Zirconium Alloys in CANDU Reactors", Atomic Energy of Canada Ltd., Report AECL-6504, Chalk River, 1978.

5. C.E. Coleman, B.A. Cheadle, J.F.R. Ambler, P.C. Lichtenberger and R.L. Eadie, "Minimizing Hydride Cracking in Zirconium Alloys", CIM Annual Conference at Quebec City, August, 1984.

6. E.G. Price, "Highlights of the Metallurgical Behaviour of CANDU Pressure Tubes", Atomic Energy of Canada Ltd., Report AECL-8338, Chalk River, October, 1984.

7. B. Cox, "Mechanisms of Hydrogen Absorption by Zirconium Alloys", Atomic Energy of Canada Ltd. Report AECL-8702, Chalk River Nuclear Laboratories, Chalk River, January, 1985.

8. C.E. Coleman and J.F.R. Ambler, "Solubility of Hydrogen Isotopes in Stressed Hydride-forming Metals", Scripta Metallurgica, V. 17, 1983, pp. 77-82.

9. G.J.C. Carpenter, "The Ditatational Misfit of *Zirconium* Hydrides Precipitated in Zirconium", J. Nucl. Mat. 48 (1973), 264-266.

10. J.F. Kiefner, W.A. Maxey, R.J. Eiber and A.R. Duffy, "Failure Stress Levels of Flaws in Pressurized Cylinders", in J.G. Kaufman (Ed.), Progress in Flaw Growth and Fracture Toughness Testing, ASTM STP 536, American Society for Testing and Materials, Philadelphia, 1973, pp. 461-481.

11. G.T. Hahn, M. Sarrate and A.R. Rosenfield, Int. J. Fract. Mech., S, (1969) pp. 187-210.

12. E.S. Folias, Int. J. Fract. Mech., 1, (1965) pp. 104-113.

13. W.J. Langfard and L.E.J. Mooder, "Fracture Behaviour of Zirconium Alloy Pressure Tubes for Canadian Power Reactors", Int. J. Pres. Vess. and Piping, 6, (1978) pp. 275-310.

14. B.J.S. Wilkins, J.N. Barrie and R.J. Zink, "Slit-Burst Testing of Cold-Worked Zr-2.5 wt% Nb Pickering Pressure Tubing", Atomic Energy of Canada report, WNRE-426, Pinawa, Manitoba, 1978, September.

15. J.G. Kalbfleisch, "Critical Crack Lengths in Pressure Tubes", Appendix B in "Examination of the Strength of Pressure Tubes with Cracks in the Area of Rolled Joints", J. Schroeder and D.J. Burns, Waterloo Research Institute, Project No. 603-18-02, 1977, February.

16. L.E.J. Mooder, "Flaw Tolerance of Hydrided Cold-Worked Zr-2.5wt% Nb Pressure Tubes Prepared for Task Group III", Unpublished report, CRNL-2452, Atomic Energy of Canada Ltd. Chalk River, Ontario, 1983, May.

17. C.E. Coleman and C.A. Wills, "Regression Analysis of Slit Burst Test Data for Cold-Worked Zr-2.5wt% Nb Pressure Tubes", Atomic Energy of Canada Report, CRNL-2501, Chalk River, Ontario, 1983, March.

18. L.A. Simpson and B.J.S. Wilkins, "Prediction of Fast Fracture in Zr-2.5wt% Nb Pressure Tubes Using Elastic-Plastic Fracture Mechanics", in K.J. Miller and R.D. Smith (Eds.), "Mechanical Behaviour of Materials", Proc. ICM(3), Cambridge, England, 1979, (Pergamon Press, 1979).

19. L.A. Simpson, "The Application of Ductile Fracture Analysis to Predictions of Pressure Tube Failure", Atomic Energy of Canada Ltd Report AECL-6805, 981, August.

20. J.R. Rice, "A Path Independent Integral and the Approximate Analysis of Strain Concentration by Notches and Cracks", Journal of Applied Mechanics, Vol. 35, 1968, pp. 379-386.

21. J.W. Hutchinson, "Singular Behaviour at the End of a Tensile Crack in a Hardening Material", J. Mech. Phys. Solids, Vol. 16, 1968, pp. 13-31.

22. J.R. Rice and G.F. Rosengren, "Plane Strain Deformation Near a Crack Tip in a Power Law Hardening Material", J. Mech. Phys. Solils, Vol.16,1968, pp. 1–12.

23. J.A. Begley and J.D. Landes, "The J–Integral as a Fracture Criterion in Fracture Toughness Testing", in "Fracture Toughness", ASTM Special Technical Publication 514, 1972, pp. 1–23, 24–39.

24. J.R. Rice, "Elastic–Plastic Models for Stable Crack Growth", in "Mechanics and mechanisms of Crack Growth", (Proc. at Cambridge, England, april, 1973), M.J. May (Ed.), British Steel Corporation Physical Metallurgy Centre Publication, 1975, pp. 14–39.

25. S.J. Garwood, J.N. Robinson and C.E. Turner, "The Measurement of Crack Growth Resistance Curves (R–Curves) Using the J–Integral", Int. J. of Fracture, 11 (1975), pp. 528.

26. P.C. Paris, H. Tada, A. Zahoor and E. Ernst, "The Theory of Instability of the Tearing Mode of Elastic–Plastic Crack Growth", in "Elastic–Plastic Fracture", ASTM Special Technical Publication 668, 1979, pp. 5–36.

27. J.W. Hutchinson and P C. Paris, "Stability Analysis of J–Controlled Crack Growth", in "Elatic–Plastic Fracture", ASTM STP 668, 1979, pp 37–64.

28. C.F. Shih, H.G. deLorenzi, and W.R. Andrews, "Studies on Crack Initiation and Stable Crack Growth", in "Elastic–Plastic Fracture", ASTM STP 668, 1979, pp. 65–120.

29. L.A. Simpson and C.F. Clarke, "An Elastic–Plastic R–Curve Description of Fracture in Zr–2.5wt% Nb Pressure Tube Alloy", in "Elastic–Plastic Fracture", ASTM STP 668, pp. 643–662.

30. V. Kumar, M.D. German and C.F. Shih, "An Engineering Approach for Elastic- Plastic Fracture Analysis", Electric Power Research Institute Report EPRI- 1931, Research Project 1237-1, Topical Report, July, 1981.

31. L.A. Simpson, R.B. Ellis, D.J. Stark and A.J. Shillinglaw, "The Effect of Irradiation and Irradiation Temperature on the Fracture Toughness of Cold-Worked Zr-2.5wt% Nb", Atomic Energy of Canada Ltd. Report AECL-8368, Pinawa, Manitoba, September, 1984.

32. B.W. Leitch, "The Leakage Area and Crack Driving Force of a Through-Wall Crack in a Zirconium-Alloy Pressure Tube", to be published in proc. ASME Pressure Vessels and Piping Conference, New Orleans, June 24-26, 1985.

33. P.C. Paris, H. Tada, H. Ernst and A. Zahoor, "Initial Experimental Investigation of Tearing Instability Theory", Elastic-Plastic Fracture, ASTM STP 668, 1979, pp. 251-265.

34. J.A. Begley, and J.D. Landes, Int. Journal of Fracture, 12, 1976, RCR 764-766.

35. S.J. Garwood, "Effect of Specimen Geometry on Crack Growth Resistance", in Fracture Mechanics, ASTM STP 677, C.W. Smith (Ed.), 1979, pp. 511-532.

36. D.E. McCabe and H.A. Ernst, "A Perspective on R-Curves and Instability Theory", in Fracture Mechanics: Fourteenth Symposium, Volume I: Theory and Analysis, ASTM STP 791, J.C. Lewis and G. Sines (Ed.), 1983, pp I-651-I-584.

37. R.M. McMeeking and D.M. Parks, "On Criteria for J-Dominance of Crack-Tip Fields in Large-Scale Yielding", ASTM STP 668, 1979, pp. 175-194.

38. C.F. Shih and M.D. German, "Requirements for a One Parameter Characterization of Crack Tip Fields by the HRR Singularity", International Journal of Fracture, Vol. 17, No. 1, February 1981.

39. L.A. Simpson, "Effects of Specimen Geometry on Elastic-Plastic R-Curves for Zr-2.5wt% Nb", in "Advances in Fracture Research", D. Francois (Ed.), Pergamon Press, Oxford, 1980, pp. 833-841.

40. B.J.S. Wilkins, A.R. Reich and J.N. Barrie, Int. J. Pres. Vess. and Piping, 10 (1982), 69.

41. A.C. Wallace, "The Development of Curved Fracture Toughness Specimens for Predicting Crack Growth in CANDU Reactor Pressure Tubes", in "Time Dependent Fracture", A.S. Krausz (Ed.), Proc. Eleventh Canadian Fracture Conference, Ottawa, June, 1984, pp. 281-291.

42. P.H. Davies, "Curved Double Torsion Fracture Toughness Tests on Zr-2.5wt% Nb Pressure Tube Material", Ontario Hydro Research Division Report No. M83-56- K, file 826.231, April, 1983.

43. P.H. Davies and G.K. Shek, "Comparison of Zircaloy-2 Pressure Tube Burst Test with Curved Double Torsion Results", Ontario Hydro Research Division Report No. 84-392-K, File 823.211, January, 1985.

44. C.K. Chow and L.A. Simpson, "An Analysis of The Unstable Fracture of a Reactor Pressure Tube Using Fracture Toughness Mapping", Proc. ASTM Symposium on Case Histories Involving Fatigue and Fracture Mechanics, Charleston, S.C., March, 1985.

45. J.L. Meriam, "Static - SI Version", 2nd Edition, John Wiley & sons, 1975, pp 367.

46. D.M. Parks, "A Stiffness Derivative Finite Element Technique for Determination of Elastic Crack Tip Stress Intensity Factors", Int. J. Fract., 10, pp. 487-502, 1974.

47. R.S. Barsoum, "On the Use of Isoparametric Finite Elements in Linear Fracture Mechanics", Int. J. Num. Meth. Eng., 10, pp. 25-38, 1976.

48. EPRI NP-1735, "Methodology for Plastic Fracture", Electric Power Research Institute, Palo Alto, California, March, 1981.

49. D.R.J. Owen and A.J. Faukes, "Engineering Fracture Mechanics: Numerical Methods and Applications", Pineridge Press, Swansea, U.K., 1983.

50. C.E. Fedderson in Discussion, "Plane Strain Crack Toughness Testing of High Strength Metallic Materials", ASTM STP 410, Brown, W.F. and Srawley, J.E., Eds., American Society for Testing and Materials, 1967, pp. 77–79.

51. J. Eftis and H. Liebowitz, "On the Modified Westergaard Equations for Certain Plane Crack Problems", Int. J. Fract. Mech., 8 (1972), pp. 383–392.

52. J. Schijve and U. De Koning, "A Specimen for a Constant Stress Intensity Factor", Eng. Fract. 1977, Vol. 9, pp. 331–340.

53. D. Broek, "Elementary Engineering Fracture Mechanics", Noordhoft International Publishing, Leyden, Netherlands.

Table 1 – Comparison of Theoretical Strains[1] in a Pressurized Tube and Those Predicted in the Specimen from Radius Increase Produced by a Given Rotation

Rotation Angle[2] (degrees)	Average Radius Increase (mm)	Strain on Deformed Surface	Theoretical Strain
1	0.6015	.011677	.011680
2	1.2058	.023415	.023414
3	1.8119	.035192	.035183
4	2.4190	.046981	.046971
5	3.0261	.058789	.058759

1 – $$\varepsilon_{cir} = \frac{R_i - r_i}{r_i}$$

r_i = undeformed internal radius

R_i = average deformed internal radius

2 – rotation applies to one half of grips only – the other half will also rotate by the same amount.

Table 2 - Finite Element Stress Intensity Factor Estimates

2a/W	Load (kN)	K_I (MPa $\sqrt{m}$)
0.2	14.706	8.64 $\pm$ 0.12
	28.829	17.07 $\pm$ 0.28
	42.848	25.51 $\pm$ 0.44
	55.208	32.93 $\pm$ 0.65
	65.799	39.33 $\pm$ 0.88
	75.212	45.08 $\pm$ 1.13
	82.652	49.48 $\pm$ 1.39
0.4	13.588	12.38 $\pm$ 0.12
	26.616	24.71 $\pm$ 0.24
	39.799	36.74 $\pm$ 0.23
	52.175	48.42 $\pm$ 0.06
	62.605	58.37 $\pm$ 0.03
	72.338	68.21 $\pm$ 0.15
	80.364	76.66 $\pm$ 0.31
0.5	12.724	13.96 $\pm$ 0.26
	25.251	27.80 $\pm$ 0.47
	37.517	41.65 $\pm$ 0.57
	49.686	55.11 $\pm$ 0.57
	59.641	67.13 $\pm$ 0.93
	69.189	79.01 $\pm$ 1.57
	77.544	90.34 $\pm$ 2.21
0.6	11.757	15.41 $\pm$ 0.34
	23.199	30.72 $\pm$ 0.63
	34.600	45.98 $\pm$ 0.77
	45.996	61.38 $\pm$ 1.08
	55.826	75.89 $\pm$ 1.91
	64.619	90.25 $\pm$ 3.31
	72.331	105.10 $\pm$ 5.14
0.8	9.126	18.63 $\pm$ 0.44
	18.007	37.12 $\pm$ 0.78
	26.926	55.64 $\pm$ 0.98
	35.466	74.97 $\pm$ 1.97
	42.998	95.75 $\pm$ 4.45
	47.931	115.27 $\pm$ 3.99
	50.244	149.78 $\pm$ 16.54

Table 3 – Experimental Compliance Data

Specimen I.D.	Normalized Crack Length (2a/W)	Normalized Compliance (EBC)
#1	.154	.2789
	.277	.4499
	.289	.4826
	.322	.5399
	.364	.6041
	.396	.6503
#2	.167	.2642
	.236	.3881
	.283	.4867
	.342	.5980
	.409	.7292
	.509	.8908
	.604	1.1567
#3	.166	.2769
	.376	.6773
	.468	.8393
	.551	1.0491
	.617	1.2409
	.694	1.5092
	.759	1.7988

TABLE 4 - Curved Specimen K Calibration Analysis
Comparison of Compliance K vs Theoretical Flat Plate K

****
** 2a/W = .2 **
****

LOAD (MN)	K(THEORETICAL) ($MPa\sqrt{m}$)	K(EXPERIMENTAL) ($MPa\sqrt{m}$)
0.01	5.72	7.93
0.02	11.45	15.85
0.03	17.17	23.78
0.04	22.89	31.71
0.05	28.61	39.63
0.06	34.34	47.56
0.07	40.06	55.49
0.08	45.78	63.42
0.09	51.51	71.34
0.10	57.23	79.27

****
** 2a/W = .3 **
****

LOAD (MN)	K(THEORETICAL) ($MPa\sqrt{m}$)	K(EXPERIMENTAL) ($MPa\sqrt{m}$)
0.01	7.24	9.22
0.02	14.48	18.45
0.03	21.72	27.67
0.04	28.97	36.90
0.05	36.21	46.12
0.06	43.45	55.34
0.07	50.69	64.57
0.08	57.93	73.79
0.09	65.17	83.01
0.10	72.41	92.24

****
** 2a/W = .4 **
****

LOAD (MN)	K(THEORETICAL) (MPa$\sqrt{m}$)	K(EXPERIMENTAL) (MPa$\sqrt{m}$)
0.01	8.78	10.36
0.02	17.55	20.72
0.03	26.33	31.08
0.04	35.10	41.44
0.05	43.88	51.80
0.06	52.65	62.16
0.07	61.43	72.52
0.08	70.20	82.88
0.09	78.98	93.24
0.10	87.75	103.60

****
** 2a/W = .5 **
****

LOAD (MN)	K(THEORETICAL) (MPa$\sqrt{m}$)	K(EXPERIMENTAL) (MPa$\sqrt{m}$)
0.01	10.49	11.38
0.02	20.99	22.77
0.03	31.48	34.15
0.04	41.98	45.53
0.05	52.47	56.91
0.06	62.96	68.30
0.07	73.46	79.68
0.08	83.95	91.06
0.09	94.45	102.44
0.10	104.94	113.83

****
** 2a/W = .6 **
****

LOAD (MN)	K(THEORETICAL) (MPa$\sqrt{m}$)	K(EXPERIMENTAL) (MPa$\sqrt{m}$)
0.01	12.61	12.32
0.02	25.22	24.64
0.03	37.83	36.96
0.04	50.43	49.28
0.05	63.04	61.60
0.06	75.65	73.93
0.07	88 26	86.25
0.08	100.87	98.57
0.09	113.48	110.89
0.10	126.09	123.21

****
** 2a/W = .7 **
****

LOAD (MN)	K(THEORETICAL) $(MPa\sqrt{m})$	K(EXPERIMENTAL) $(MPa\sqrt{m})$
0.01	15.50	13.19
0.02	30.99	26.39
0.03	46.49	39.58
0.04	61.98	52.77
0.05	77.48	65.96
0.06	92.98	79.16
0.07	108.47	92.35
0.08	123.97	105.54
0.09	139.47	118.73
0.10	154.96	131.93

****
** 2a/W = .8 **
****

LOAD (MN)	K(THEORETICAL) $(MPa\sqrt{m})$	K(EXPERIMENTAL) $(MPa\sqrt{m})$
0.01	20.08	14.01
0.02	40.16	28.02
0.03	60.24	42.03
0.04	80.32	56.04
0.05	100.40	70.05
0.06	120.48	84.06
0.07	140.56	98.07
0.08	160.64	112.08
0.09	180.72	126.09
0.10	200.80	140.10

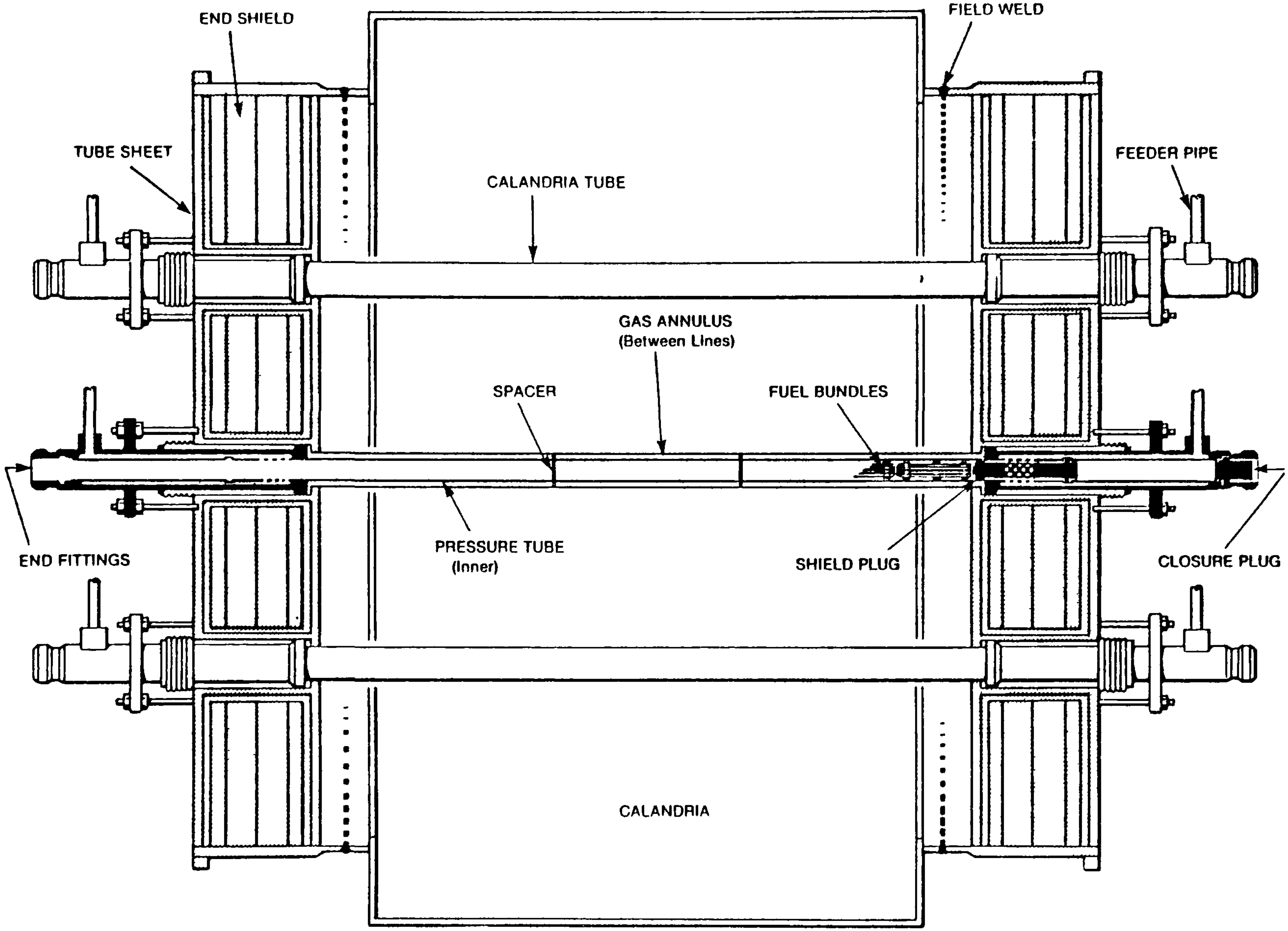

FIGURE 1

SCHEMATIC OF THE CANDU REACTOR SHOWING FUEL CHANNELS

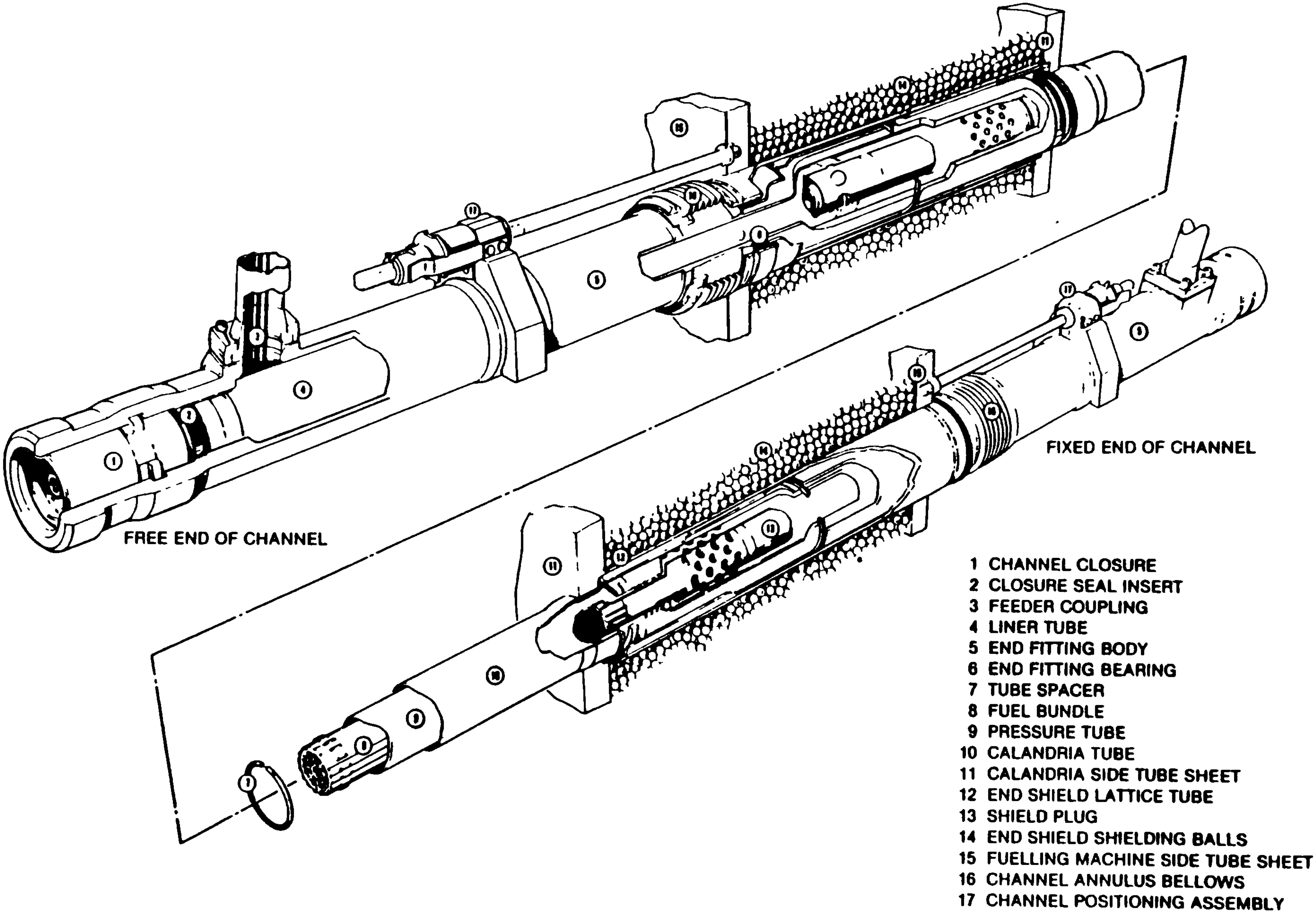

FIGURE 2
FUEL CHANNEL ASSEMBLY

17449G-RD

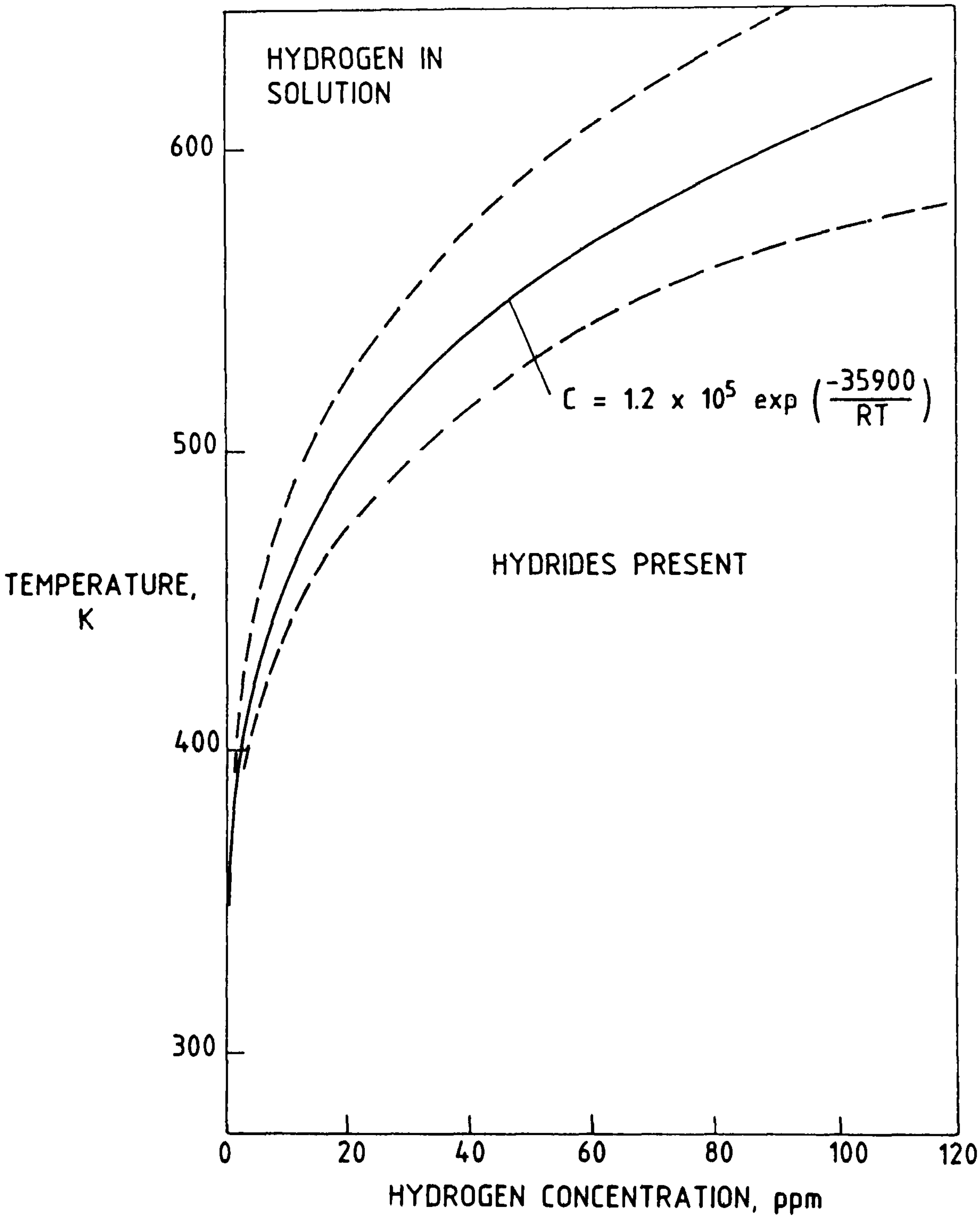

FIGURE 3
SOLUBILITY OF HYDROGEN IN ZIRCONIUM

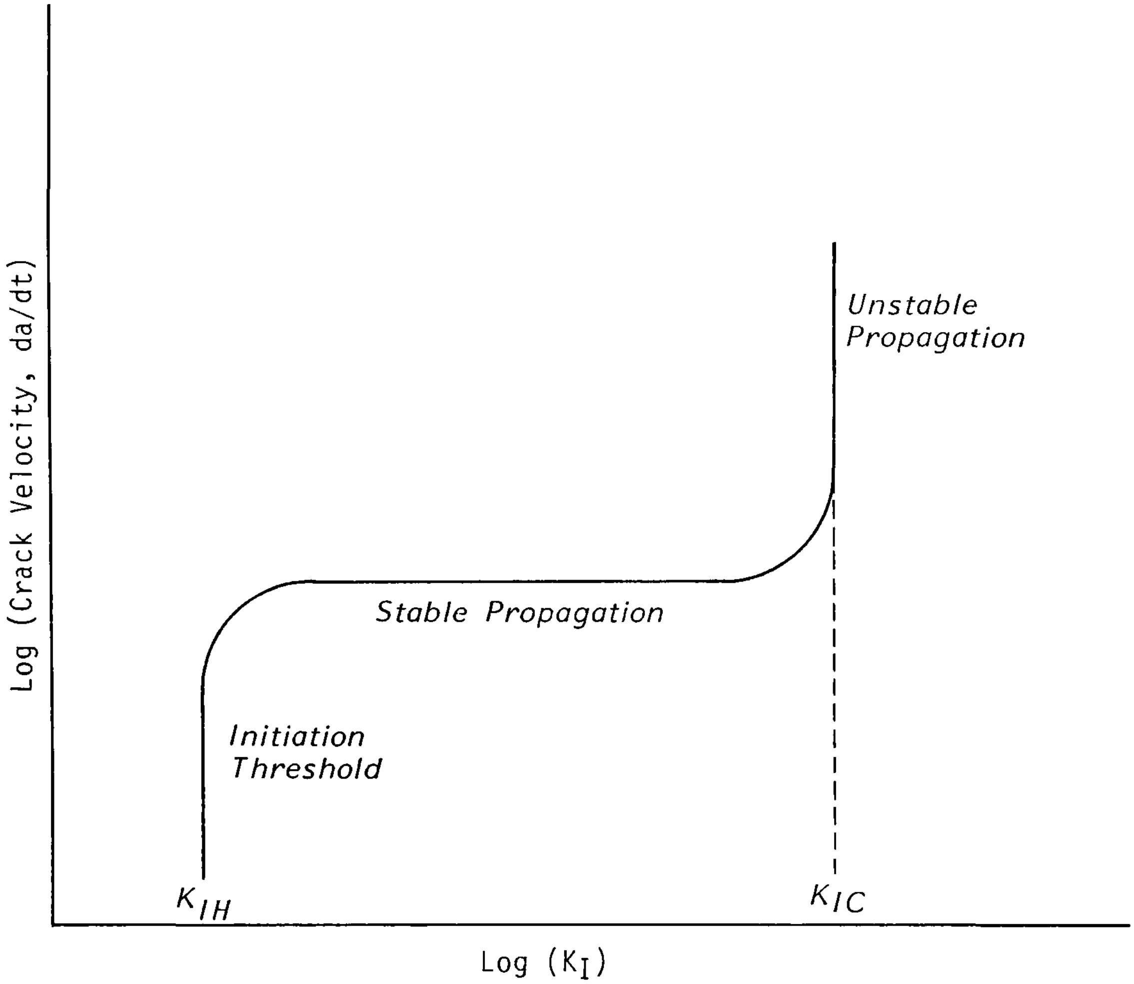

FIGURE 4

THE DEPENDENCE OF HYDRIDE CRACKING VELOCITY (da/dt)
ON THE STRESS INTENSITY FACTOR (K_I)

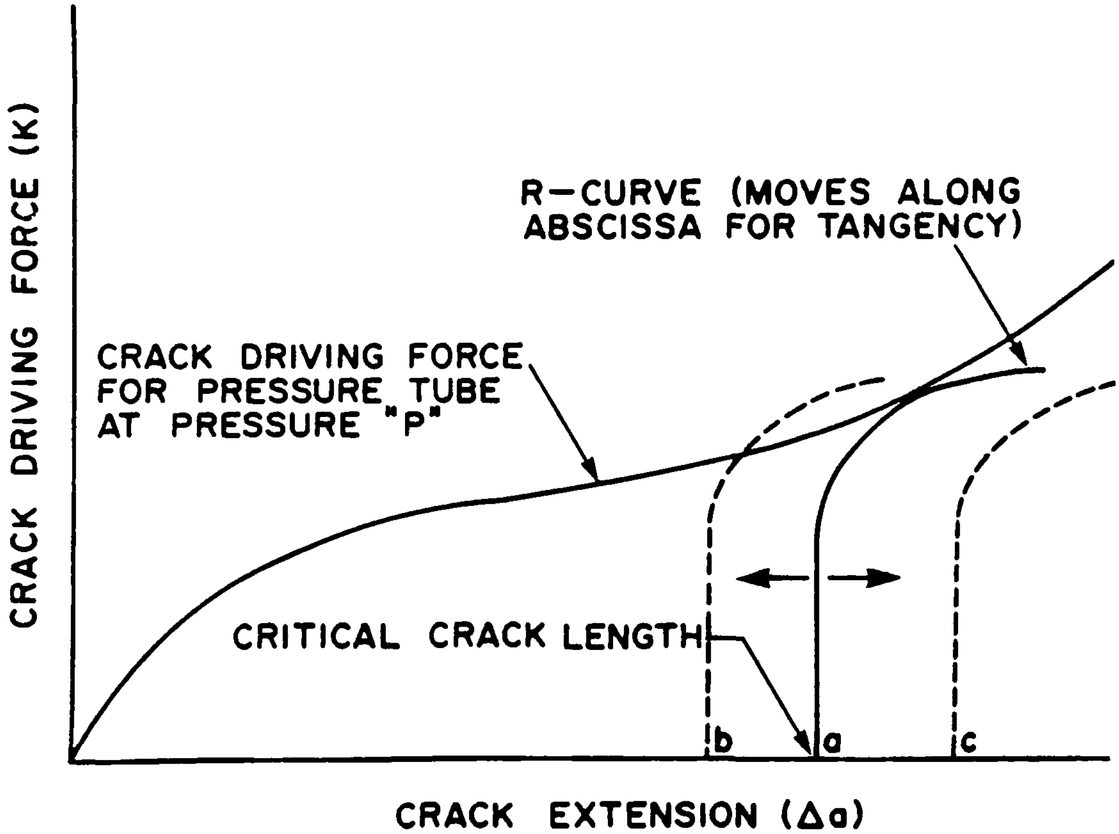

FIGURE 5

DEMONSTRATION OF THE TANGENCY METHOD OF ESTIMATING CRITICAL CRACK LENGTH WITH THE R-CURVE (REFERENCE 19)

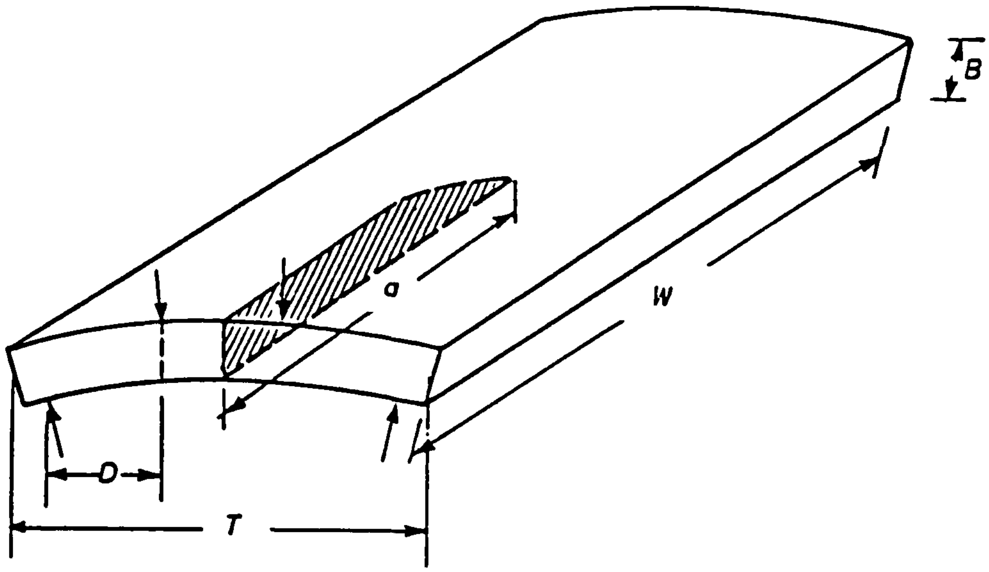

Four-point loading applied by means of rollers on upper plate surface and roller bearings on lower plate surface.

FIGURE 6

CURVED DOUBLE TORSION SPECIMEN CONFIGURATION

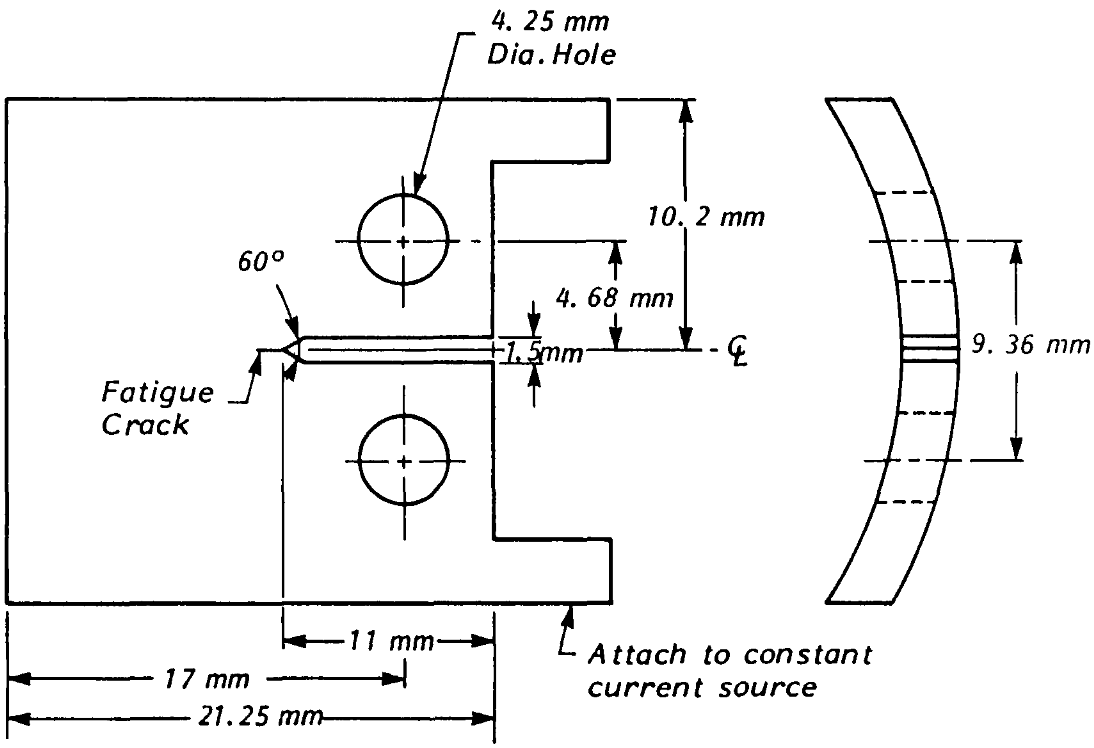

FIGURE 7

CURVED COMPACT-TENSION SPECIMEN

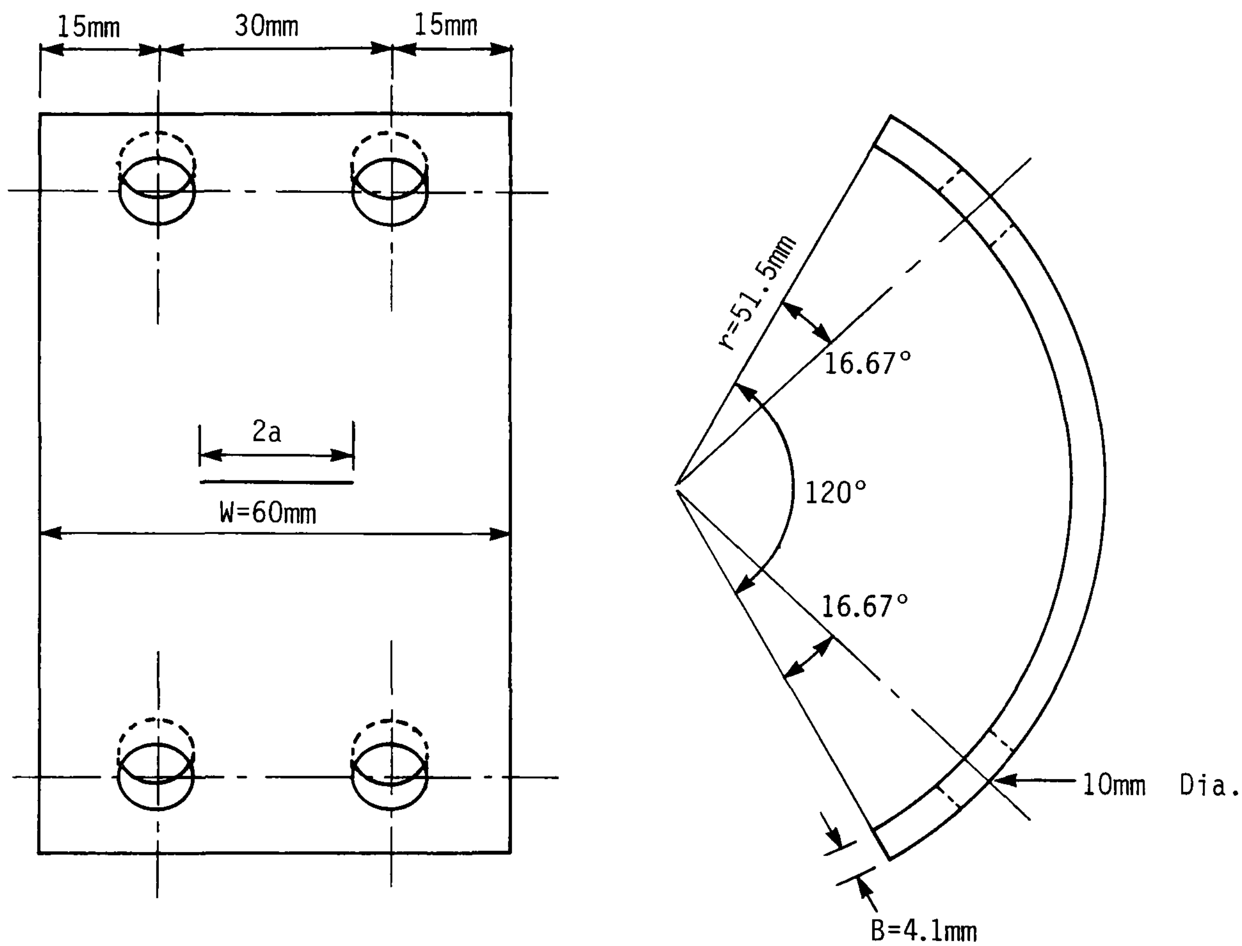

FIGURE 8
CURVED CENTRE CRACKED SPECIMEN

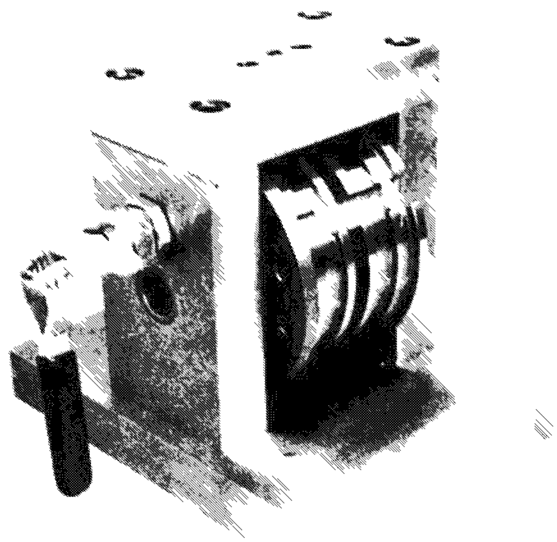

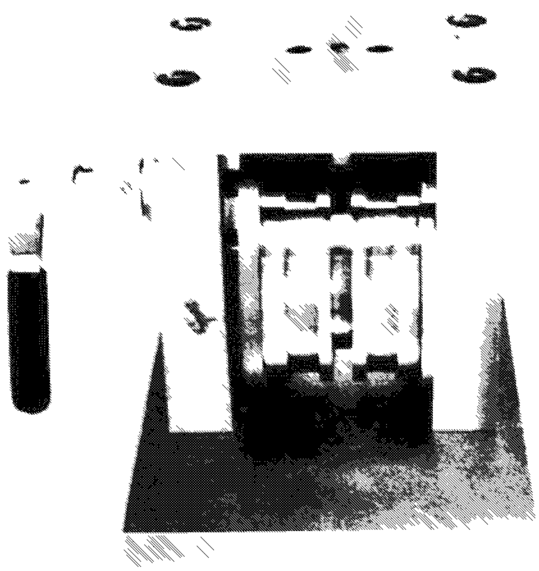

FIGURE 9

2 VIEWS OF DRILLING JIG USED TO PRECISELY POSITION HOLES IN THE CURVED SPECIMEN

172524 RD

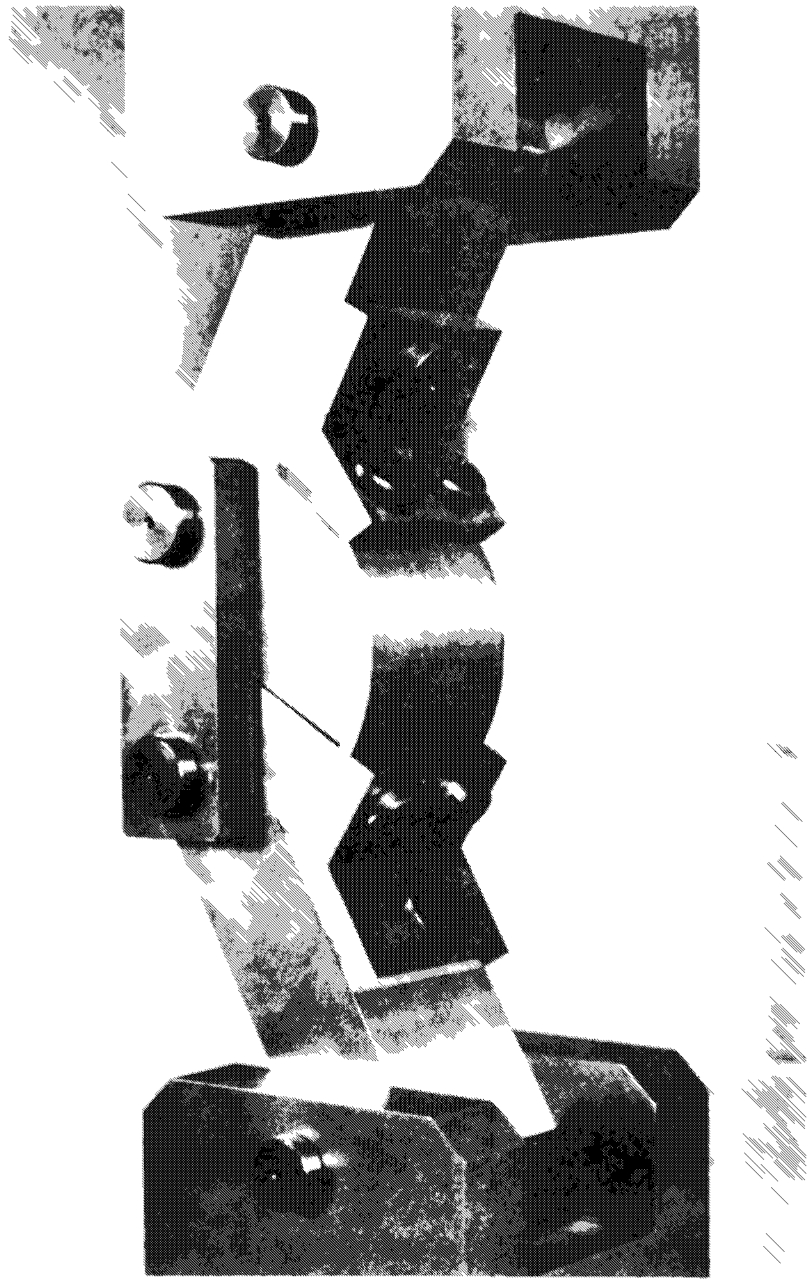

FIGURE 19

VIEW OF AN UNNOTCHED SPECIMEN
MOUNTED IN THE GRIPS

172808 RD

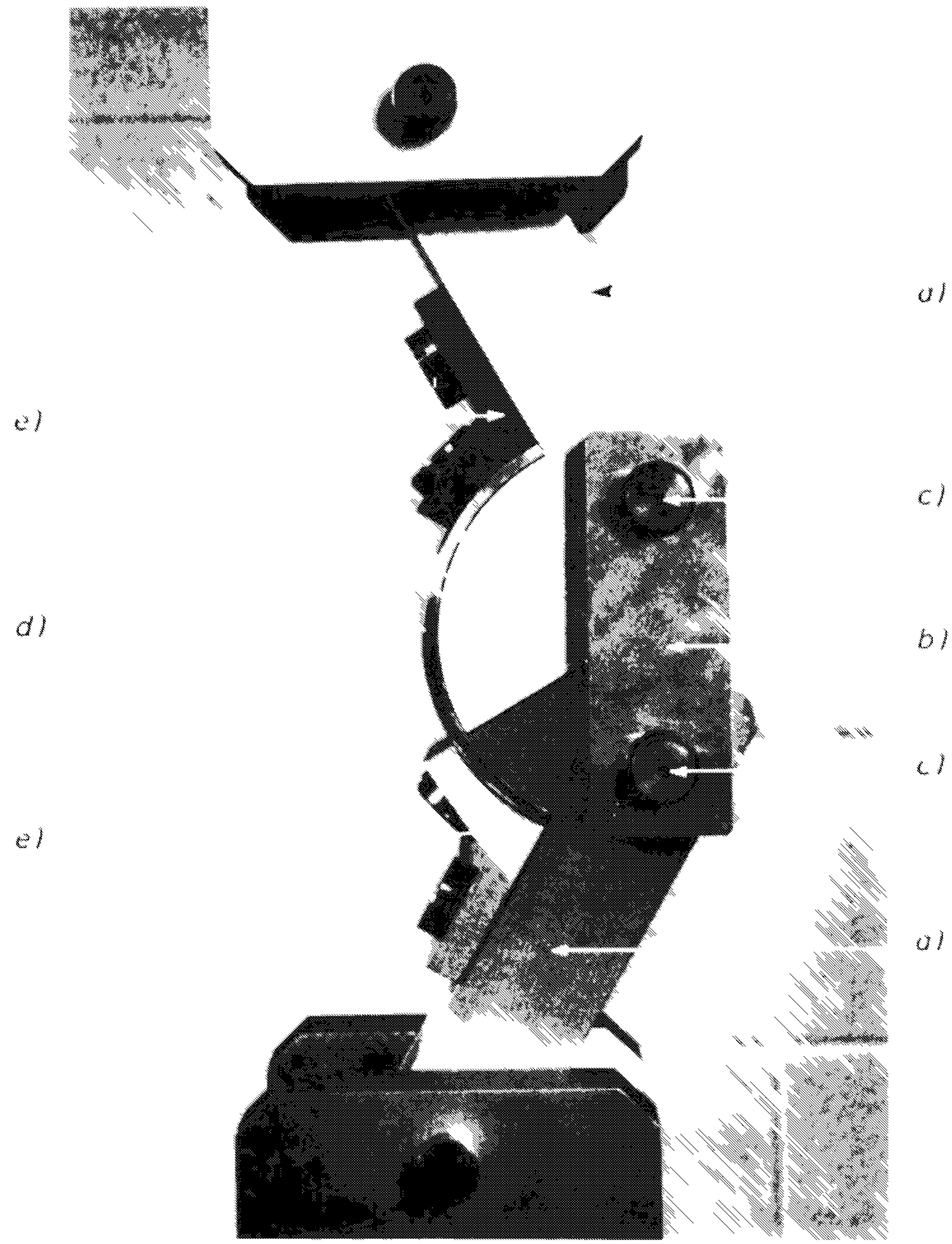

FIGURE 11

SIDE VIEW OF SPECIMEN MOUNTED IN GRIPS
WITH VARIOUS COMPONENTS IDENTIFIED

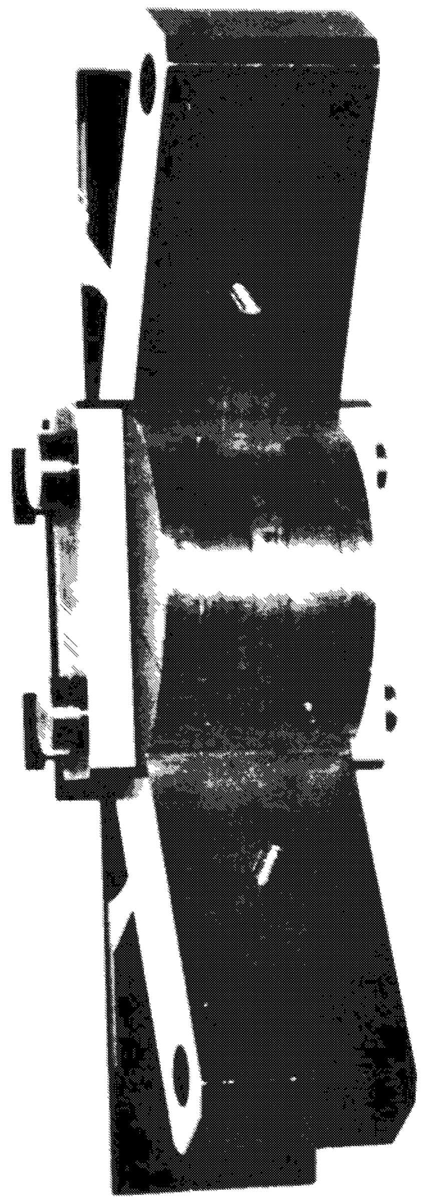

FIGURE 12

GRIPS IN THEIR INITIAL CLOSED POSITION

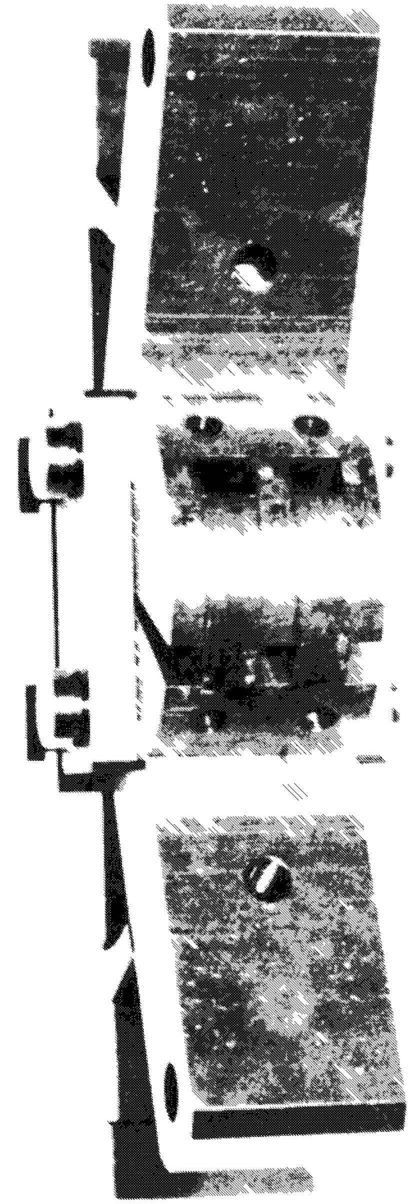

FIGURE 13

GRIPS AFTER OPENING UNDER LOAD

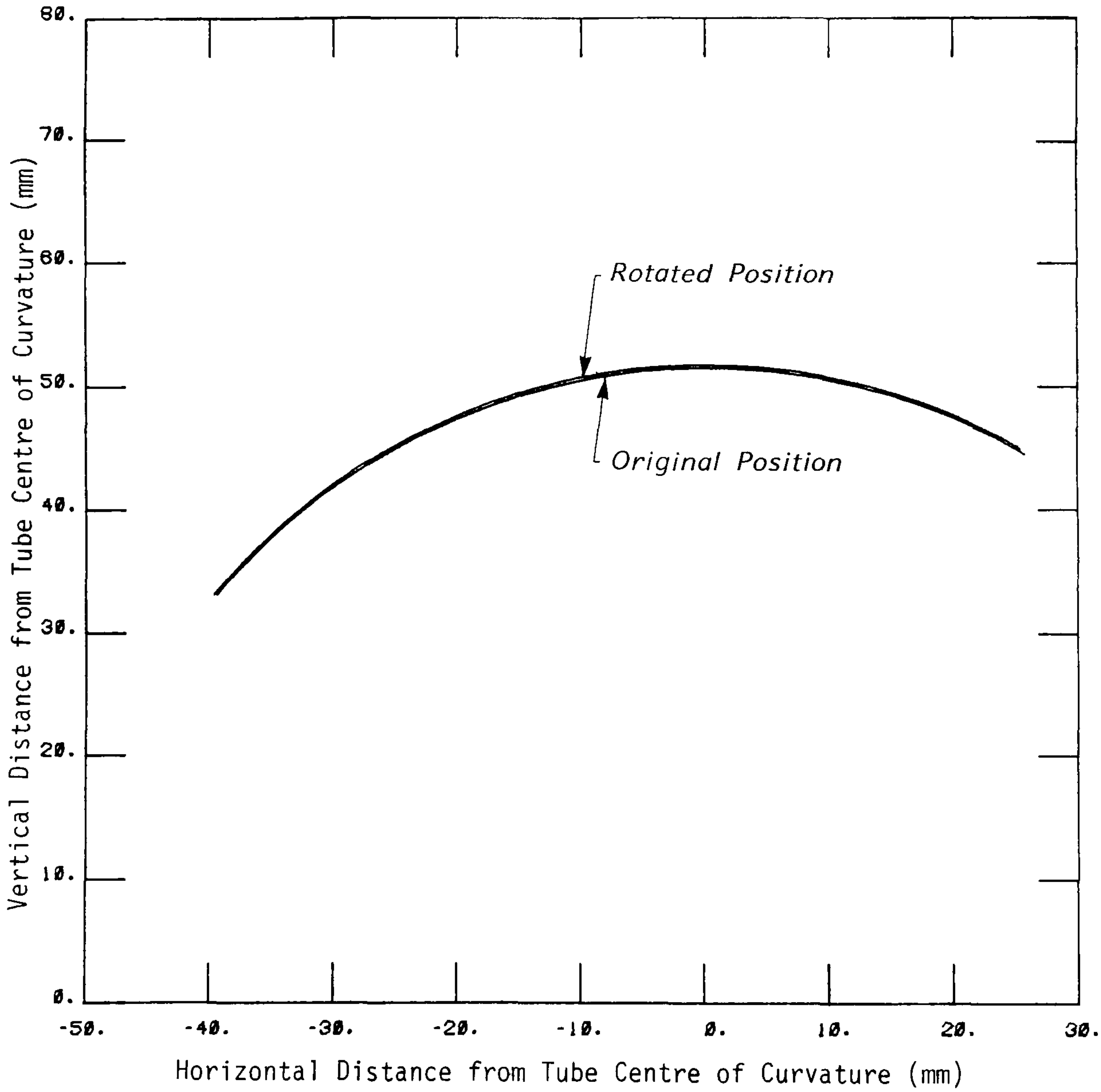

FIGURE 14

DEFORMATION ANALYSIS FOR GRIP-HALF ROTATION OF 0.4°

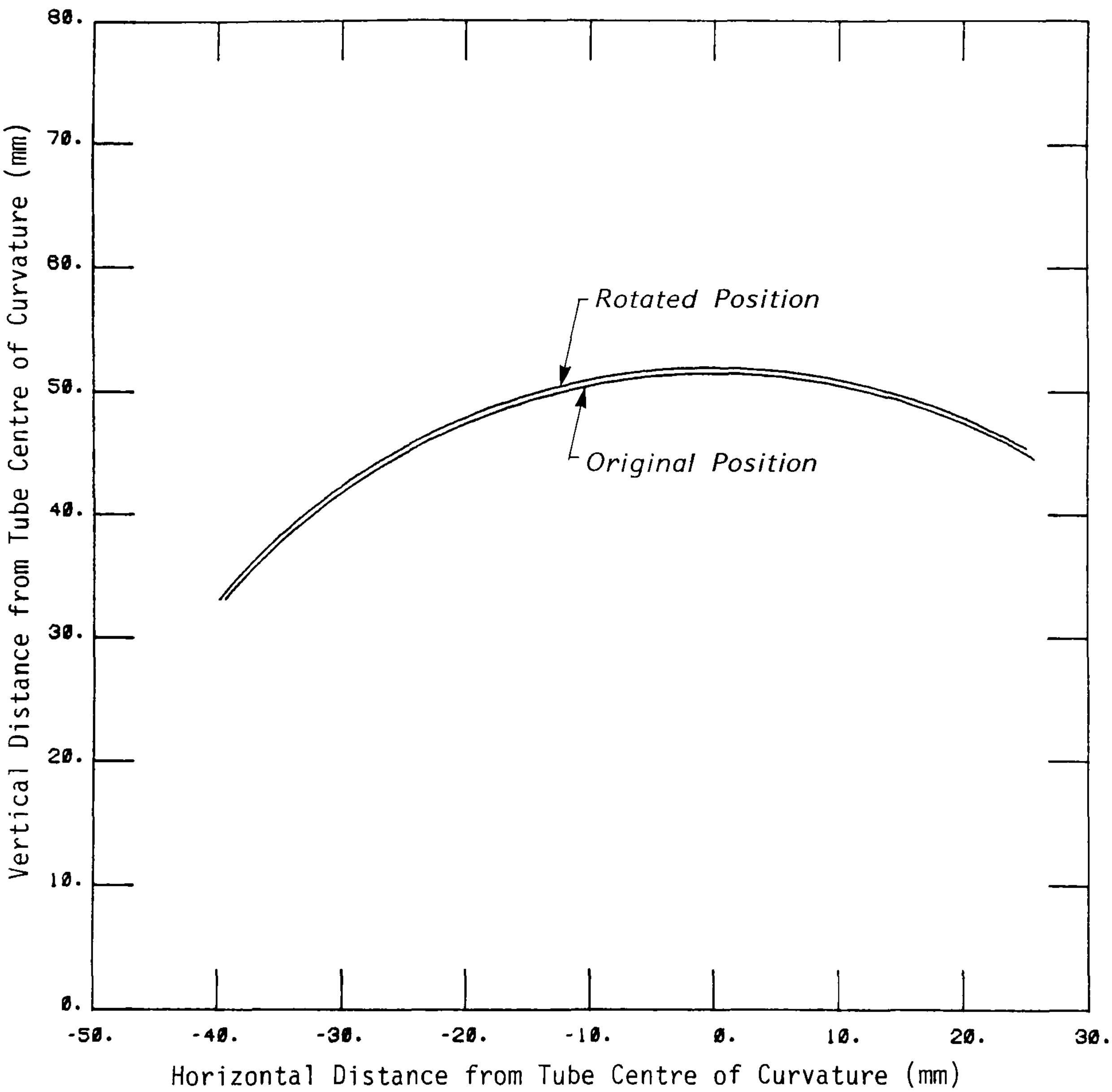

FIGURE 15

DEFORMATION ANALYSIS FOR GRIP-HALF ROTATION OF 0.8°

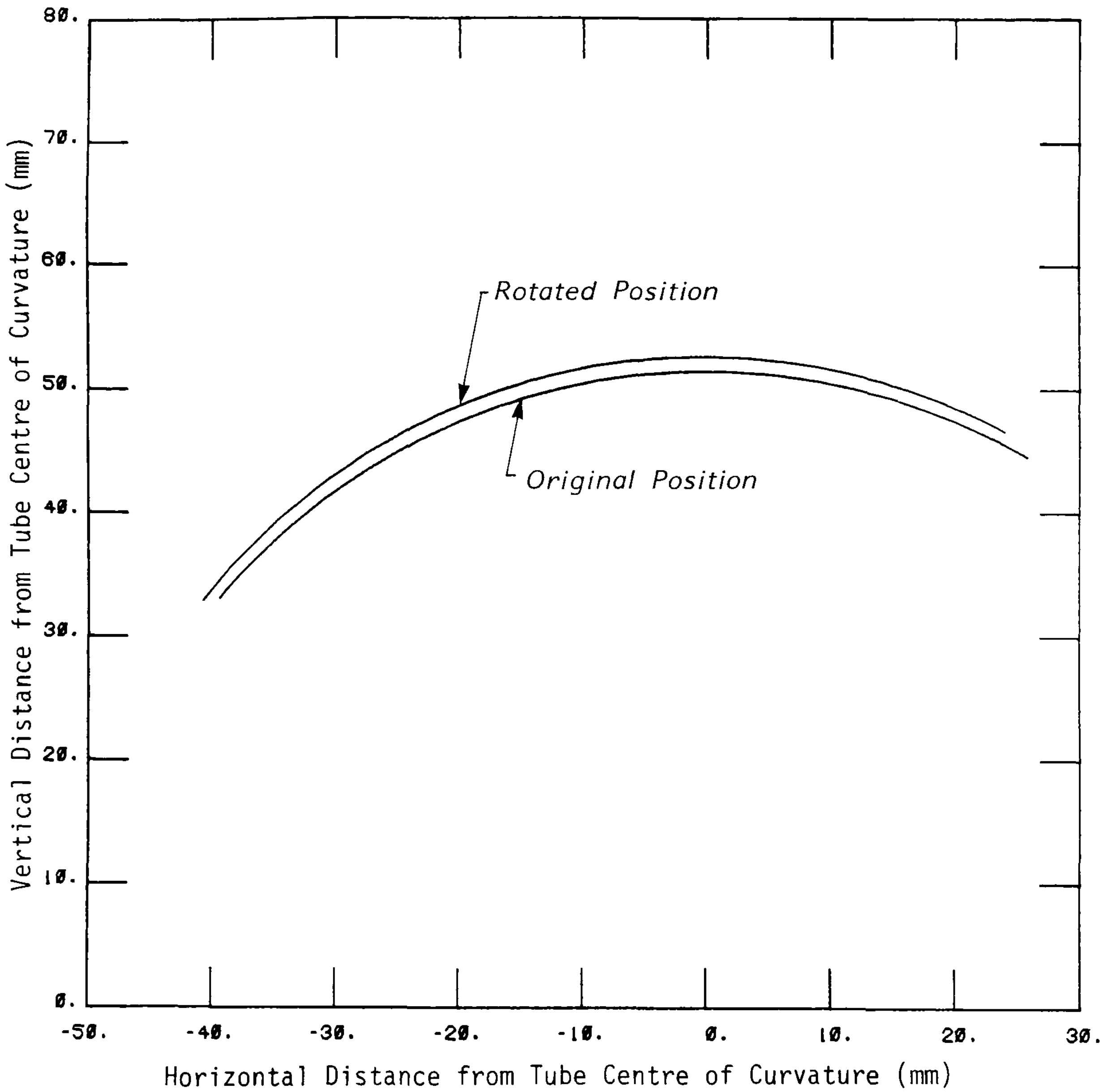

FIGURE 16

DEFORMATION ANALYSIS FOR GRIP-HALF ROTATION OF 2°

172528 RD

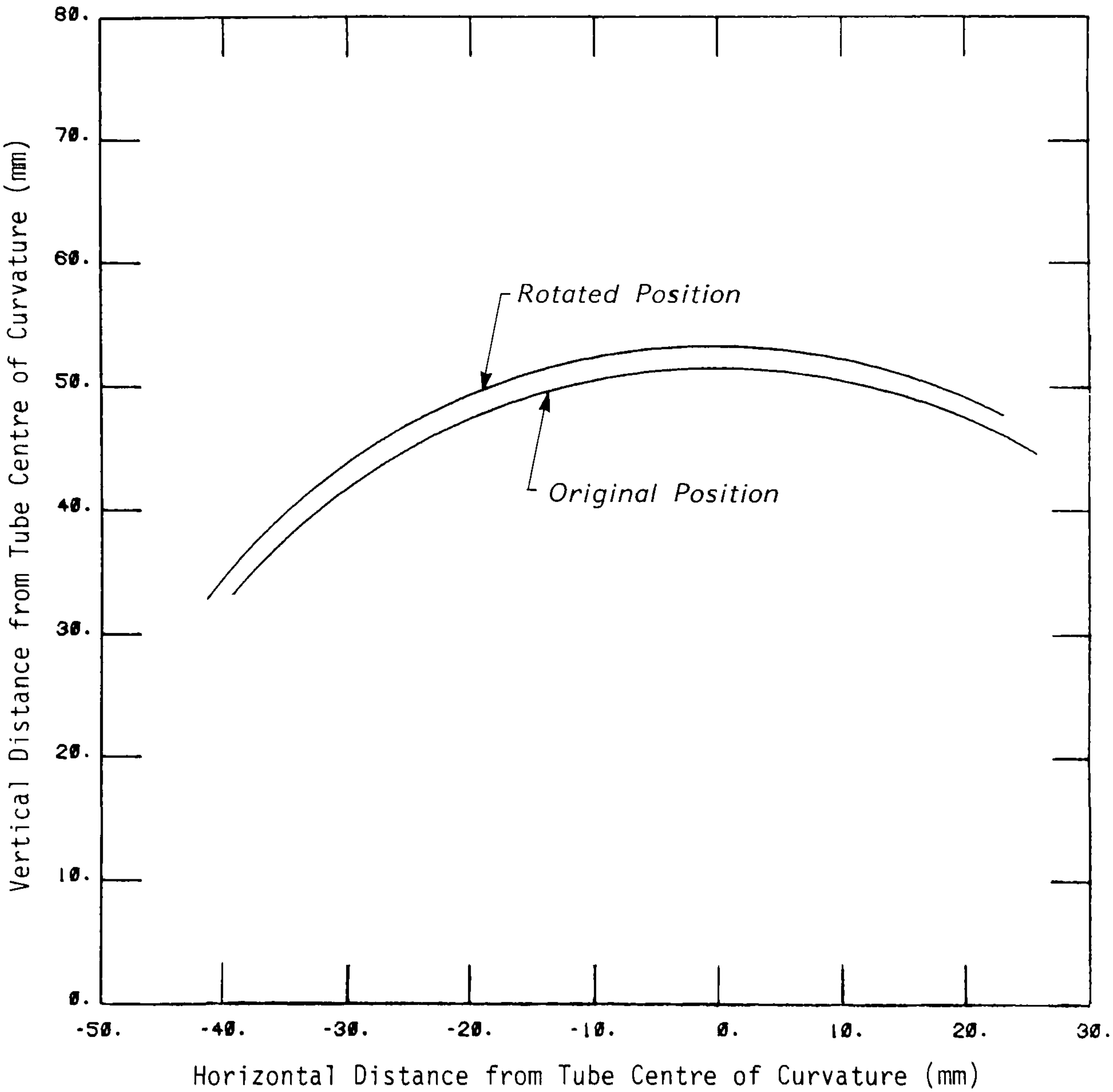

FIGURE 17

DEFORMATION ANALYSIS FOR GRIP-HALF ROTATION OF 3°

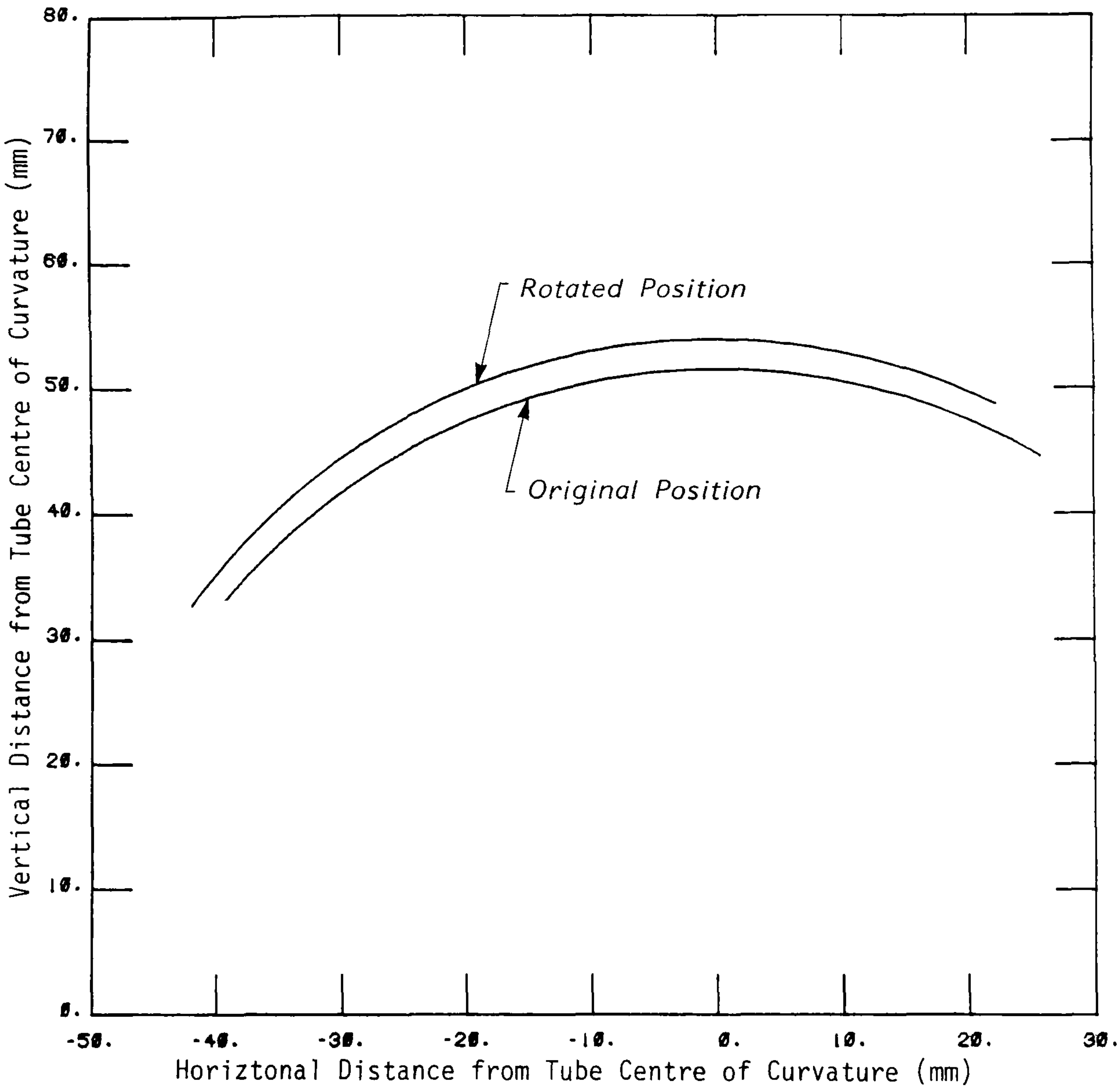

FIGURE 18

DEFORMATION ANALYSIS FOR GRIP-HALF ROTATION OF 4°

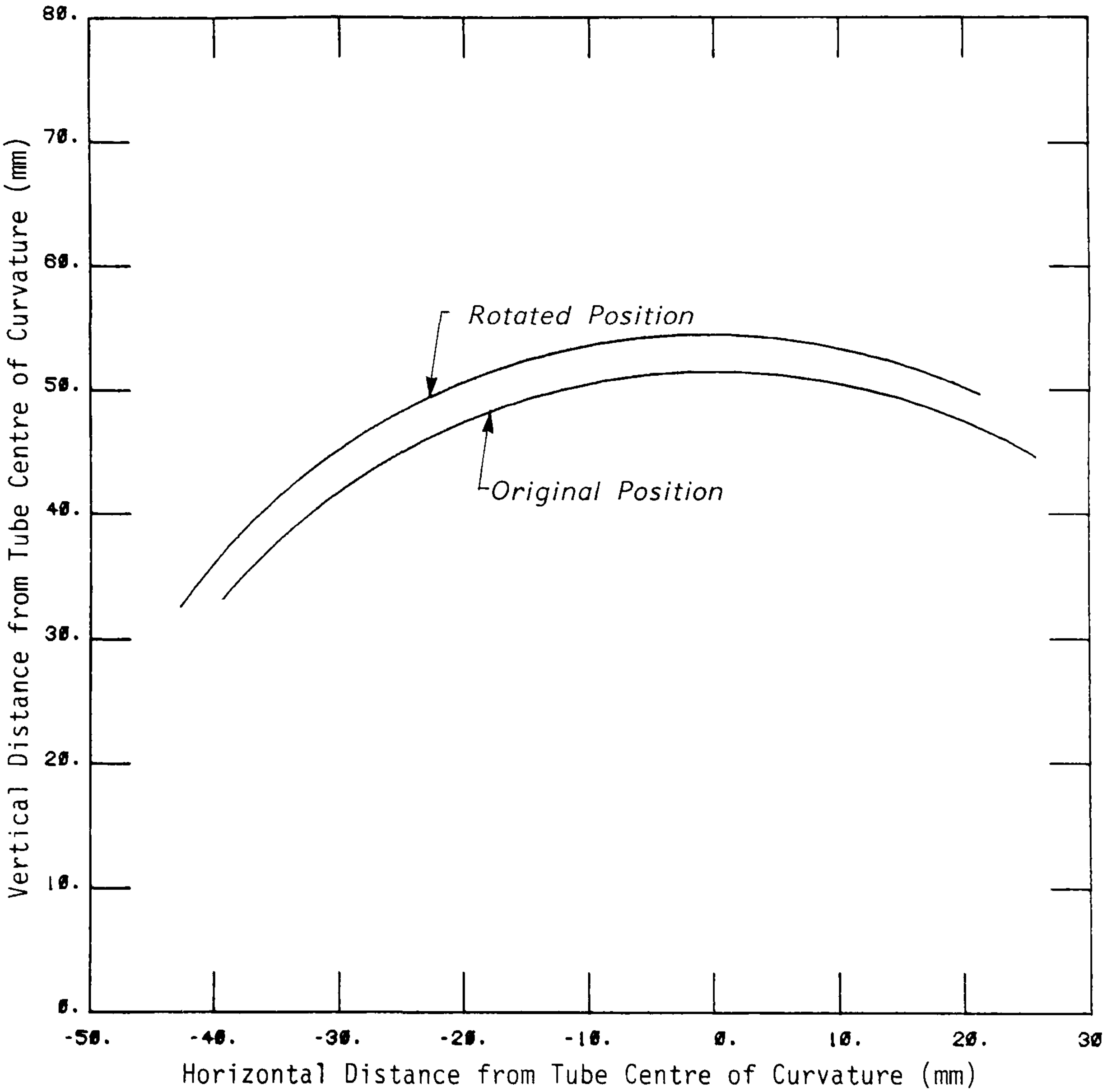

FIGURE 19

DEFORMATION ANALYSIS FOR GRIP-HALF ROTATION OF 5°

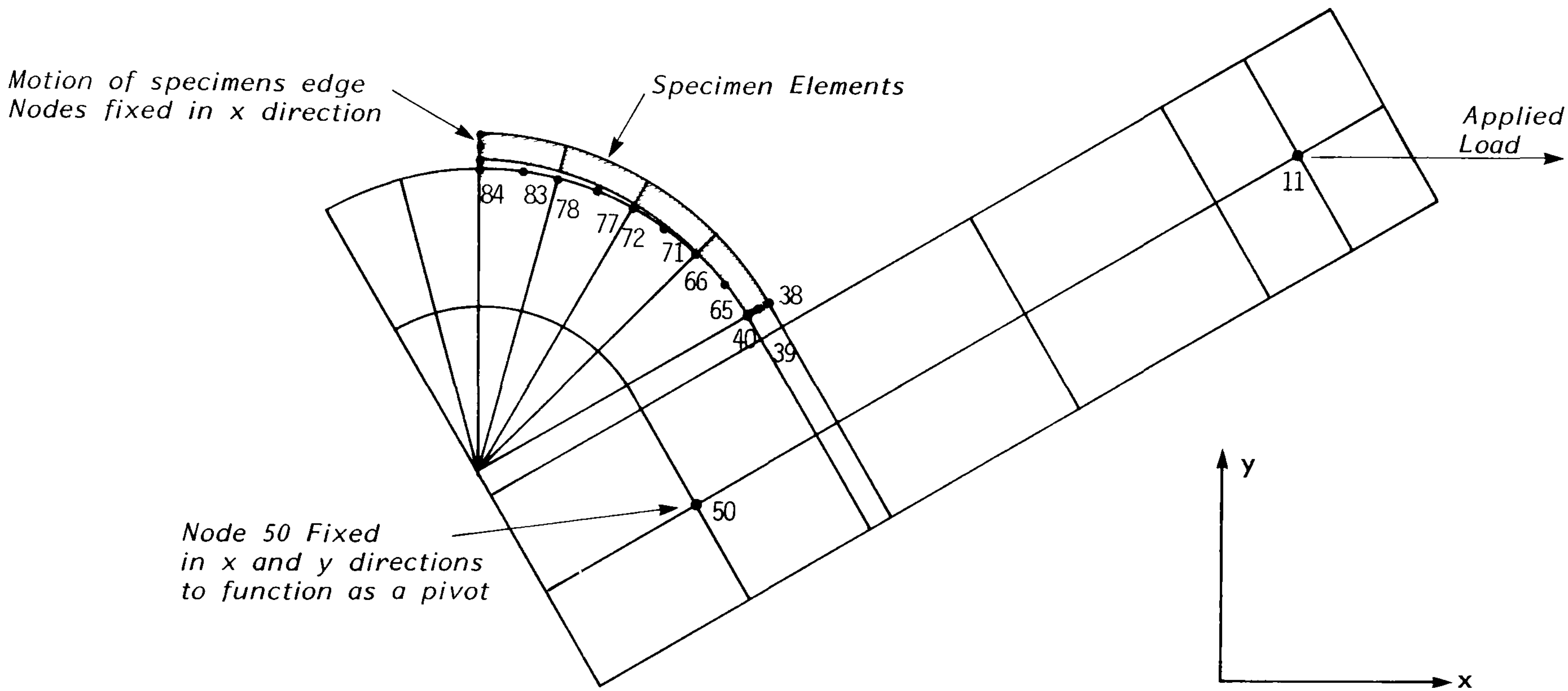

FIGURE 20

MESH USED IN TWO-DIMENSIONAL FINITE ELEMENT ANALYSIS OF BEHAVIOUR OF SPECIMEN AND GRIPS UNDER LOAD. ONE HALF OF THE SPECIMEN AND ONE HALF OF THE GRIPS ARE MODELLED

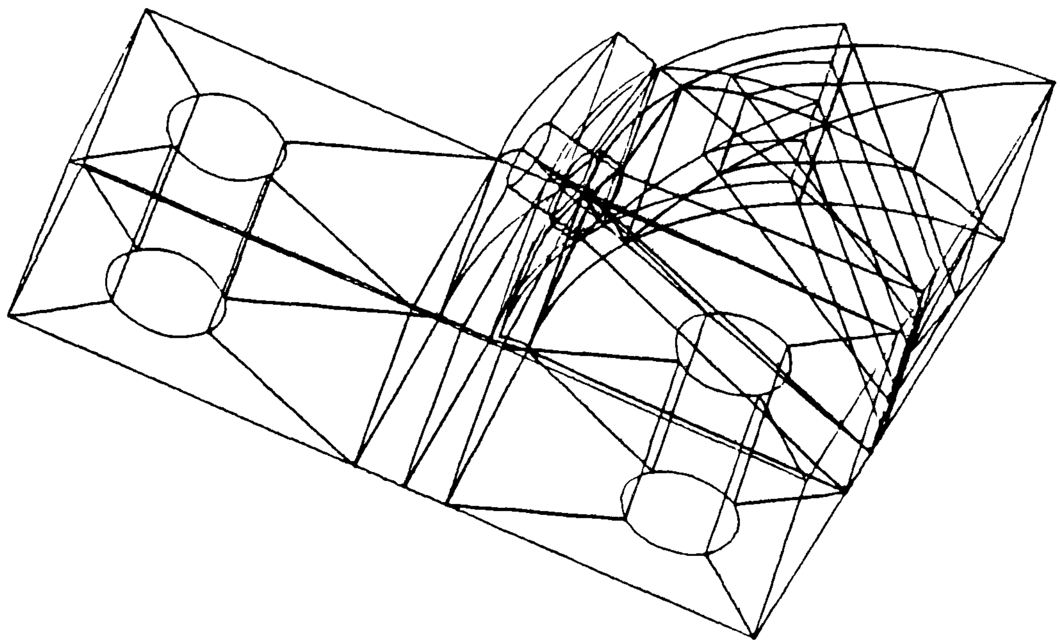

FIGURE 21

MESH USED FOR UNSUCCESSFUL ATTEMPT AT MODELLING SPECIMEN AND GRIPS IN 3 DIMENSIONS

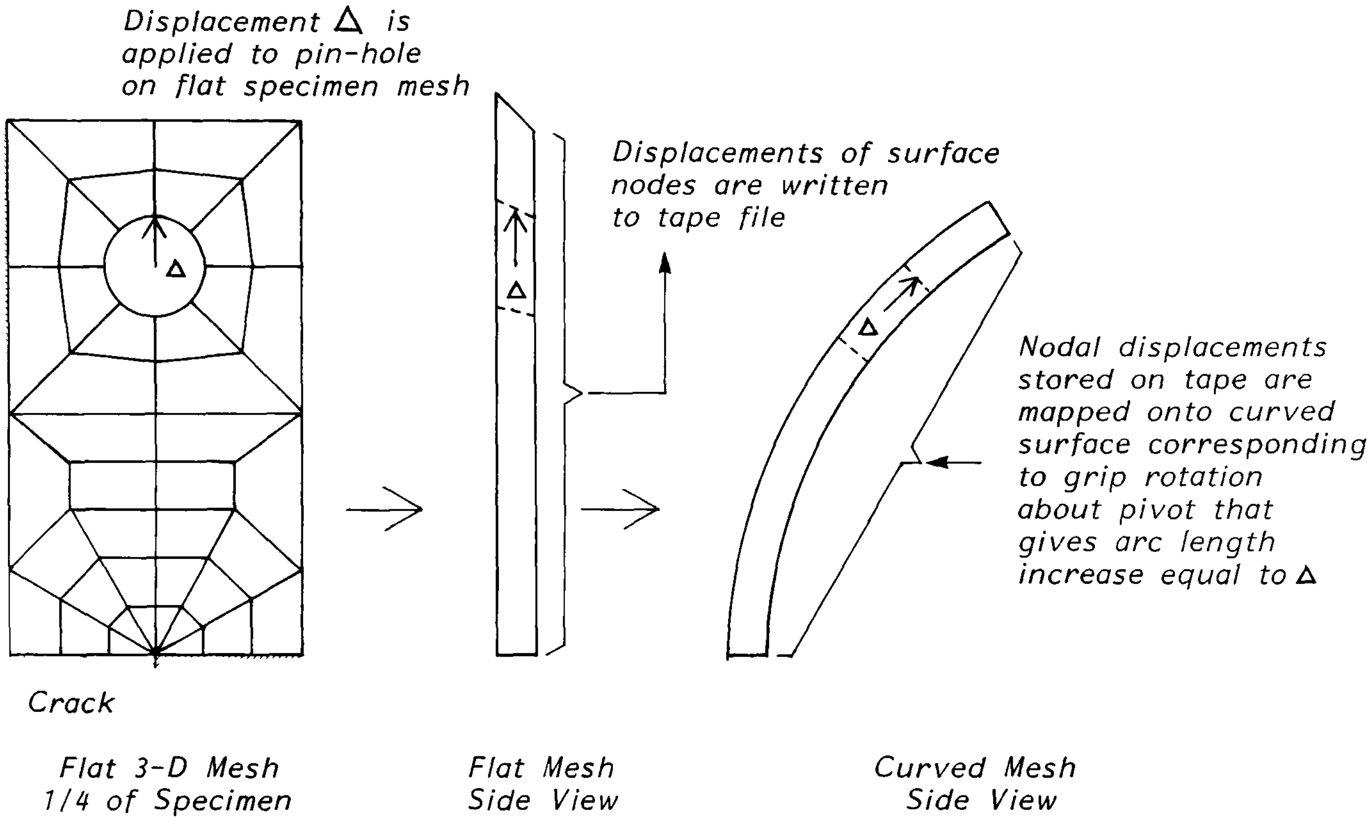

FIGURE 22

ILLUSTRATION OF MAPPING OF FLAT SPECIMEN MESH ONTO CURVED GEOMETRY AND TRANSFER OF INSIDE SURFACE NODAL DISPLACEMENTS BETWEEN GEOMETRIES

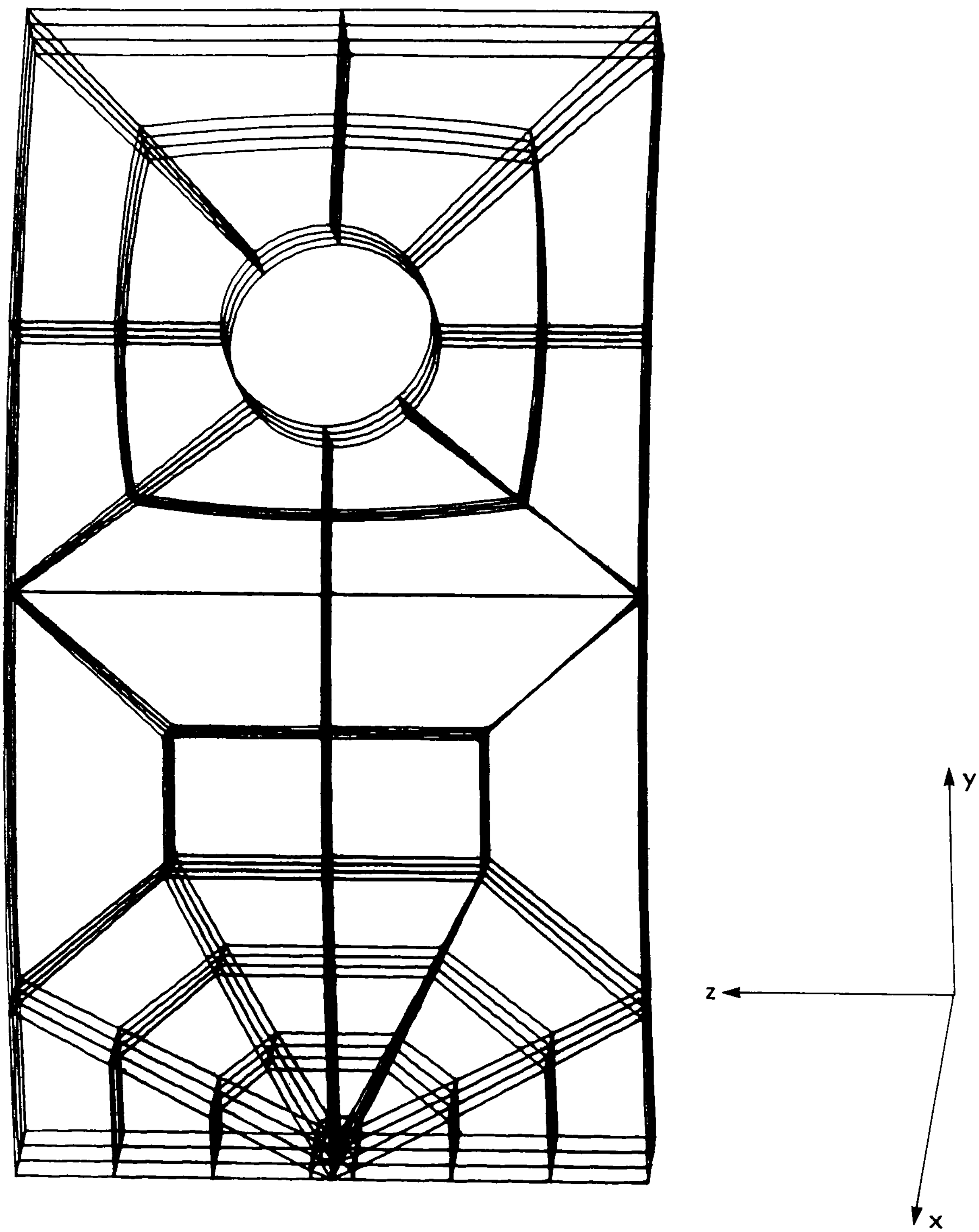

FIGURE 23

3-DIMENSIONAL, NON-HIDDEN LINE PLOT OF CURVED SPECIMEN MESH USED IN ANALYSIS

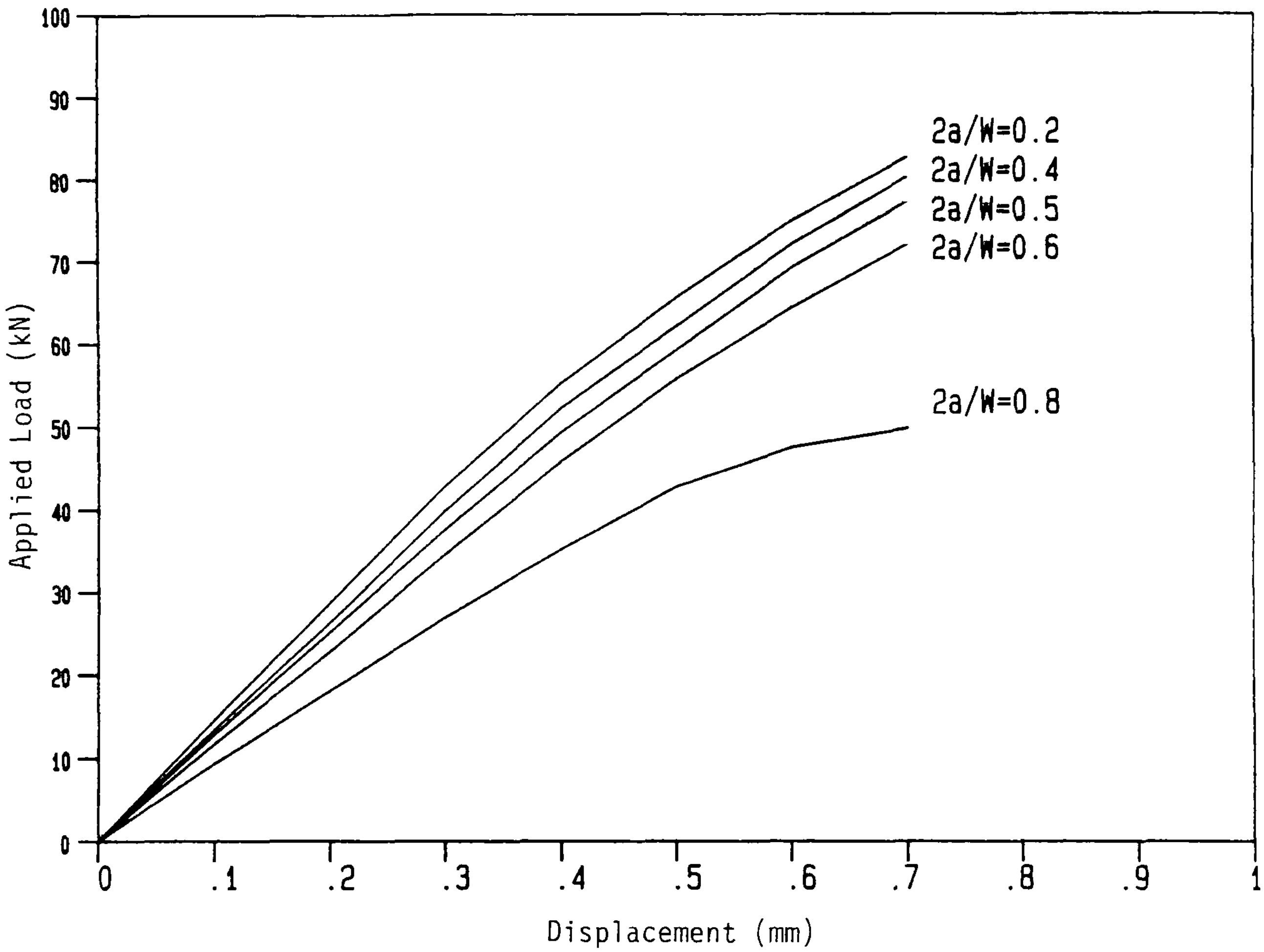

FIGURE 24

FINITE ELEMENT PREDICTIONS OF LOAD VERSUS DISPLACEMENT MEASURED ALONG THE CURVED SPECIMEN INSIDE SURFACE

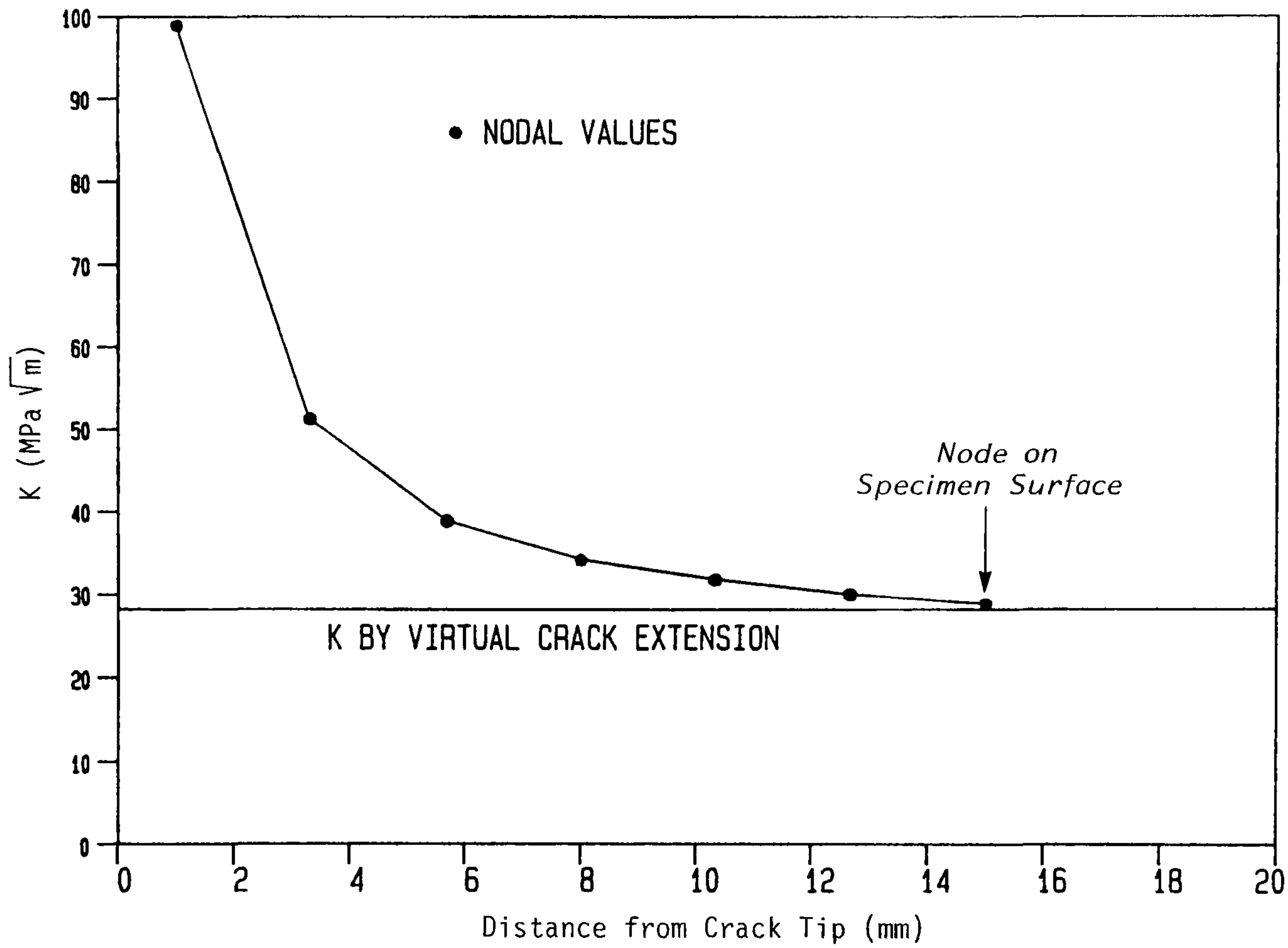

FIGURE 25

VERIFICATION OF FINITE ELEMENT K CALCULATIONS
BY EXTRAPOLATION OF NODAL K VALUES
(DATA FROM 2a/W = 0.5, INCREMENT 2)

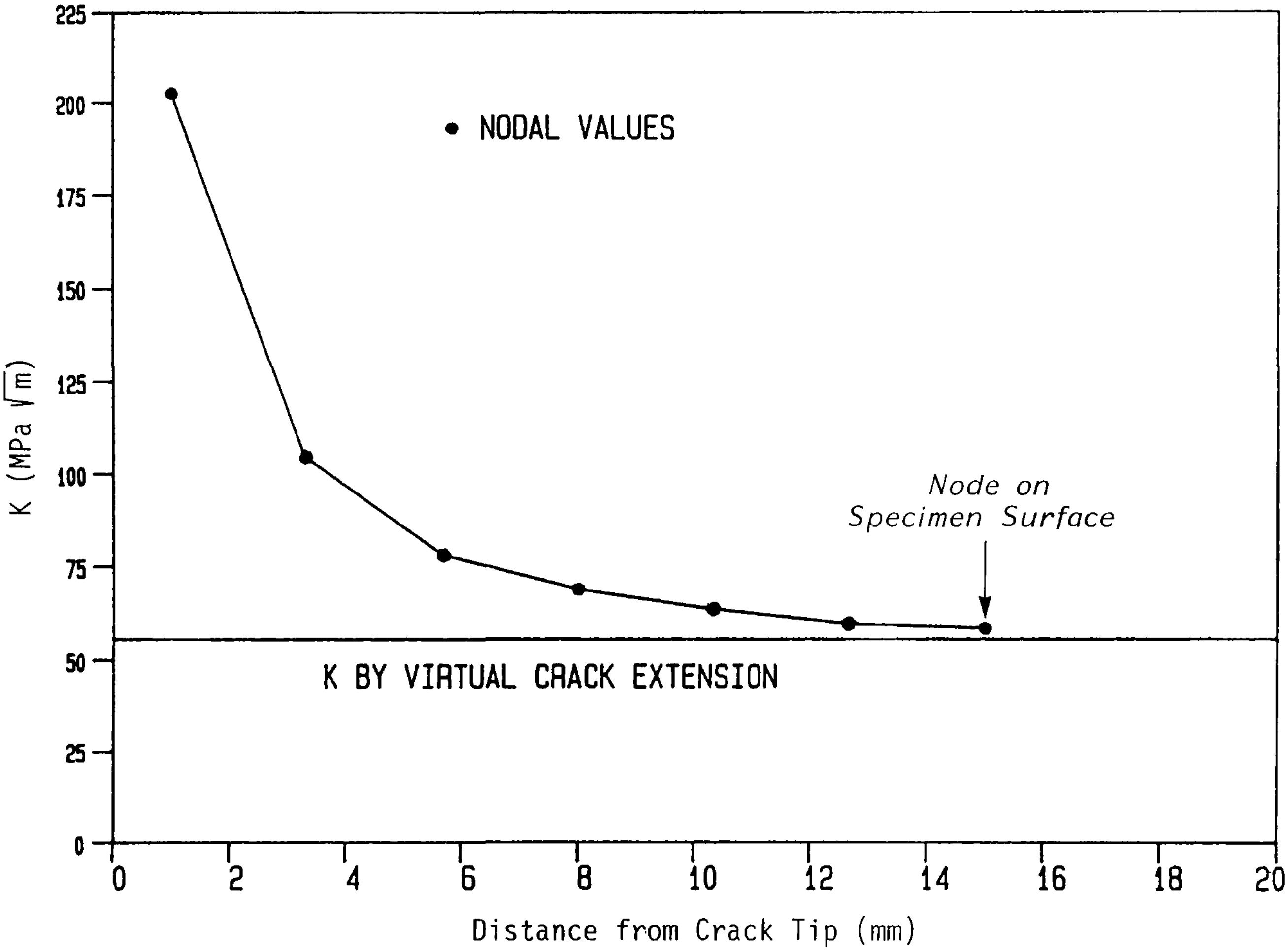

FIGURE 26

VERIFICATION OF FINITE ELEMENT K CALCULATIONS
BY EXTRAPOLATION OF NODAL K VALUES
(DATA FROM 2a/W = 0.5, INCREMENT 4)

172538 RD

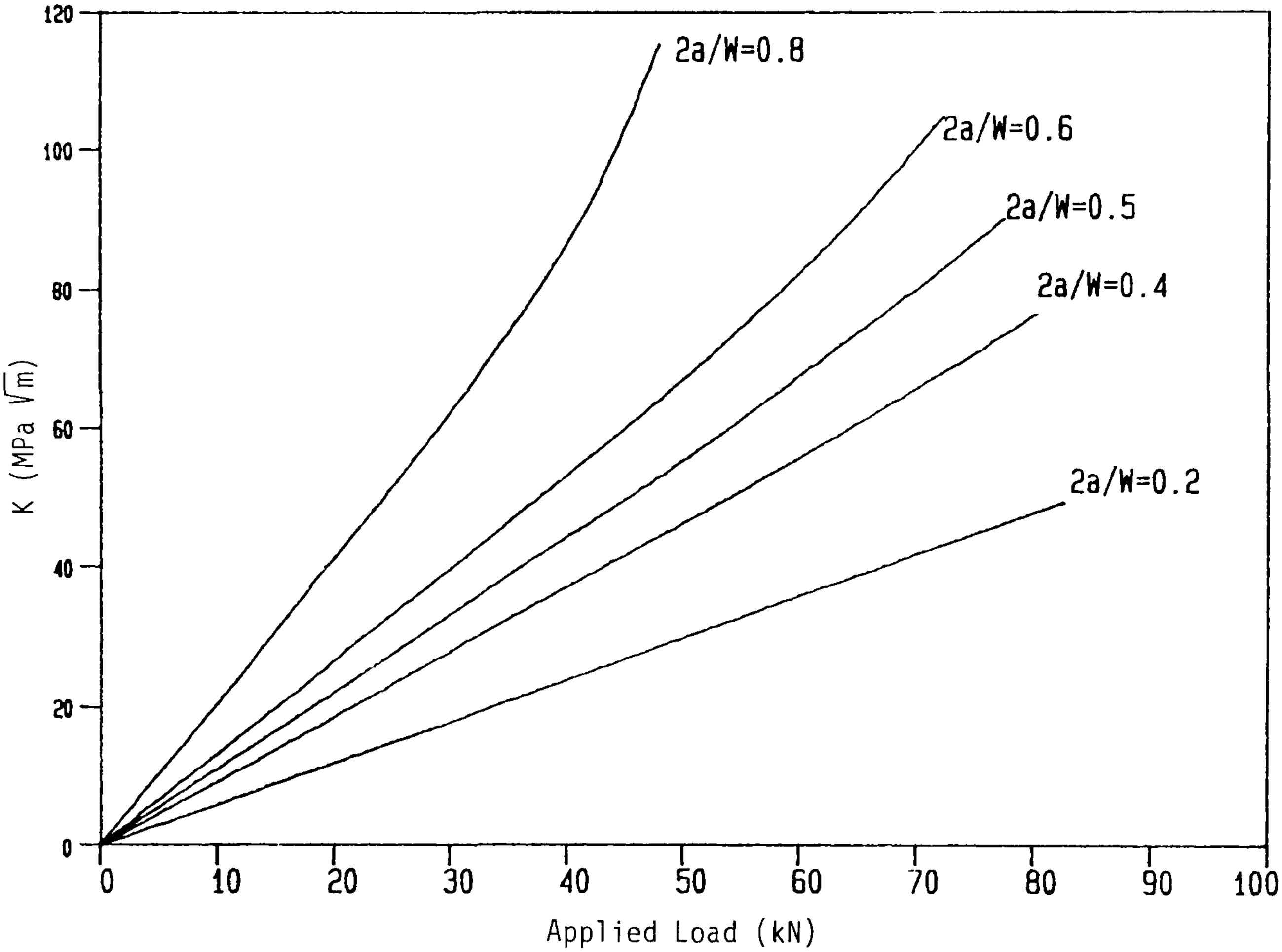

FIGURE 27

FINITE ELEMENT PREDICTIONS OF K VERSUS APPLIED LOAD FOR DIFFERENT CRACK LENGTH RATIOS (2a/W)

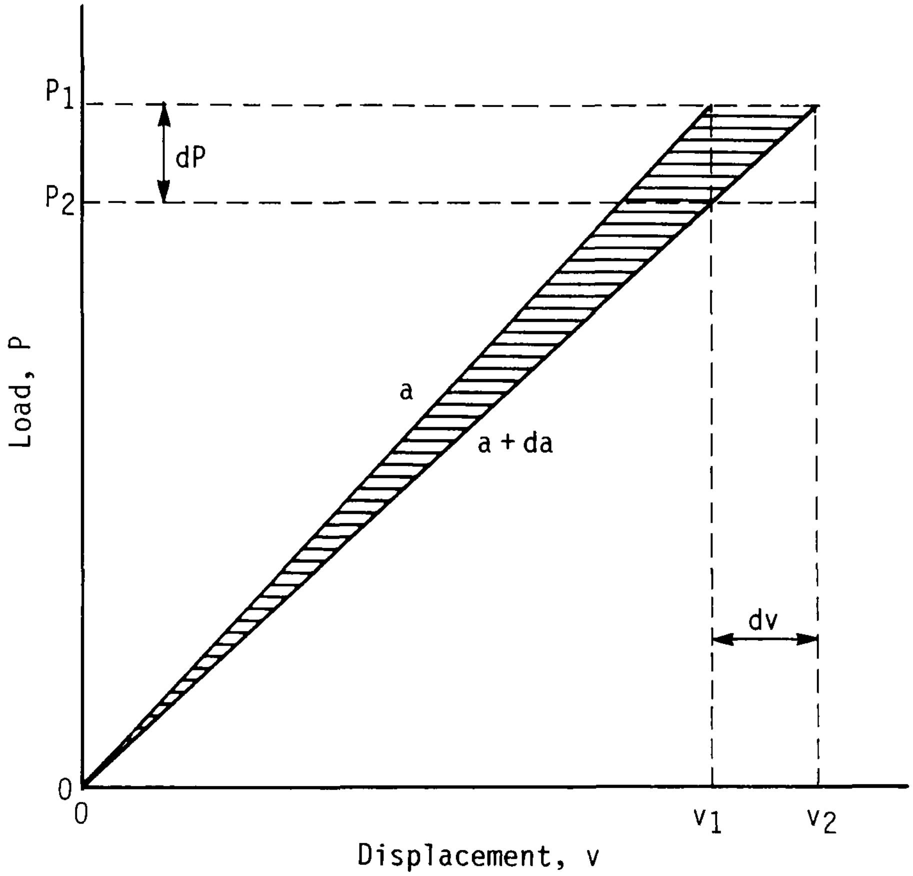

FIGURE 28

ELASTIC LOADING CURVES
FOR CRACK LENGTHS a AND a+da

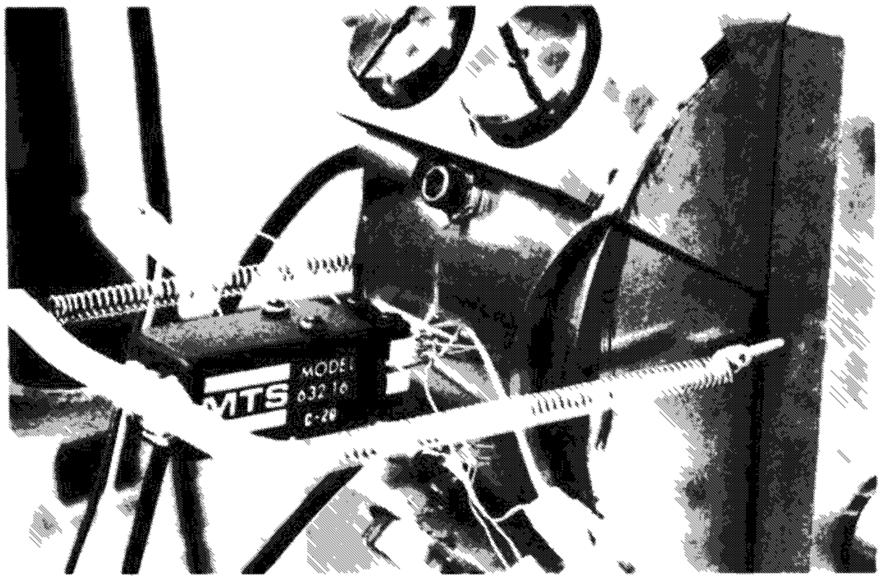

FIGURE 29

VIEW OF EXTENSOMETER USED FOR DISPLACEMENT MEASUREMENTS, (THE SPECIMEN SHOWN DIFFERS FROM THOSE USED IN THE COMPLIANCE CALIBRATIONS)

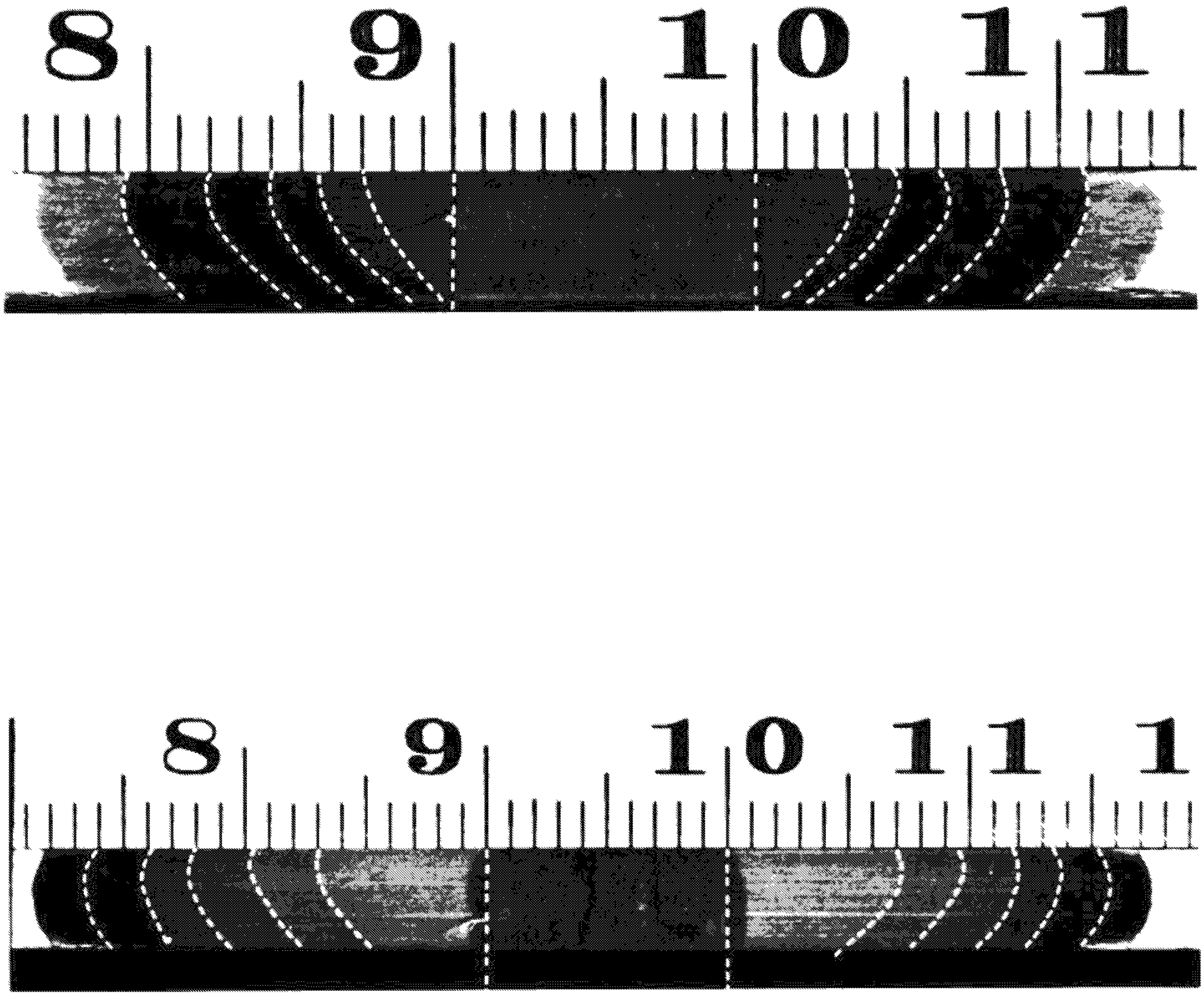

FIGURE 30

FRACTURE SURFACES OF TWO OF THE CALIBRATION SPECIMENS SHOWING TENDENCY FOR SKEWED CRACK FRONTS AT SHORTER CRACK LENGTHS. THE SCALE IS IN cm AND IS ADJACENT TO THE SPECIMEN INSIDE SURFACE. CRACK FRONTS AT EACH HEAT TINT BAND HAVE BEEN HIGHLIGHTED FOR BETTER VISIBILITY.

172810 RD

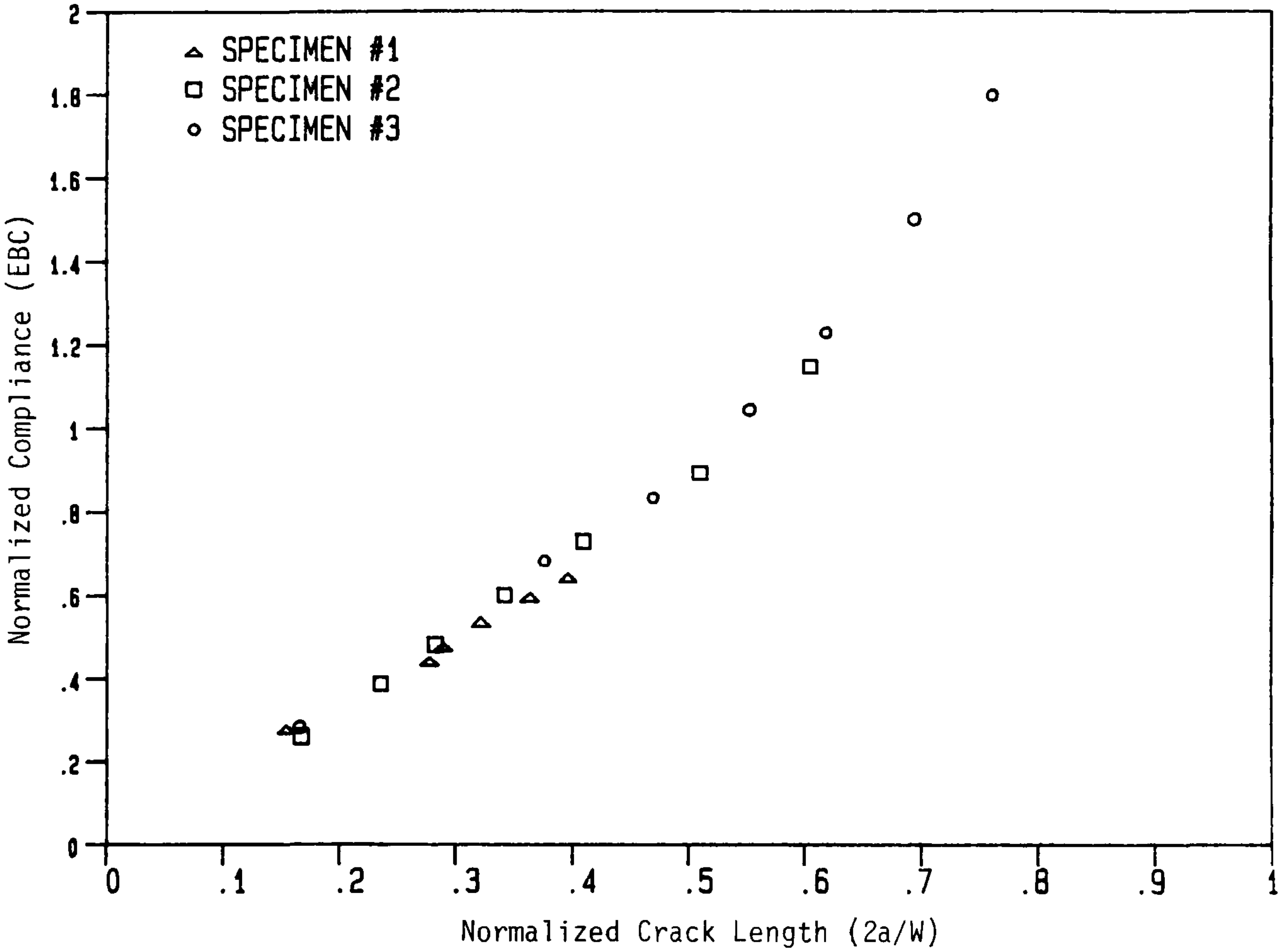

FIGURE 31
COMPLIANCE DATA FROM 3 TEST SPECIMENS

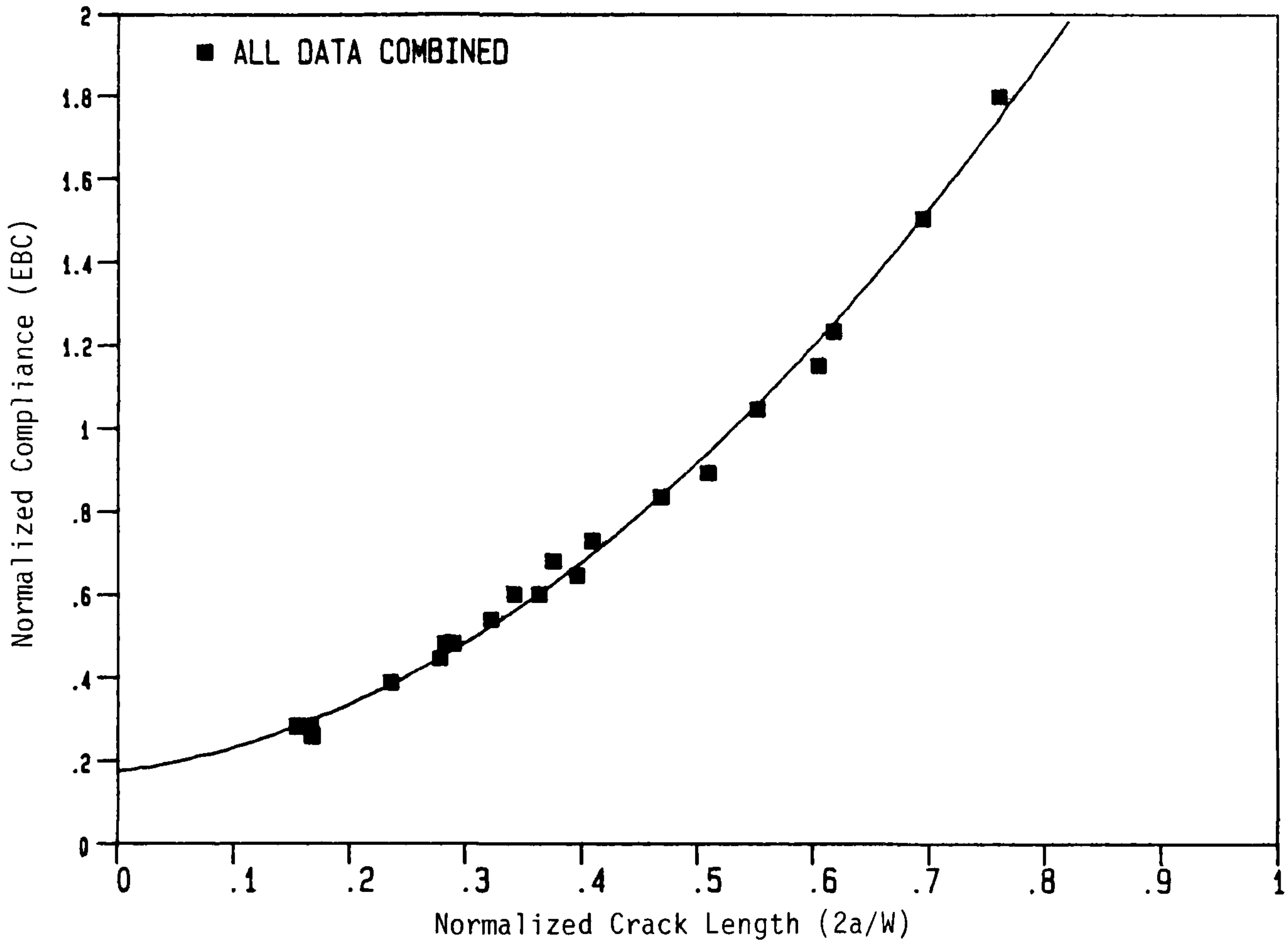

FIGURE 32

CURVE REPRESENTING SECOND DEGREE POLYNOMIAL FIT TO COMPLIANCE DATA FROM 3 SPECIMENS IN FIGURE 31

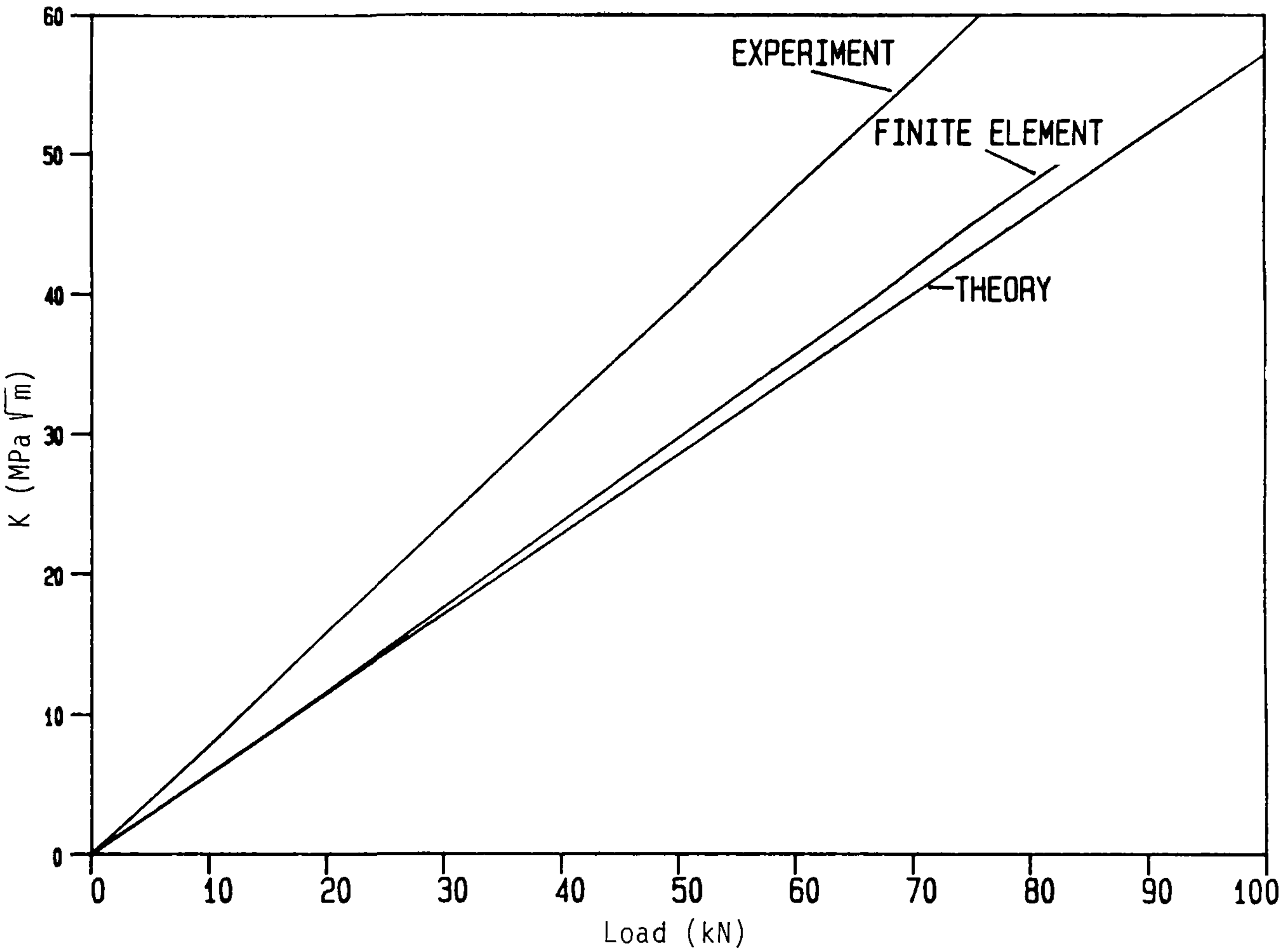

FIGURE 33

COMPARISON OF K VALUES OBTAINED FROM EXPERIMENTAL COMPLIANCE, FINITE ELEMENT ANALYSIS AND THEORETICAL FLATE PLATE EQUATION FOR 2a/W=0.2

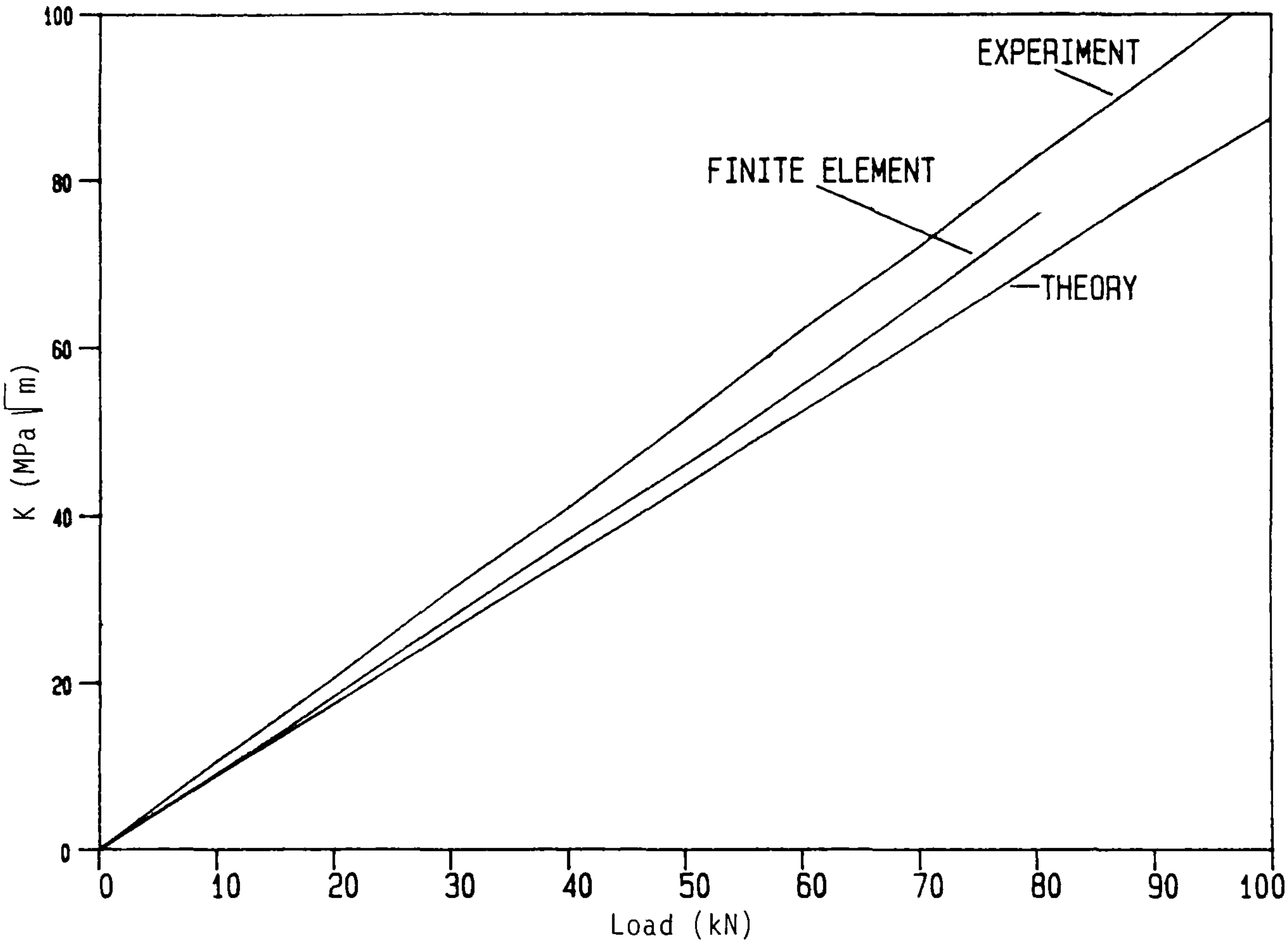

FIGURE 34

COMPARISON OF K VALUES OBTAINED FROM EXPERIMENTAL COMPLIANCE, FINITE ELEMENT ANALYSIS AND THEORETICAL FLAT PLATE EQUATION FOR 2a/W = 0.4

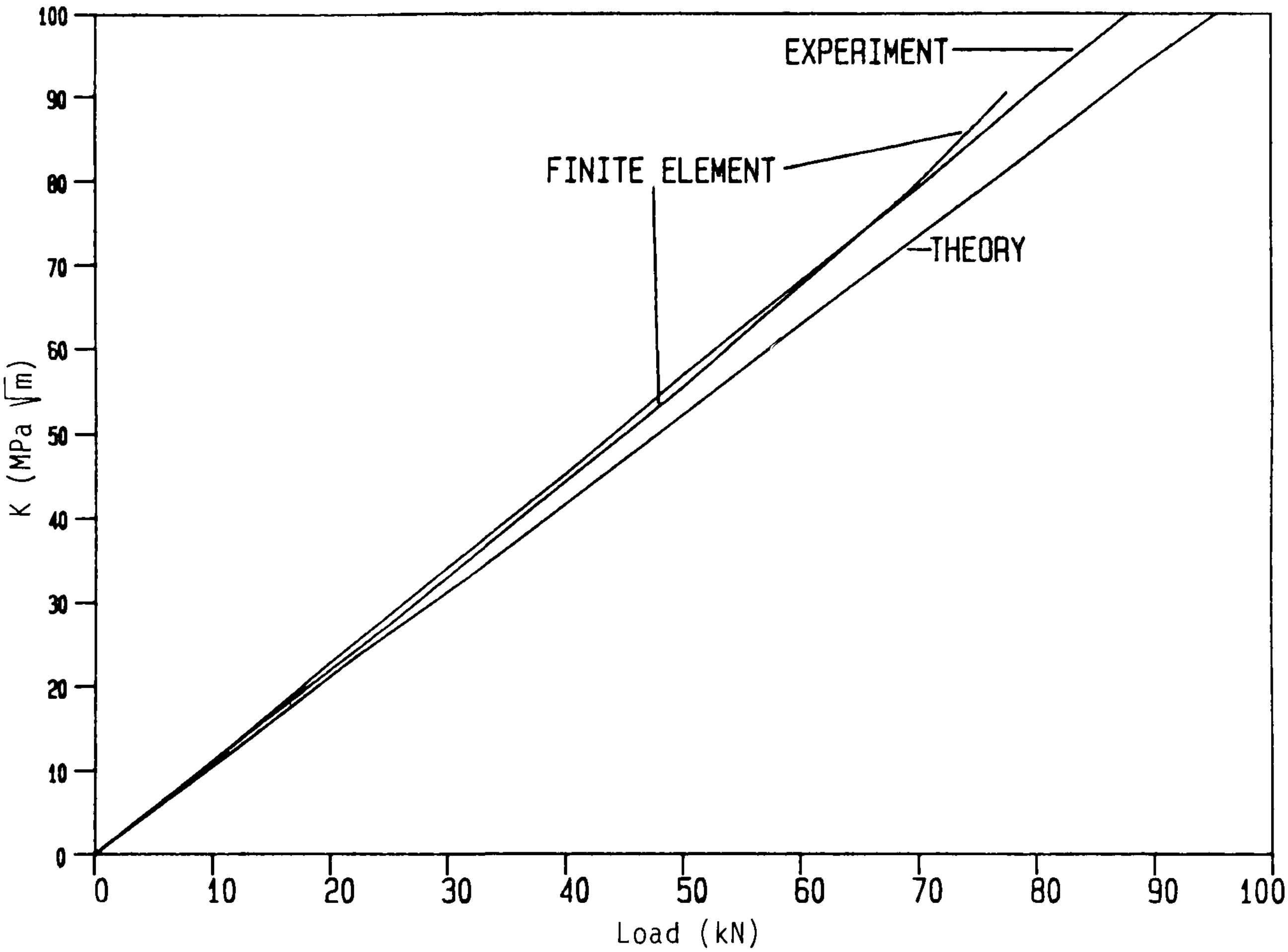

FIGURE 35

COMPARISON OF K VALUES OBTAINED FROM EXCPERIMENTAL COMPLIANCE, FINITE ELEMENT ANALYSIS AND THEORETICAL FLAT PLATE EQUATION FOR 2a/W = 0.5

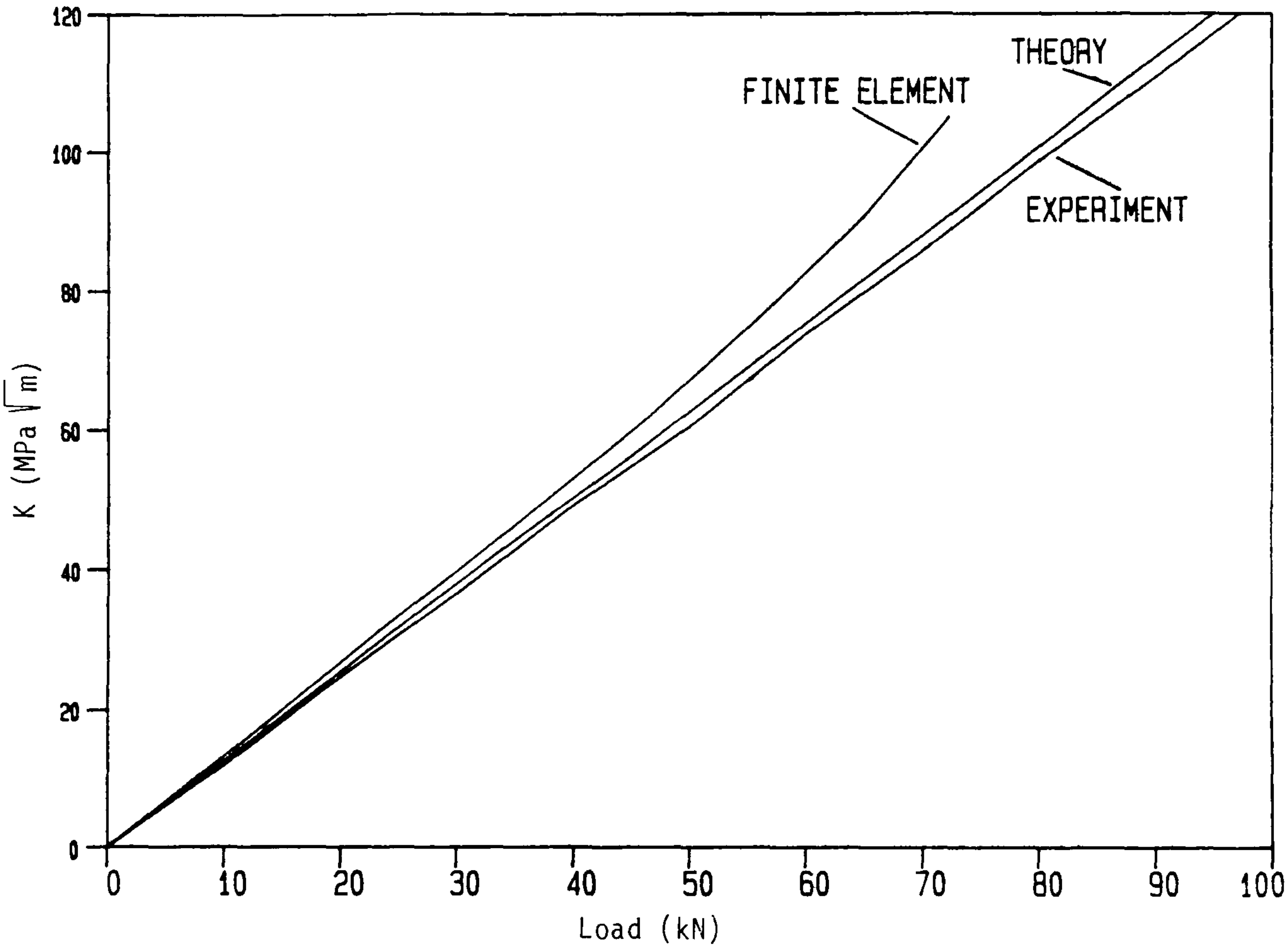

FIGURE 36

COMPARISON OF K VALUES OBTAINED FROM EXPERIMENTAL COMPLIANCE, FINITE ELEMENT ANALYSIS AND THEORETICAL FLAT PLATE EQUATION FOR 2a/W = 0.6

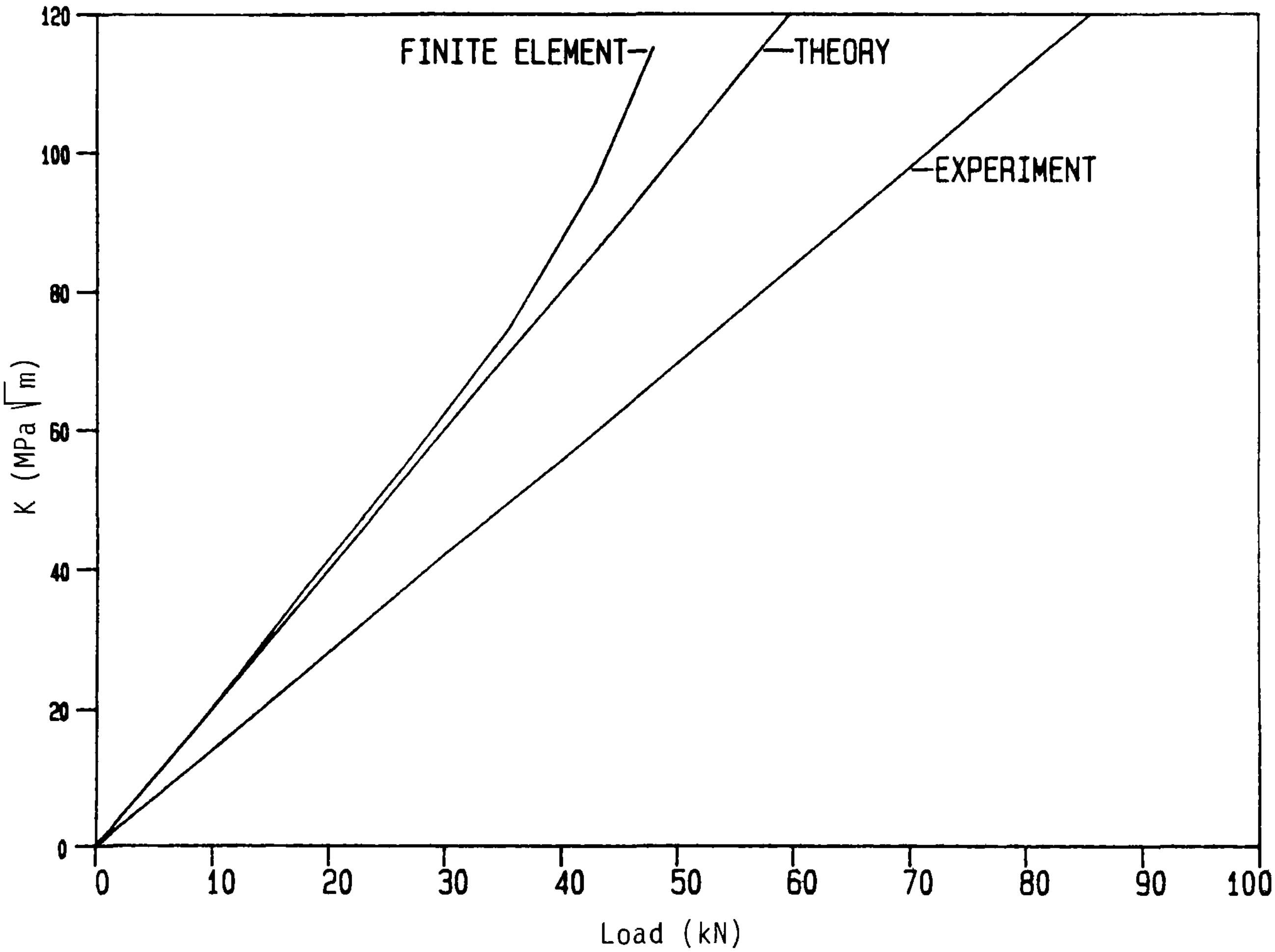

FIGURE 37

COMPARISON OF K VALUES OBTAINED FROM EXPERIMENTAL COMPLIANCE, FINITE ELEMENT ANALYSUS AND THEORETICAL FLAT PLATE EQUATION FOR 2a/W = 0.8

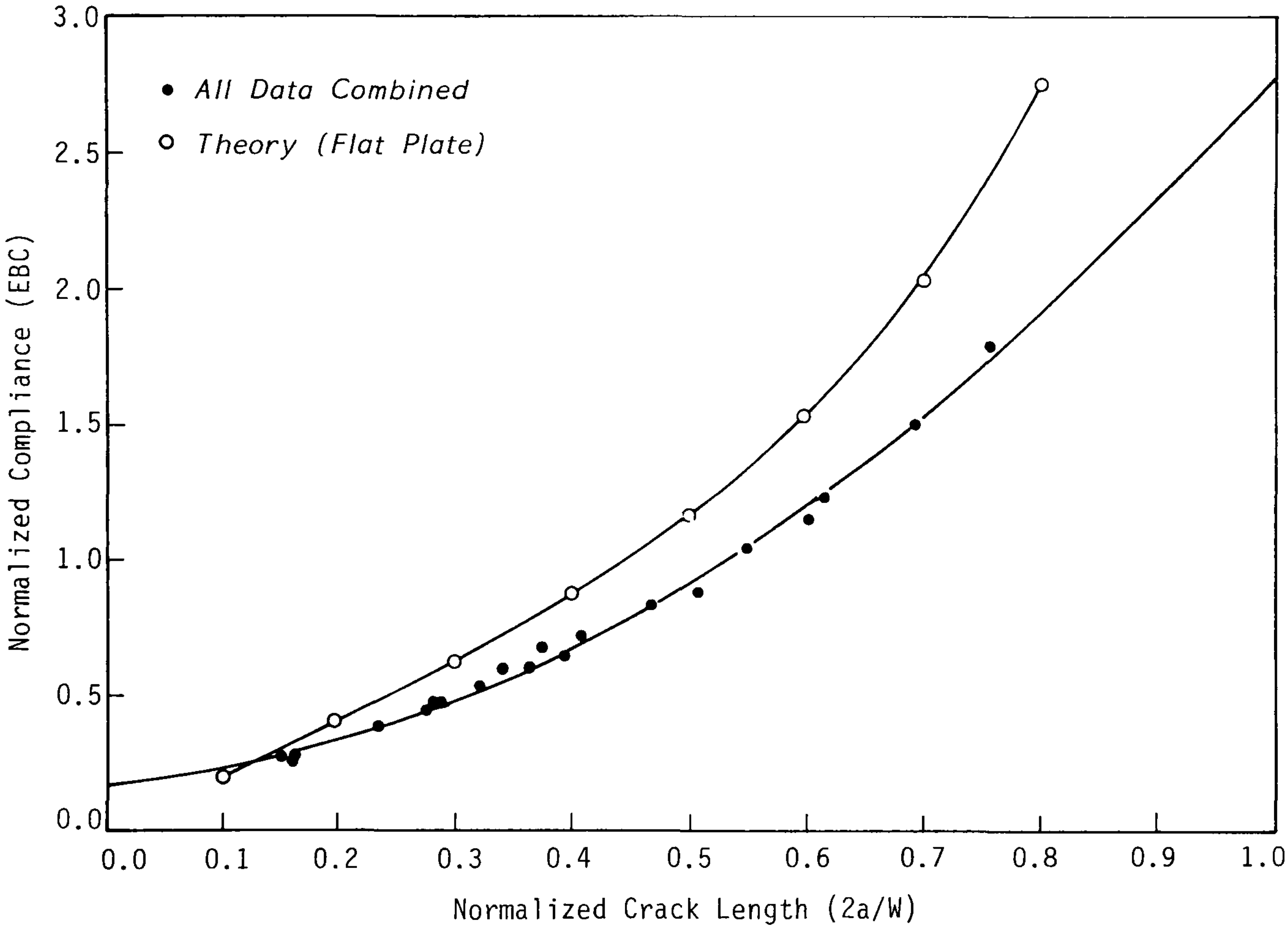

FIGURE 38

COMPARISON OF EXPERIMENTAL COMPLIANCE DATA WITH A THEORETICAL COMPLIANCE RELATION FOR A FLAT PLATE

APPENDIX A

Program CSMESH

Listing of input coding to MARC-MESH3D-CDC Revision K.1-1 to generate a 3D flat specimen mesh with 2a/W = 0.5.

Meshes for different values of 2a/W were generated by altering the coordinates of points 33-47 and 80-94 on pages 1, 2 and 3 of the input listing.

Figures A.1 to A.5 show 3D hidden line plots of the meshes generated in this way for ratios of 2a/W of 0.2, 0.4, 0.5, 0.6 and 0.8.

Listings of element connectivity and nodal coordinates are omitted for brevity.

Note: In order to simplify the later transformation to a curved geometry, the x-coordinate of thee meshes were generated in degrees. These coordinates were later transformed into millimeters via subroutines in the analyses programs.

M A R C - C D C

C A R D   I N P U T   D A T A

P A G E   1

```
                5   10   15   20   25   30   35   40   45   50   55   60   65   70   75   80
           ------------------------------------------------------------------------------------
                 30000
                2   20         1                   94
             1000  200
              150   20
CARD   5   POINT
                1        60.            51.45       -15.
                2        43.3           51.45       -15.
                3        30.            51.45       -15.
                4         9.            51.45       -15.
CARD  10        5         0.            51.45       -15.
                6        23.            51.45        -7.5
                7        16.            51.45        -7.5
                8        60.            51.45         0.
                9        48.9           51.45         0.
CARD  15       10        48.4           51.45        -1.9
               11        47.2           51.45        -3.5
               12        45.4           51.45        -4.6
               13        43.3           51.45        -5.0
               14        41.2           51.45        -4.6
CARD  20       15        39.4           51.45        -3.5
               16        38.2           51.45        -1.9
               17        37.8           51.45         0.
               18        30.            51.45         0.
               19        48.4           51.45         1.9
CARD  25       20        47.2           51.45         3.5
               21        45.4           51.45         4.6
               22        43.3           51.45         5.
               23        41.2           51.45         4.6
               24        39.4           51.45         3.5
CARD  30       25        38.2           51.45         1.9
               26        60.            51.45       15.
               27        43.3           51.45       15.
               28        30.            51.45       15.
               29         9.            51.45       15.
CARD  35       30         0.            51.45       15.
               31        23.            51.45         7.5
               32        16.            51.45         7.5
               33         0.            51.45       -1.
               34         0.5           51.45       -1.
CARD  40       35         1.0           51.45       -0.5
               36         1.0           51.45        0.
               37         1.0           51.45        0.5
               38         0.5           51.45        1.0
               39         0.            51.45        1.
CARD  45       40         0.            51.45        0.
           ------------------------------------------------------------------------------------
                5   10   15   20   25   30   35   40   45   50   55   60   65   70   75   80
```

```
       5   10   15   20   25   30   35   40   45   50   55   60   65   70   75   80
------------------------------------------------------------------------------------
```

	41	0.	51.45	-0.25
	42	0.125	51.45	-0.25
	43	0.25	51.45	-0.125
	44	0.25	51.45	0.0
CARD 50	45	0.25	51.45	0.125
	46	0.125	51.45	0.25
	47	0.	51.45	0.25
	48	60.	55.55	-15.
	49	43.3	55.55	-15.
CARD 55	50	30.	55.55	-15.
	51	9.	55.55	-15.
	52	0.	55.55	-15.
	53	23.	55.55	-7.5
	54	16.	55.55	-7.5
CARD 60	55	60.	55.55	0.
	56	48.4	55.55	0.
	57	48.	55.55	-1.9
	58	46.9	55.55	-3.5
	59	45.3	55.55	-4.6
CARD 65	60	43.3	55.55	-5.0
	61	41.3	55.55	-4.6
	62	39.7	55.55	-3.5
	63	38.6	55.55	-1.9
	64	38.2	55.55	0.
CARD 70	65	30.	55.55	0.
	66	48.0	55.55	1.9
	67	46.9	55.55	3.5
	68	45.3	55.55	4.6
	69	43.3	55.55	5.0
CARD 75	70	41.3	55.55	4.6
	71	39.7	55.55	3.5
	72	38.6	55.55	1.9
	73	60.	55.55	15.
	74	43.3	55.55	15.
CARD 80	75	30.	55.55	15.
	76	9.	55.55	15.
	77	0.	55.55	15.
	78	23.	55.55	7.5
	79	16.	55.55	7.5
CARD 85	80	0.	55.55	-1.0
	81	0.5	55.55	-1.0
	82	1.0	55.55	-0.5
	83	1.	55.55	0.
	84	1.	55.55	0.5
CARD 90	85	0.5	55.55	1.
	86	0.	55.55	1.
	87	0.	55.55	0.
	88	0.	55.55	-0.25
	89	0.125	55.55	-0.25
CARD 95	90	0.25	55.55	-0.125

```
------------------------------------------------------------------------------------
       5   10   15   20   25   30   35   40   45   50   55   60   65   70   75   80
```

```
                 5   10   15   20   25   30   35   40   45   50   55   60   65   70   75   80
               ---------------------------------------------------------------------------------
                91         0.25          55.55          0.
                92         0.25          55.55          0.125
                93         0.125         55.55          0.25
                94         0.0           55.55          0.25
CARD  100      DEFINE   BLK1
                 1   0    0   21    3    2    3    1   12    0    0
               MAP      BLK1
                 0   10
                 1    8
CARD  105        2    9
                 3   56
                 4   55
                 5    1
                 6   11
CARD  110        7   58
                 8   48
                18   10
                19   57
               DEFINE   BLK2
CARD  115        2    0   0   21    3    2    3    1   12    0    2
               MAP      BLK2
                 0   10
                 1    1
                 2   11
CARD  120        3   58
                 4   48
                 5    2
                 6   13
                 7   60
CARD  125        8   49
                18   12
                19   59
               MERGE
                 1    2
CARD  130      DEFINE   BLK3
                 2    0   0   21    3    2    3    1   12    0    4
               MAP      BLK3
                 0   10
                 1    2
CARD  135        2   13
                 3   60
                 4   49
                 5    3
                 6   15
CARD  140        7   62
                 8   50
                18   14
                19   61
               MERGE
CARD  145        1    2
               ---------------------------------------------------------------------------------
                 5   10   15   20   25   30   35   40   45   50   55   60   65   70   75   80
```

```
         5    10   15   20   25   30   35   40   45   50   55   60   65   70   75   80
    --------------------------------------------------------------------------------
    DEFINE   BLK4
         2    0    0   21    3    2    3    1   12    0    6
    MAP      BLK4
         0   10
         1    3
         2   15
         3   62
         4   50
         5   18
         6   17
         7   64
         8   65
        18   16
        19   63
    MERGE
         1    2
    DEFINE   BLK5
         2    0    0   21    3    2    3    1   12    0    8
    MAP      BLK5
         0   10
         1   18
         2   17
         3   64
         4   65
         5   28
         6   24
         7   71
         8   75
        18   25
        19   72
    MERGE
         1    2
    DEFINE   BLK6
         2    0    0   21    3    2    3    1   12    0   10
    MAP      BLK6
         0   10
         1   28
         2   24
         3   71
         4   75
         5   27
         6   22
         7   69
         8   74
        18   23
        19   70
    MERGE
         1    2
    DEFINE   BLK7
         2    0    0   21    3    2    3    1   12    0   12
    --------------------------------------------------------------------------------
         5    10   15   20   25   30   35   40   45   50   55   60   65   70   75   80
```

```
                     5   10   15   20   25   30   35   40   45   50   55   60   65   70   75   80
                 ----------------------------------------------------------------------------------
                 MAP      BLK7
                     0   10
                     1   27
                     2   22
CARD  200            3   69
                     4   74
                     5   26
                     6   20
                     7   67
CARD  205            8   73
                    18   21
                    19   68
                 MERGE
                     1    2
CARD  210        DEFINE   BLK8
                     2    0    0   21    3    2    3    1   12    0   14
                 MAP      BLK8
                     0   10
                     1   26
CARD  215            2   20
                     3   67
                     4   73
                     5    8
                     6    9
CARD  220            7   56
                     8   55
                    18   19
                    19   66
                 MERGE
CARD  225            1    2
                 DEFINE   BLK9
                     2    0    0   21    3    1    3    2   10    0    6
                 MAP      BLK9
                     0   10
CARD  230            1    6
                     2    3
                     3   50
                     4   53
                     5   31
CARD  235            6   28
                     7   75
                     8   78
                    18   18
                    19   65
CARD  240        MERGE
                     1    2
                 DEFINE   BLK10
                     2    0    0   21    3    1    3    2    8    0    6
                 MAP      BLK10
CARD  245            0    8
                 ----------------------------------------------------------------------------------
                     5   10   15   20   25   30   35   40   45   50   55   60   65   70   75   80
```

```
                     5    10   15   20   25   30   35   40   45   50   55   60   65   70   75   80
                 ----------------------------------------------------------------------------------
                     1    7
                     2    6
                     3   53
                     4   54
CARD  250            5   32
                     6   31
                     7   78
                     8   79
                 MERGE
CARD  255            1    2
                 DEFINE   BLK11
                     2    0    0   21    3    1    3    1    8    0    4
                 MAP      BLK11
                     0    8
CARD  260            1    4
                     2    3
                     3   50
                     4   51
                     5    7
CARD  265            6    6
                     7   53
                     8   54
                 MERGE
                     1    2
CARD  270        DEFINE   BLK12
                     2    0    0   21    3    1    3    1    8    0   10
                 MAP      BLK12
                     0    8
                     1   32
CARD  275            2   31
                     3   78
                     4   79
                     5   29
                     6   28
CARD  280            7   75
                     8   76
                 MERGE
                     1    2
                 DEFINE   BLK13
CARD  285            2    0    0   21    3    3    3    1    2    0    2
                 MAP      BLK13
                     0    8
                     1   33
                     2    5
CARD  290            3   52
                     4   80
                     5   34
                     6    4
                     7   51
CARD  295            8   81
                 ----------------------------------------------------------------------------------
                     5    10   15   20   25   30   35   40   45   50   55   60   65   70   75   80
```

```
    5   10   15   20   25   30   35   40   45   50   55   60   65   70   75   80
--------------------------------------------------------------------------------
MERGE
    1    2
DEFINE   BLK14
    2    0    0   21    3    3    3    1    2    0    4
MAP      BLK14
    0    8
    1   34
    2    4
    3   51
    4   81
    5   35
    6    7
    7   54
    8   82
MERGE
    1    2
DEFINE     BLK15
    2    0    0   21    3    3    3    2    2    0    6
MAP      BLK15
    0   10
    1   35
    2    7
    3   54
    4   82
    5   37
    6   32
    7   79
    8   84
   17   36
   20   83
MERGE
    1    2
DEFINE   BLK16
    2    0    0   21    3    3    3    1    2    0   10
MAP      BLK16
    0    8
    1   37
    2   32
    3   79
    4   84
    5   38
    6   29
    7   76
    8   85
MERGE
    1    2
DEFINE   BLK17
    2    0    0   21    3    3    3    1    2    0   12
MAP      BLK17
    0    8
--------------------------------------------------------------------------------
    5   10   15   20   25   30   35   40   45   50   55   60   65   70   75   80
```

```
         5    10   15   20   25   30   35   40   45   50   55   60   65   70   75   80
    --------------------------------------------------------------------------------
         1    38
         2    29
         3    76
         4    85
         5    39
         6    30
         7    77
         8    86
    MERGE
         1     2
    DEFINE     BLK18
         2     0    0   21    3    1    3    1    0    0    2
    MAP        BLK18
         0    14
         1    40
         2    33
         3    80
         4    87
         5    40
         6    34
         7    81
         8    87
         9    41
        11    88
        13    42
        15    89
        17    40
        20    87
    MERGE
         1     2
    DEFINE     BLK19
         2     0    0   21    3    1    3    1    0    0    4
    MAP        BLK19
         0    14
         1    40
         2    34
         3    81
         4    87
         5    40
         6    35
         7    82
         8    87
         9    42
        11    89
        13    43
        15    90
        17    40
        20    87
    MERGE
         1     2
    --------------------------------------------------------------------------------
         5    10   15   20   25   30   35   40   45   50   55   60   65   70   75   80
```

```
        5   10   15   20   25   30   35   40   45   50   55   60   65   70   75   80
-----------------------------------------------------------------------------------
DEFINE     BLK20
        2    0    0   21    3    1    3    1    0    0    6
MAP        BLK20
        0   14
        1   40
        2   35
        3   82
        4   87
        5   40
        6   36
        7   83
        8   87
        9   43
       11   90
       13   44
       15   91
       17   40
       20   87
MERGE
        1    2
DEFINE     BLK21
        2    0    0   21    3    1    3    1    0    0    8
MAP        BLK21
        0   14
        1   40
        2   36
        3   83
        4   87
        5   40
        6   37
        7   84
        8   87
        9   44
       11   91
       13   45
       15   92
       17   40
       20   87
MERGE
        1    2
DEFINE     BLK22
        2    0    0   21    3    1    3    1    0    0   10
MAP        BLK22
        0   14
        1   40
        2   37
        3   84
        4   87
        5   40
        6   38
-----------------------------------------------------------------------------------
        5   10   15   20   25   30   35   40   45   50   55   60   65   70   75   80
```

```
                5   10   15   20   25   30   35   40   45   50   55   60   65   70   75   80
           ---------------------------------------------------------------------------------
                7   85
                8   87
                9   45
               11   92
CARD 450       13   46
               15   93
               17   40
               20   87
           MERGE
CARD 455        1    2
           DEFINE    BLK23
                2    0    0   21    3    1    3    1    0    0   12
           MAP       BLK23
                0   14
CARD 460        1   40
                2   38
                3   85
                4   87
                5   40
CARD 465        6   39
                7   86
                8   87
                9   46
               11   93
CARD 470       13   47
               15   94
               17   40
               20   87
           MERGE
CARD 475        1    2
           JOIN
                1  117    1
               12    0    0   12    0   16
               12    1    0   12    1   16
CARD 480       12    2    0   12    2   16
               12    3    0   12    3   16
               12    4    0   12    4   16
               12    5    0   12    5   16
               12    6    0   12    6   16
CARD 485       13    0    0   13    0   16
               13    2    0   13    2   16
               13    4    0   13    4   16
               13    6    0   13    6   16
               14    0    0   14    0   16
CARD 490       14    1    0   14    1   16
               14    2    0   14    2   16
               14    3    0   14    3   16
               14    4    0   14    4   16
               14    5    0   14    5   16
CARD 495       14    6    0   14    6   16
           ---------------------------------------------------------------------------------
                5   10   15   20   25   30   35   40   45   50   55   60   65   70   75   80
```

5 10 15 20 25 30 35 40 45 50 55 60 65 70 75 80

	5	10	15	20	25	30
	15	0	0	15	0	16
	15	2	0	15	2	16
	15	4	0	15	4	16
	15	6	0	15	6	16
CARD 500	16	0	0	16	0	16
	16	1	0	16	1	16
	16	2	0	16	2	16
	16	3	0	16	3	16
	16	4	0	16	4	16
CARD 505	16	5	0	16	5	16
	16	6	0	16	6	16
	11	0	6	10	0	5
	11	2	6	10	2	5
	11	4	6	10	4	5
CARD 510	11	6	6	10	6	5
	12	0	6	10	0	4
	12	1	6	10	1	4
	12	2	6	10	2	4
	12	3	6	10	3	4
CARD 515	12	4	6	10	4	4
	12	5	6	10	5	4
	12	6	6	10	6	4
	11	0	10	10	0	11
	11	2	10	10	2	11
CARD 520	11	4	10	10	4	11
	11	6	10	10	6	11
	12	0	10	10	0	12
	12	1	10	10	1	12
	12	2	10	10	2	12
CARD 525	12	3	10	10	3	12
	12	4	10	10	4	12
	12	5	10	10	5	12
	12	6	10	10	6	12
	0	0	2	0	0	3
CARD 530	0	0	2	0	0	4
	0	0	2	0	0	5
	0	0	2	0	0	6
	0	0	2	0	0	7
	0	0	2	0	0	8
CARD 535	0	0	2	0	0	9
	0	0	2	0	0	10
	0	0	2	0	0	11
	0	0	2	0	0	12
	0	0	2	0	0	13
CARD 540	0	0	2	0	0	14
	0	1	2	0	1	4
	0	1	2	0	1	6
	0	1	2	0	1	8
	0	1	2	0	1	10
CARD 545	0	1	2	0	1	12

5 10 15 20 25 30 35 40 45 50 55 60 65 70 75 80

```
                    5   10   15   20   25   30   35   40   45   50   55   60   65   70   75   80
                -------------------------------------------------------------------------------
                    0    1    2    0    1   14
                    0    2    2    0    2    3
                    0    2    2    0    2    4
                    0    2    2    0    2    5
CARD  550           0    2    2    0    2    6
                    0    2    2    0    2    7
                    0    2    2    0    2    8
                    0    2    2    0    2    9
                    0    2    2    0    2   10
CARD  555           0    2    2    0    2   11
                    0    2    2    0    2   12
                    0    2    2    0    2   13
                    0    2    2    0    2   14
                    0    3    2    0    3    4
CARD  560           0    3    2    0    3    6
                    0    3    2    0    3    8
                    0    3    2    0    3   10
                    0    3    2    0    3   12
                    0    3    2    0    3   14
CARD  565           0    4    2    0    4    3
                    0    4    2    0    4    4
                    0    4    2    0    4    5
                    0    4    2    0    4    6
                    0    4    2    0    4    7
CARD  570           0    4    2    0    4    8
                    0    4    2    0    4    9
                    0    4    2    0    4   10
                    0    4    2    0    4   11
                    0    4    2    0    4   12
CARD  575           0    4    2    0    4   13
                    0    4    2    0    4   14
                    0    5    2    0    5    4
                    0    5    2    0    5    6
                    0    5    2    0    5    8
CARD  580           0    5    2    0    5   10
                    0    5    2    0    5   12
                    0    5    2    0    5   14
                    0    6    2    0    6    3
                    0    6    2    0    6    4
CARD  585           0    6    2    0    6    5
                    0    6    2    0    6    6
                    0    6    2    0    6    7
                    0    6    2    0    6    8
                    0    6    2    0    6    9
CARD  590           0    6    2    0    6   10
                    0    6    2    0    6   11
                    0    6    2    0    6   12
                    0    6    2    0    6   13
                    0    6    2    0    6   14
CARD  595       OUTPUT
                -------------------------------------------------------------------------------
                    5   10   15   20   25   30   35   40   45   50   55   60   65   70   75   80
```

PAGE 13

```
              5    10   15   20   25   30   35   40   45   50   55   60   65   70   75   80
          --------------------------------------------------------------------------------
              1
          DATA
              1
          PLOT
CARD 600      1
          2A/W=0.5
                 30.       100.        0.
                 30.       55.55       0.
                 60.       55.55       0.
CARD 605       [illegible].      [illegible].
              [illegible]    1
          END
          --------------------------------------------------------------------------------
              5    10   15   20   25   30   35   40   45   50   55   60   65   70   75   80
          --------------------------------------------------------------------------------
          --------------------------------------------------------------------------------
```

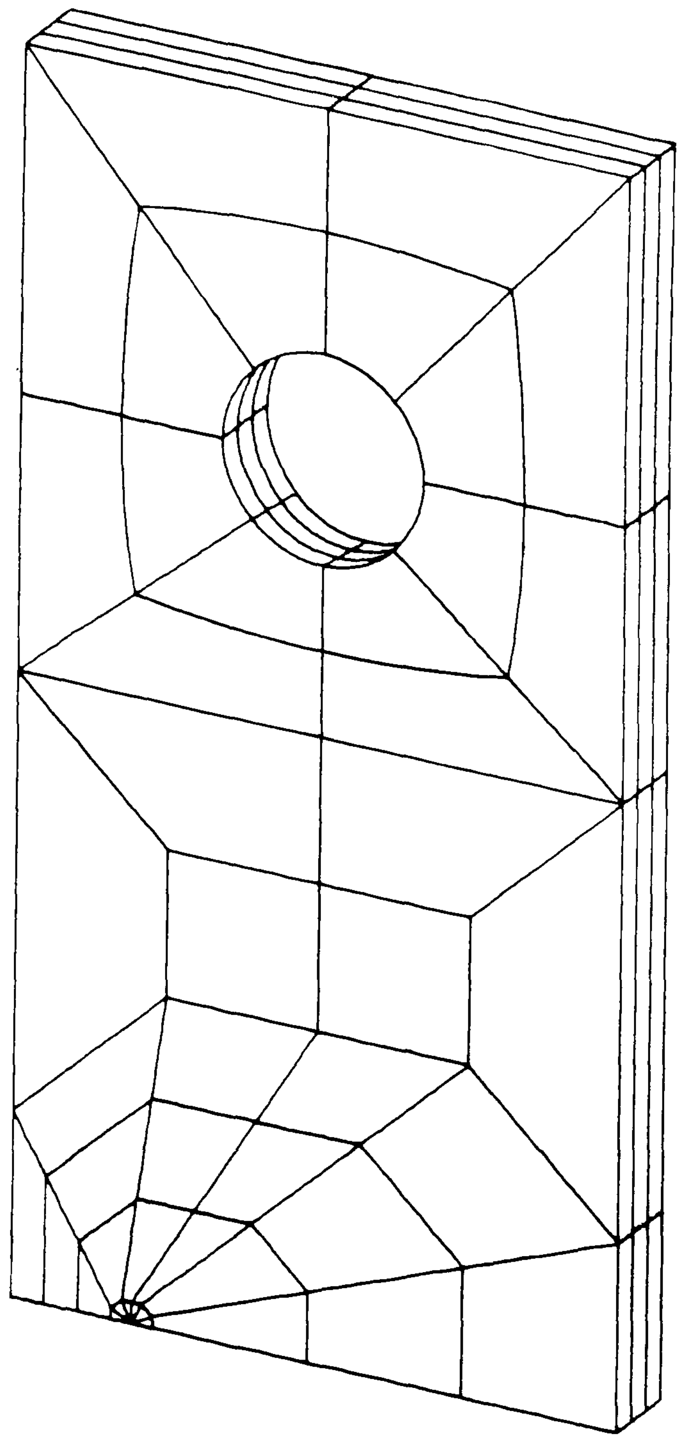

FIGURE A-1

FLAT SPECIMEN MESH FOR 2a/W=0.2
(ONE QUARTER OF FULL SPECIMEN IS MODELLED)

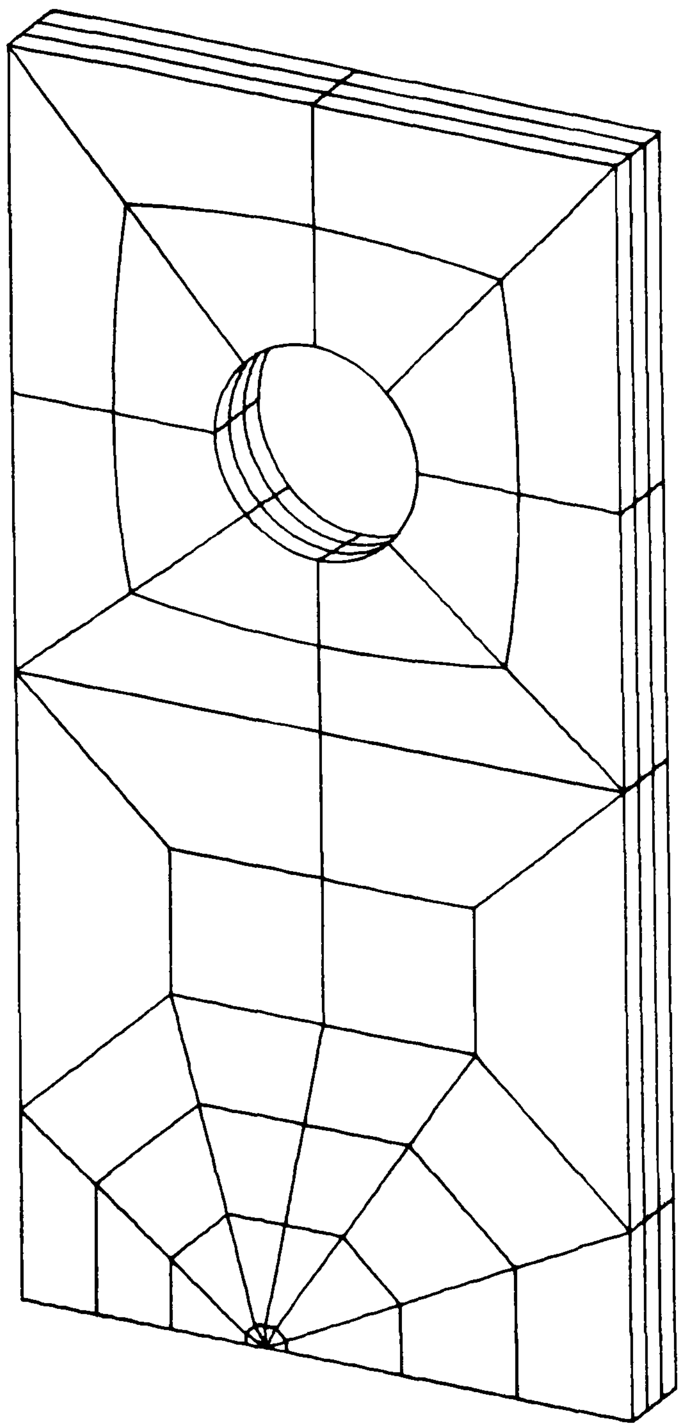

FIGURE A-2
FLAT SPECIMEN MESH FOR 2a/W = 0.4

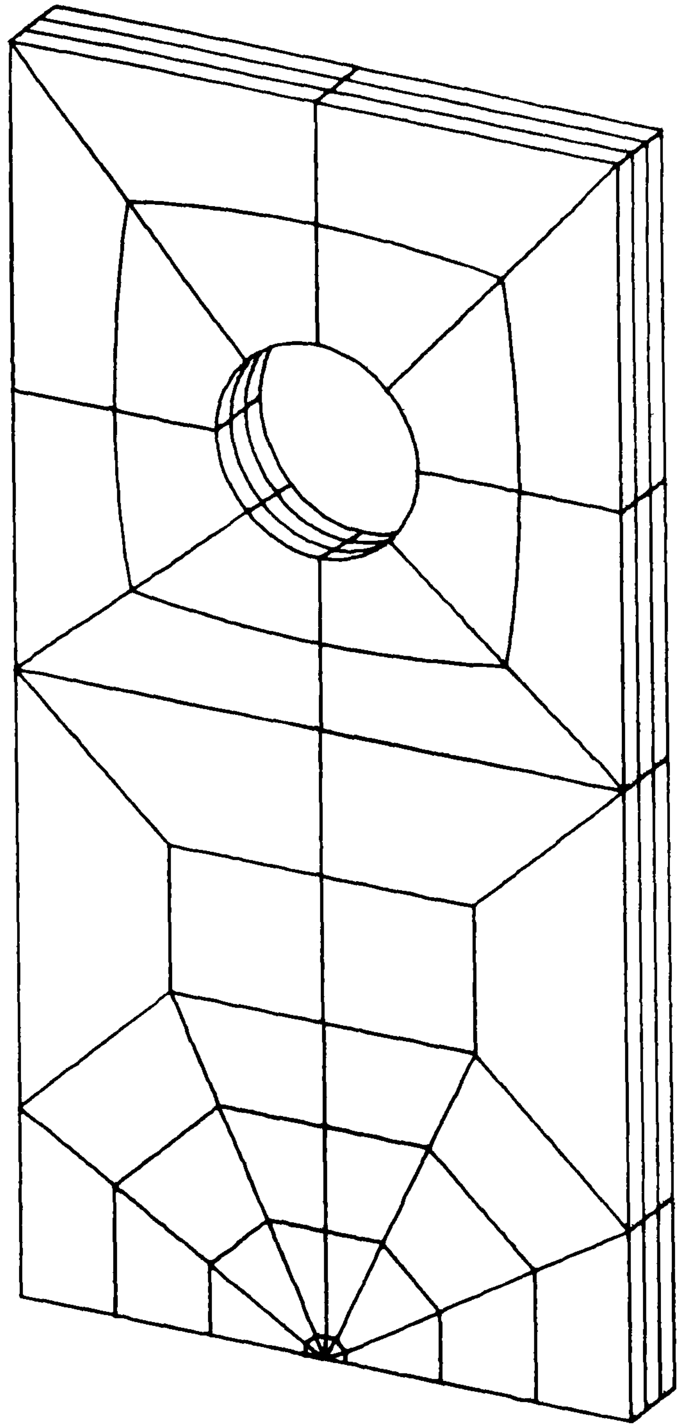

FIGURE A-3
FLAT SPECIMEN MESH FOR 2a/W = 0.5

172551 RD

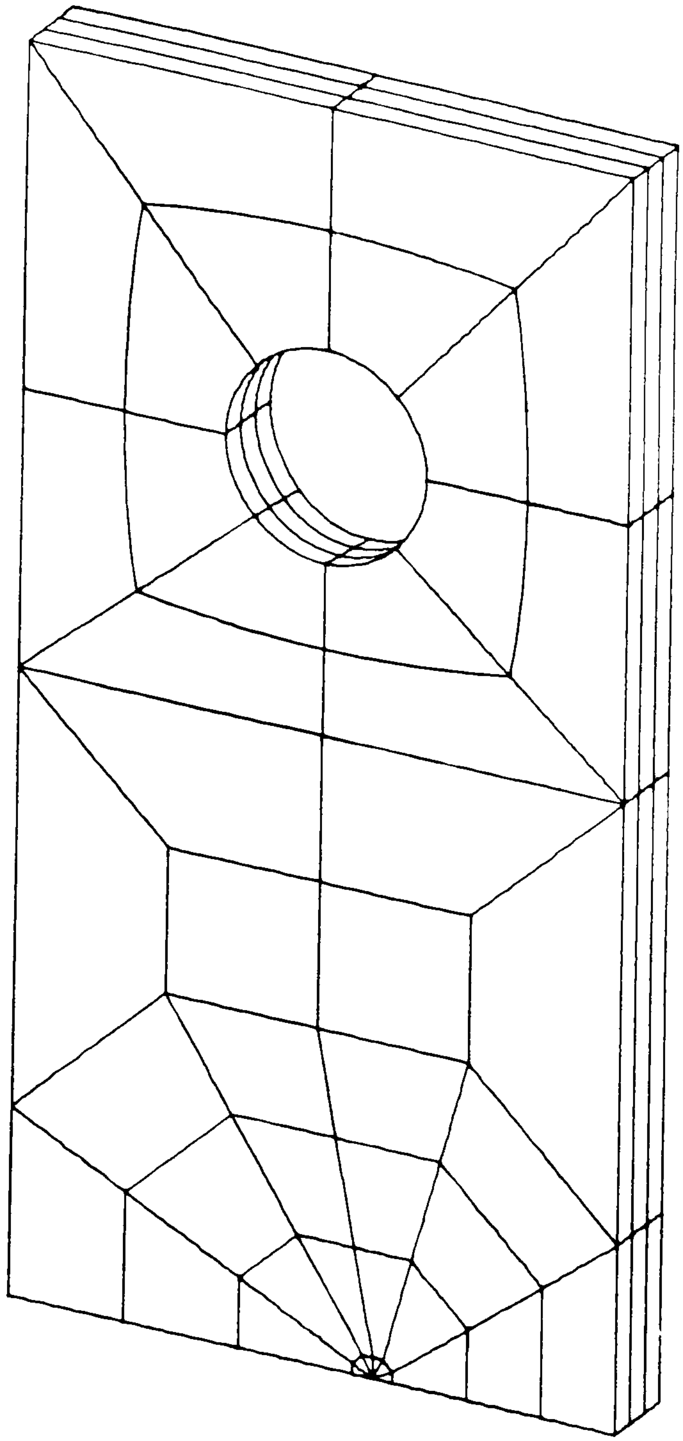

FIGURE A-4
FLAT SPECIMEN MESH FOR 2a/W = 0.6

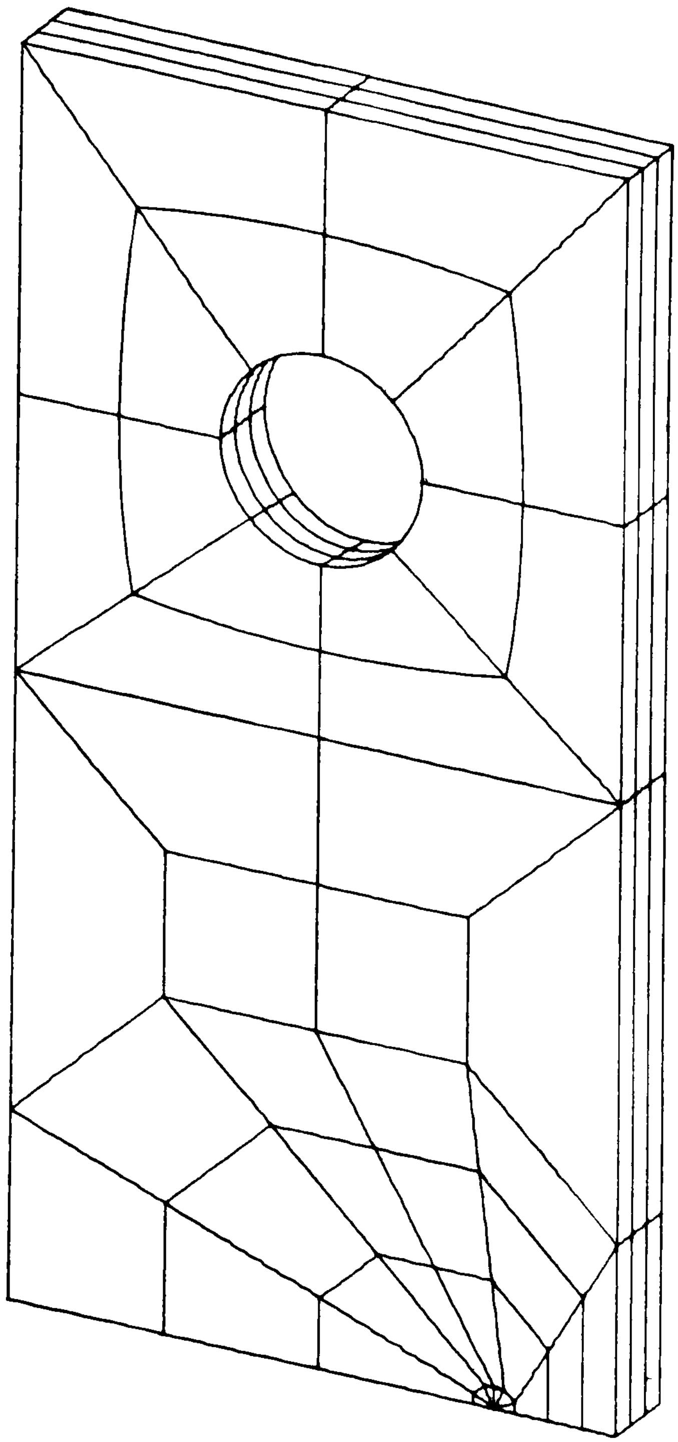

FIGURE A-5
FLAT SPECIMEN MESH FOR 2a/W = 0.8

APPENDIX B

Program NDISP

Listing of MARC–CDC input for a typical run of program NDISP, in this case increment 6 with 2a/W = .8. The program determines the displacements of inside surface nodes following an incremental displacement of the pin–hole nodes of 0.05 mm, for a flat specimen. These nodal displacements are stored for later use by the probram CURK, which does the K calculations for the curved specimen.

Subroutine UFXORD contains FORTRAN coding to transform the flat mesh coordinates from degrees to millimeters.

Subroutine FORCDT applies the incremental displacements to the pin–hole nodes.

Subroutine IMPD writes the displacements for the nodes that will be on the curved specimen inside surface to a tape file for later access by program CURK. It also sums and prints the reaction forces for the nodes in the specimen uncracked ligament, providing an easy way to determine the load corresponding to a given displacement.

Only the listing is given. The output is not included since it is of no importance and was never used.

```
      SUBROUTINE UFXORD(XORD,NCRD,N)
      DIMENSION XORD(NCRD),CRD(3)
      XORD(1)=XORD(1)*3.1415927*XORD(2)/180.
      RETURN
      END
```

```
SYMBOLIC REFERENCE MAP (R=1)

ENTRY POINTS
   3  UFXORD

VARIABLES      SN  TYPE            RELOCATION
  14  CRD          REAL      *UNDEF                     0  N        INTEGER   *UNUSED   F.P.
   0  NCRD         INTEGER             F.P.             0  XORD     REAL       ARRAY    F.P.

STATISTICS
  PROGRAM LENGTH                  17B      15
        60000B CM USED
```

```
      SUBROUTINE FORCDT(U,V,A,DP,DU,TIME,DTIME,NDEG,NODE,
     +UG,XORD,NCRD,IACFLG,INC)
      DIMENSION U(NDEG),V(NDEG),DP(NDEG),DU(NDEG),UG(NDEG),
     +XORD(NCRD)
C     DISPLACEMENTS SPECIFIED FOR PIN HOLE NODES
      XMIN=46.89*3.1415927*XORD(2)/180.
      XMAX=48.91*3.1415927*XORD(2)/180.
      IF(XORD(1).GE.XMIN.AND.XORD(1).LE.XMAX) GO TO 30
      GO TO 50
   30 CONTINUE
      ZMIN=-3.51
      ZMAX=3.51
      IF(XORD(3).GE.ZMIN.AND.XORD(3).LE.ZMAX) GO TO 40
      GO TO 50
   40 CONTINUE
      DU(1)=.05
      U(1)=U(1)+.05
   50 CONTINUE
      RETURN
      END
```

SYMBOLIC REFERENCE MAP (R=1)

TRY POINTS
3 FORCDT

ARIABLES		SN TYPE		RELOCATION					
0	A	REAL	*UNUSED	F.P.	0	DP	REAL	ARRAY	F.P.
0	DTIME	REAL	*UNUSED	F.P.	0	DU	REAL	ARRAY	F.P.
0	IACFLG	INTEGER	*UNUSED	F.P.	0	INC	INTEGER	*UNUSED	F.P.
0	NCRD	INTEGER		F.P.	0	NDEG	INTEGER		F.P.
0	NODE	INTEGER	*UNUSED	F.P.	0	TIME	REAL	*UNUSED	F.P.
0	U	REAL	ARRAY	F.P.	0	UG	REAL	ARRAY	F.P.
0	V	REAL	ARRAY	F.P.	37	XMAX	REAL		
36	XMIN	REAL			0	XORD	REAL	ARRAY	F.P.
41	ZMAX	REAL			40	ZMIN	REAL		

23 50

```
      SUBROUTINE IMPD(N,DD,TD,XORD,F,V,A,NDEG,NCRD)
      DIMENSION DD(NDEG),TD(NDEG),XORD(NCRD),F(NDEG),V(NDEG),A(NDEG)

      XMIN=46.89*3.1415927*XORD(2)/180.
      XMAX=48.91*3.1415927*XORD(2)/180.
      IF(XORD(1).GE.XMIN.AND.XORD(1).LE.XMAX) GO TO 20
      GO TO 50
   20 CONTINUE
      ZMIN=-3.51
      ZMAX=3.51
      IF(XORD(3).GE.ZMIN.AND.XORD(3).LE.ZMAX) GO TO 30
      GO TO 50
   30 CONTINUE
      IF(N.EQ.5) GO TO 35
      READ(22,*) F1
      REWIND 22
      F(1)=F(1)+F1
      IF(N.EQ.328) GO TO 40
   35 CONTINUE
      WRITE(22,*) F(1)
      REWIND 22
      GO TO 50
   40 CONTINUE
      WRITE(6,99) F(1)
   99 FORMAT(1X,*REACTION FORCE AT PIN =*,F10.3,* N*)
   50 CONTINUE
      YMIN=51.46
      IF(XORD(2).GE.YMIN) GO TO 100
      TD(1)=TD(1)+XORD(1)
      WRITE(24,*) N,DD(1),TD(1)
      N3=797
      IF(N.EQ.N3) GO TO 60
      GO TO 100
   60 REWIND 24

  100 CONTINUE
      RETURN
      END
```

SYMBOLIC REFERENCE MAP (R=1)

```
ENTRY POINTS
    3  IMPD

VARIABLES        SN  TYPE           RELOCATION
    0  A             REAL        ARRAY     F.P.          0  DD        REAL        ARRAY     F.P.
    0  F             REAL        ARRAY     F.P.        124  F1        REAL
    0  N             INTEGER               F.P.          0  NCRD      INTEGER               F.P.
    0  NDEG          INTEGER               F.P.        126  N3        INTEGER
    0  TD            REAL        ARRAY     F.P.          0  V         REAL        ARRAY     F.P.
  121  XMAX          REAL                              120  XMIN      REAL
    0  XORD          REAL        ARRAY     F.P.        125  YMIN      REAL
  123  ZMAX          REAL                              122  ZMIN      REAL
```

M A R C - C D C

C A R D   I N P U T   D A T A

P A G E   1

```
    5   10   15   20   25   30   35   40   45   50   55   60   65   70   75   80
--------------------------------------------------------------------------------
TITLE,FLAT CURVED SPECIMEN ANALYSIS
SIZING,40000,138,800,250,10,21,
INPUT TAPE,1,
MESH PLOT,1,
ALL POINTS
LOAD COR
TAPES,22,1000,
TAPES,24,2000,
ELSTO
VECSTO
ECS,45,
FORCDT,29,
RESTART
END
NEW
CONNECTIVITY
138,1,
COORDINATES
3,800,1,
UFXORD
1 TO 800 BY 1
DEFINE    NODE SET XLIG
726,727,728,729,730,731,732,733,734,735,736,737,738,739,740,CONTINUE
741,742,743,744,745,746,747,748,749,750,751,752,753,754,755,CONTINUE
756,757,758,759,760,761,762,763,764,765,766,768,769,771,772,CONTINUE
774,775,797,798,799,800,
DEFINE    NODE SET ZEDGE
42,47,50,55,58,63,66,71,74,77,80,83,88,91,96,CONTINUE
99,104,107,112,115,118,121,124,129,132,137,140,145,148,411,CONTINUE
412,413,414,415,416,417,418,419,420,421,447,451,458,462,469,CONTINUE
473,480,484,488,492,496,
DEFINE    NODE SET PINH
5,8,13,16,21,24,29,32,35,38,41,46,49,54,57,CONTINUE
62,65,70,292,295,300,303,308,311,316,319,322,325,328,
FORCDT
PINH
UDUMP
1,138,1,800,
PROPERTY
1,
95000,.38,,,,800,
1 TO 138
WORK HARD
2,
1666.67,0,
--------------------------------------------------------------------------------
    5   10   15   20   25   30   35   40   45   50   55   60   65   70   75   80
```

```
    5   10   15   20   25   30   35   40   45   50   55   60   65   70   75   80
--------------------------------------------------------------------------------
0,,.03
PRINT CHOICE
1,6,1,
133,138,
5,70,292,328,447,447,480,480,726,775,797,800,
14,
BOUNDARY CONDITIONS
3,
0,
1,
XLIG AND PINH
0,
2,
55,301,462,747,
0,
3,
ZEDGE
CONTROL
20,3,0,0,
.1,
RESTART
3,,5,
OPTIMIZE,1,
150,,,,300,
END OPTION
AUTO LOAD
1,
CONTINUE
PLOT TYPE
1,
15,1000,0,
SECTIONING
0,0,
0,30,52.8,54.2,-15,15,
SCALING
1,
10,10,
CONTOURS
11,2,6,5,1,5,,,1,
-200,800,
SLICE
1,
5,
3,4,9,10,15,16,21,22,27,28,33,34,39,40,45,CONTINUE
46,50,53,56,59,62,65,70,71,72,79,80,81,88,89,CONTINUE
90,97,98,99,106,107,108,115,116,117,122,125,128,131,134,CONTINUE
137,
TITLE
X-DIR. STRESS/MID WALL/D=.30MM
CONTINUE
--------------------------------------------------------------------------------
    5   10   15   20   25   30   35   40   45   50   55   60   65   70   75   80
```

```
     5   10   15   20   25   30   35   40   45   50   55   60   65   70   75   80
--------------------------------------------------------------------------------
PLOT TYPE
1,
0,1000,0,
SECTIONING
1,
70,79,88,97,106,115,122,125,128,131,134,137,
SCALING
1,
10,10,
CONTOURS
11,2,5,5,1,4,,,1,
0,800,
SLICE
1,
5,
70,79,88,97,106,115,122,125,128,131,134,137,
TITLE
X-STRESS/MID-WALL/D=.30MM
CONTINUE
END PLOT
1,
--------------------------------------------------------------------------------
     5   10   15   20   25   30   35   40   45   50   55   60   65   70   75   80
--------------------------------------------------------------------------------
--------------------------------------------------------------------------------
```

APPENDIX C

Program LARC

Program LARC was a FORTRAN program to determine the relation between grip-half rotation angle about the pivot point, and the corresponding increase in the length of the specimen inside surface, measured between the loading pins and the crack plane (line y=0).

LARC gave as output the equation of a 4th degree polynomial fit giving rotation angle as a function of arc length increase.

This was used as input to program DEFIT.
The relationship determined by LARC is plotted in Figure C.1.

```
      PROGRAM LARC(INPUT,OUTPUT,PLOT,TAPE5=INPUT,TAPE6=OUTPUT)

C     PURPOSE OF PROGRAM IS TO DETERMINE WHAT INCREMENTAL LENGTH
C     INCREASES ARE PRODUCED BY CORRESPONDING INCREMENTAL ROTATIONS
C     AROUND THE GRIP PIVOT POINTS. THE DISTANCE OF CONCERN IS
C     THAT BETWEEN THE Y-AXIS AND THE LEAD I.D. PIN-HOLE NODE.

      REAL X0(100),Y0(100),XD(100),YD(100),YF(100),W(100),P(10),
     +E(10,10),WS(1250),DIST(100),THET(100)
      INTEGER MA
      COMMON/SCALES/XMIN,XMAX,TICX,FXSCAL,YMIN,YMAX,TICY,FYSCAL
      COMMON/FORMAT/XL,YL,FTITLE(8),FSUBTIT(8),FXAXTIT(8),FYAXTIT(8),
     +NSTVARS,STVARS(10)

C     FOLLOWING DETERMINES ORIGINAL UNDEFORMED ARC LENGTH,S0.

      S0=51.45*48.9*3.1415927/180.
      WRITE(6,1001) S0
 1001 FORMAT(1X,*THEORETICAL UNDEFORMED LENGTH =*,F10.5,* MM*)

      XPIV=34.5
      YPIV=-5.5

C     FIRST APPLY METHOD TO ORIGINAL UNDEFORMED SURFACE

      DO 10 I=1,100
      DX0=.5
      X0(I)=(I*DX0)+(38.7708-50)
      Y0(I)=SQRT(51.45**2-(ABS(X0(I)))**2)
   10 CONTINUE

C     FIND ORIGINAL ARC LENGTH BY APPROXIMATION FOR COMPARISON
C     TO THEORETICAL

      DXS=X0(100)/500.
      S=0.
      DO 20 I=1,500
      X1=(I-1)*DXS
      X2=I*DXS
      Y1=SQRT(51.45**2-X1**2)
      Y2=SQRT(51.45**2-X2**2)
      XL=ABS(X2-X1)
      YL=ABS(Y2-Y1)
      DS=SQRT(XL**2+YL**2)
      S=S+DS
   20 CONTINUE
      WRITE(6,1002) S
 1002 FORMAT(1X,*APPROXIMATED UNDEFORMED ARC LENGTH =*,F10.5,* MM*)

C     FOLLOWING DETERMINES EQUATIONS FOR AND LENGTH INCREASES OF
C     ARCS DEFORMED IN INCREMENTS OF 0.04 DEG.
      DO 100 ITHET=1,100
      DEFANG=ITHET*.04

C     FOLLOWING CALCULATES EQN OF DEFORMED SURFACE

      DO 30 I=1,100
```

REASON FOR NEGATIVE X VALUES?
possibly to determine whether y was larger for +ve or negative x

```
      DX=XO(I)-XPIV
      DY=YO(I)-YPIV
      R=SQRT((ABS(DX))**2+(ABS(DY))**2)
      PIVANG=ATAN2(DY,DX)
      ANG1=PIVANG-DEFANG*3.1415927/180.
      XD(I)=R*COS(ANG1)+XPIV
      YD(I)=R*SIN(ANG1)+YPIV
   30 CONTINUE
      N=100
      NE=10
      MA=9
      CALL PRESET(YF(1),100,0.)
      CALL PRESET(W(1),100,1.)
      CALL PRESET(P(1),10,0.)
      CALL PRESET(E(1),100,0.)
      CALL PRESET(WS(1),1250,0.)

      CALL POLFIT(XD,YD,W,YF,P,N,MA,E,NE,SSR,WS)

C     FOLLOWING CALCULATES INCREASE IN ARC LENGTH

      DXS =XD(100)/500.
      Y1=0.
      Y2=0.
      S=0.

      DO 40 I=1,500
      X1=(I-1)*DXS
      X2=I*DXS
      Y1=P(1)+P(2)*X1
      Y2=P(1)+P(2)*X2
      DO 50 J=3,10
      Y1=Y1+P(J)*X1**(J-1)
      Y2=Y2+P(J)*X2**(J-1)
   50 CONTINUE

      XL=ABS(X2-X1)
      YL=ABS(Y2-Y1)
      DS=SQRT(XL**2+YL**2)
      S=S+DS
   40 CONTINUE

      DIST(ITHET)=S-S0
      THET(ITHET)=DEFANG

  100 CONTINUE

      DO 1000 MA=1,9
      CALL PRESET(YF(1),100,0.)
      CALL PRESET(W(1),100,1.)
      CALL PRESET(P(1),10,0.)
      CALL PRESET(E(1),100,0.)
      CALL PRESET(WS(1),1250,0.)

      CALL POLFIT(DIST,THET,W,YF,P,N,MA,E,NE,SSR,WS)

      WRITE(6,1003)
```

USE MORE POINTS?

- PERHAPS MAKE FIT COVER LESS NEGATIVE X ARC

```
        1003 FORMAT(1H1,*COEFFICIENTS OF ANG(DEG) AS A FUNCTION OF DISP(MM)*//)
             WRITE(6,1006) MA
        1006 FORMAT(1X,*FIT OF DEGREE*,I2/)
             WRITE(6,1004) (P(I),I=1,10)
        1004 FORMAT(1X,E15.8)
             WRITE(6,1005) SSR
        1005 FORMAT(1H0,*SUM OF SQUARES OF RESIDUALS = *,E15.8)

             FXAXTIT(1)=10H(*PIVOT PO
             FXAXTIT(2)=10HINT ROTATI
             FXAXTIT(3)=10HON ANGLE (
             FXAXTIT(4)=6HDEG)*)
             FYAXTIT(1)=10H(*ARC LENG
             FYAXTIT(2)=10HTH INCREAS
             FYAXTIT(3)=8HE (MM)*)
             FTITLE(1)=10H(*ARC LENG
             FTITLE(2)=10HTH INCREAS
             FTITLE(3)=10HE VS. ROTA
             FTITLE(4)=10HTION ANGLE
             FTITLE(5)=10H BETWEEN Y
             FTITLE(6)=10H-AXIS AND
             FTITLE(7)=10HLEAD PIN-H
             FTITLE(8)=10HOLE NODE*)
             FSUBTIT(1)=10H(*FIT OF D
             FSUBTIT(2)=10HEGREE*,F2.
             FSUBTIT(3)=10H0,* - SSR
             FSUBTIT(4)=9H=*,E15.8)

             XMIN=0.
             XMAX=4.
             XL=150.
             YL=150.
             TICX=.5
             TICY=.5
             NSTVARS=2
             STVARS(1)=FLOAT(MA)
             STVARS(2)=SSR

             CALL SIMPLTM(1,THET,DIST,N,1,0)
        1000 CONTINUE

             STOP
             END
```

SYMBOLIC REFERENCE MAP (R=3)

```
ENTRY POINTS      DEF LINE      REFERENCES
 6216  LARC           1

VARIABLES        SN  TYPE            RELOCATION
  6773  ANG1          REAL                                REFS        63       64    DEFINED      62
  6766  DEFANG        REAL                                REFS        62      101    DEFINED      53
 12650  DIST          REAL        ARRAY                   REFS         8      112        153    DEFINED      100
```

```
FIT OF DEGREE 4

 .17783106E-03
 .10060928E+01
-.53484934E-02
 .61616981E-04
-.66571727E-06
0.
0.
0.
0.
0.

SUM OF SQUARES OF RESIDUALS =    .12674783E-13
```

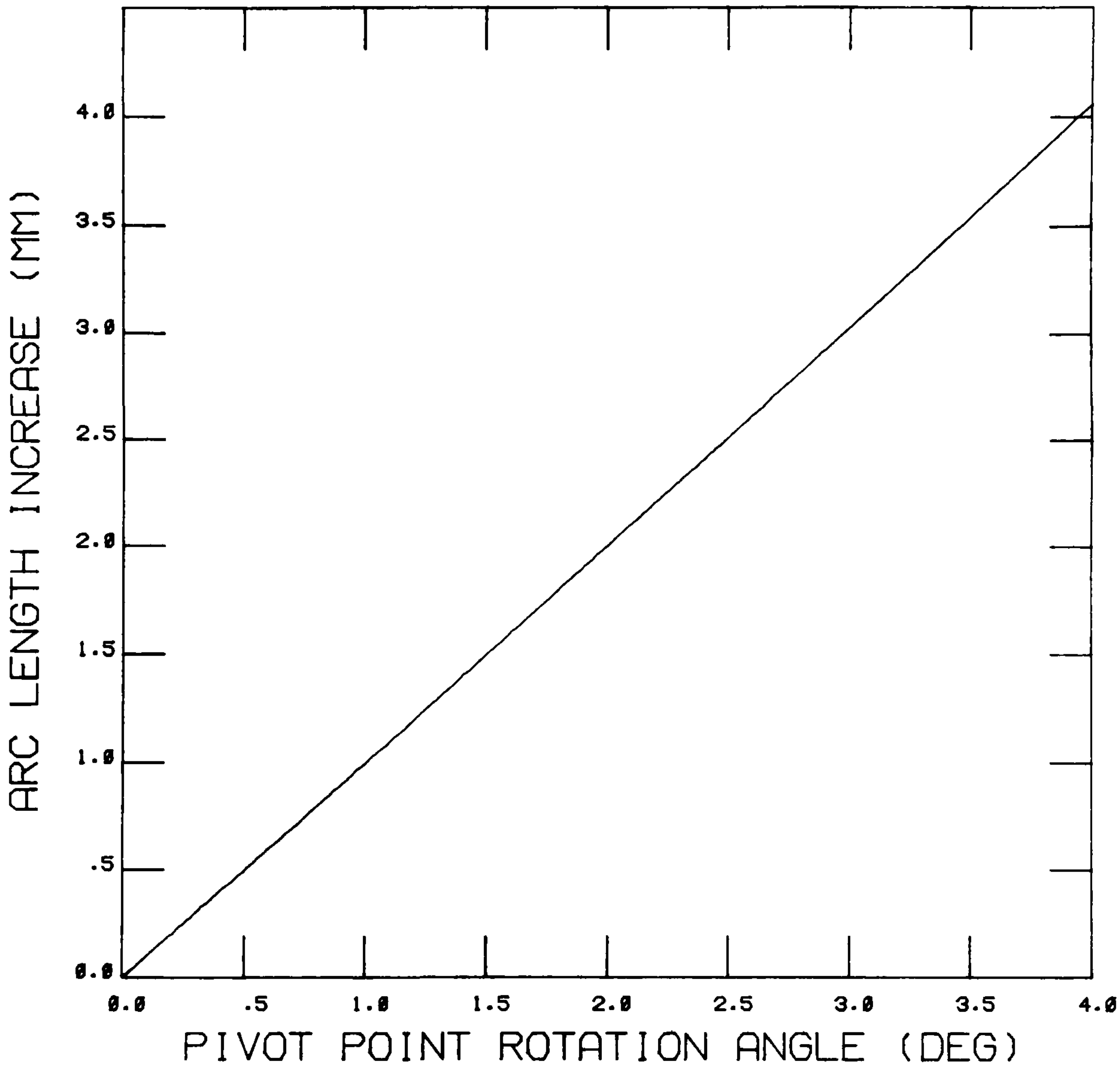

FIGURE C-1

RELATION BETWEEN GRIP CURVED SURFACE ARC LENGTH INCREASE AND GRIP PIVOT POINT ROTATION ANGLE. ARC LENGTH IS MEASURED BETWEEN THE CRACK PLANE AND THE TOP EDGE OF THE SPECIMEN MOUNTING PIN-HOLE. THE ROTATION ANGLE IS FOR ONE HALF OF THE GRIPS ONLY

APPENDIX D

Program DEFIT

DEFIT was a FORTRAN program that used the equation generated by LARC to determine the rotation angles that would produce curved surface length increases of .05, .10, .15, .20,..., 2.00 mm.

Then, based soley on geometry, DEFIT would calculate the 10th degree polynomial equation for the resulting curved surface in an x-y plane.

This equation was used as input by the analysis program CURK, which used it to locate positions of nodes on that surface.

```
      PROGRAM DEFIT(INPUT,OUTPUT,TAPE5=INPUT,TAPE6=OUTPUT)

      REAL XO(100),YO(100),XD(100),YD(100),YF(100),W(100),P(10),
     +E(10,10),WS(1250),DIST(100),DTHET(40),PP(5)
      INTEGER MA

      XPIV=34.5
      YPIV=-5.5

C     FOLLOWING DETERMINES POINTS ON UNDEFORMED SURFACE

      DO 10 I=1,100
      DXO=.5
      XO(I)=(I*DXO)+(44.557-50)
      YO(I)=SQRT(51.45**2-(ABS(XO(I)))**2)
   10 CONTINUE
C     FOLLOWING CALCULATES EQN OF DEFORMED SURFACE FOR ROTATION DTHET(I)
C     FOLLOWING ARE COEFFICIENTS OF 4TH DEGREE FIT GIVING
C     DTHETA AS F(DS):
      PP(1)=.17783106E-03
      PP(2)=.10060928E+01
      PP(3)=-.53434934E-02
      PP(4)=.61616981E-04
      PP(5)=-.66571727E-06
C
      DO 100 I=1,40
      DS=I*.05
      DTHET(I)=PP(1)+PP(2)*DS
      DO 20 J=3,5
      DTHET(I)=DTHET(I)+PP(J)*DS**(J-1)
   20 CONTINUE
C
C     FOLLOWING FINES EQUATION OF CURVED SURFACE
C     AFTER PIVOT POINT ROTATION OF DTHET(I)
C

      DEFANG=DTHET(I)
      DO 30 J=1,100
      DX=XO(J)-XPIV
      DY=YO(J)-YPIV
      R=SQRT((ABS(DX))**2+(ABS(DY))**2)
      PIVANG=ATAN2(DY,DX)
      ANG1=PIVANG-DEFANG*3.1415927/180.
      XD(J)=R*COS(ANG1)+XPIV
      YD(J)=P*SIN(ANG1)+YPIV
   30 CONTINUE
      N=100
      NE=10
      MA=9
      CALL PRESET(YF(1),100,0.)
      CALL PRESET(W(1),100,1.)
      CALL PRESET(P(1),10,0.)
      CALL PRESET(E(1),100,0.)
      CALL PRESET(WS(1),1250,0.)

      CALL POLFIT(XD,YD,W,YF,P,N,MA,E,NE,SSR,WS)
```

```
          WRITE(6,200) DS,DTHET(I)
      200 FORMAT(1H0,1X,*FOR ARC LENGTH INCREASE,DS =*,F5.2,* MM*/1X,*CORRES
         +PONDING ROTATION ANGLE =*,F7.4,* DEGREES*/)
          WRITE(6,300) (P(K),K=1,10)
      300 FORMAT(1X,*COEFFICIENTS OF FIT TO DEFORMED SURFACE (Y=F(X)) ARE:*/
         +(5X,E15.8))
          WRITE(6,400)
      400 FORMAT(50H--------------------------------------------------)
      100 CONTINUE
          STOP
          END
```

```
3OLIC REFERENCE MAP (R=3)

TS      DEF LINE      REFERENCES
IT          1

    SN  TYPE              RELOCATION
1       REAL                                REFS       44        45    DEFINED        43
ANG     REAL                                REFS       43   DEFINED         37
T       REAL        *UNDEF                  REFS        3
        REAL                               .REFS       28        30         58   DEFINED
.T      REAL         ARRAY                  REFS        3        30         37        59
        REAL                                REFS       41        42    DEFINED        39
        REAL                                REFS       14   DEFINED         13
        REAL                                REFS       41        42    DEFINED        40
        REAL         ARRAY                  REFS        3        53         56
        INTEGER                             REFS     2*14      2*15         27        28
                                         DEFINED       12        26
        INTEGER                             REFS     2*30        39         40        44
                                         DEFINED       29        38
        INTEGER                             REFS       61   DEFINED         61
        INTEGER                             REFS        5        56    DEFINED        49
        INTEGER                             REFS       56   DEFINED         47
        INTEGER                             REFS       56   DEFINED         43
        REAL         ARRAY                  REFS        3        52         56        61
ANG     REAL                                REFS       43   DEFINED         42
        REAL         ARRAY                  REFS        3      2*28         30   DEFINED
                                              23       24
        REAL                                REFS       44        45    DEFINED        41
      * REAL                                REFS       56
        REAL         ARRAY                  REFS        3        51         56
        REAL         ARRAY                  REFS        3        54         56
        REAL         ARRAY                  REFS        3        56    DEFINED        44
        REAL                                REFS       39        44    DEFINED         7
        REAL         ARRAY                  REFS        3        15         39   DEFINED
        REAL         ARRAY                  REFS        3        56    DEFINED        45
        REAL         ARRAY                  REFS        3        50         56
        REAL                                REFS       40        45    DEFINED         8
        REAL         ARRAY                  REFS        3        40    DEFINED        15
```

```
-----------------------------------------------------------

 FOR ARC LENGTH INCREASE,DS =    .20 MM
CORRESPONDING ROTATION ANGLE =   .2012 DEGREES

COEFFICIENTS OF FIT TO DEFORMED SURFACE (Y=F(X)) ARE:
     1  .51571458E+02
     2  .51148848E-03
     3 -.98121074E-02
     4  .76484337E-06
     5  .23684187E-05
     6 -.47124486E-06
     7  .29143010E-07
     8 -.94515071E-09
     9  .15491729E-10
    10 -.10409186E-12

-----------------------------------------------------------

 FOR ARC LENGTH INCREASE,DS =    .25 MM
CORRESPONDING ROTATION ANGLE =   .2514 DEGREES

COEFFICIENTS OF FIT TO DEFORMED SURFACE (Y=F(X)) ARE:
        .51601652E+02
        .61775348E-03
       -.98130649E-02
        .14195403E-06
        .25177130E-05
       -.48437137E-06
        .29790184E-07
       -.96173135E-09
        .15710796E-10
       -.10534450E-12

-----------------------------------------------------------

 FOR ARC LENGTH INCREASE,DS =    .30 MM
CORRESPONDING ROTATION ANGLE =   .3015 DEGREES

COEFFICIENTS OF FIT TO DEFORMED SURFACE (Y=F(X)) ARE:
        .51631824E+02
        .72467822E-03
       -.98139366E-02
       -.51697810E-06
        .26719418E-05
       -.49884159E-06
        .30450476E-07
       -.97913484E-09
        .15951175E-10
       -.10661295E-12

-----------------------------------------------------------

 FOR ARC LENGTH INCREASE,DS =    .35 MM
CORRESPONDING ROTATION ANGLE =   .3517 DEGREES

COEFFICIENTS OF FIT TO DEFORMED SURFACE (Y=F(X)) ARE:
        .51661975E+02
        .83224006E-03
       -.98147162E-02
       -.12129995E-05
```

FOR ARC LENGTH INCREASE,DS = .35 MM
CORRESPONDING ROTATION ANGLE = .3517 DEGREES

COEFFICIENTS OF FIT TO DEFORMED SURFACE (Y=F(X)) ARE:

.51661975E+02
.83224006E-03
-.98147162E-02
-.12129995E-05
.28312272E-05
-.51315720E-06
.31124138E-07
-.99656195E-09
.16185912E-10
-.10789712E-12

FOR ARC LENGTH INCREASE,DS = .40 MM
CORRESPONDING ROTATION ANGLE = .4018 DEGREES

COEFFICIENTS OF FIT TO DEFORMED SURFACE (Y=F(X)) ARE:

.51692104E+02
.94043571E-03
-.98153972E-02
-.19475[illegible]37E-05
.2[illegible]7145E-05
-.527[illegible]E-06
.31[illegible]11[illegible]24E-07
-.10142[illegible]5E-08
.164[illegible]405[illegible]E-10
-.10919730E-12

FOR ARC LENGTH INCREASE,DS = .45 MM
CORRESPONDING ROTATION ANGLE = .4518 DEGREES

COEFFICIENTS OF FIT TO DEFORMED SURFACE (Y=F(X)) ARE:

.51722212E+02
.10492561E-02
-.98159730E-02
-.27222047E-05
.31655477E-05
-.54286222E-06
.32512597E-07
-.10323105E-08
.16665663E-10
-.11051371E-12

FOR ARC LENGTH INCREASE,DS = .50 MM
CORRESPONDING ROTATION ANGLE = .5019 DEGREES

COEFFICIENTS OF FIT TO DEFORMED SURFACE (Y=F(X)) ARE:

.51752299E+02
.11586916E-02

```
 .32517597E-07
-.10323105E-08
 .16665663E-10
-.11051371E-12

--------------------------------------------------

FOR ARC LENGTH INCREASE,DS =   .50 MM
CORRESPONDING ROTATION ANGLE =   .5019 DEGREES

COEFFICIENTS OF FIT TO DEFORMED SURFACE (Y=F(X)) ARE:
 .51752299E+02
 .11586916E-02
-.98164366E-02
-.35382934E-05
 .33403741E-05
-.55826782E-06
 .33227921E-07
-.10506418E-08
 .16910775E-10
-.11184655E-12

--------------------------------------------------

FOR ARC LENGTH INCREASE,DS =   .55 MM
CORRESPONDING ROTATION ANGLE =   .5519 DEGREES

COEFFICIENTS OF FIT TO DEFORMED SURFACE (Y=F(X)) ARE:
 .51782364E+02
 .12627315E-02
-.98167305E-02
-.43973338E-05
 .35211450E-05
-.57415324E-06
 .33957668E-07
-.10692846E-08
 .17159447E-10
-.11319604E-12

--------------------------------------------------

FOR ARC LENGTH INCREASE,DS =   .60 MM
CORRESPONDING ROTATION ANGLE =   .6019 DEGREES

COEFFICIENTS OF FIT TO DEFORMED SURFACE (Y=F(X)) ARE:
 .51812408E+02
 .13793645E-02
-.98169973E-02
-.53010412E-05
 .37086152E-05
-.59022702E-06
 .34702113E-07
-.10832440E-08
 .17411731E-10
-.11456239E-12

--------------------------------------------------

FOR ARC LENGTH INCREASE,DS =   .65 MM
CORRESPONDING ROTATION ANGLE =
```

APPENDIX E

Program CURK

Program CURK was the main analysis program that calculated loads and the stress intensity factor for the actual curved specimen geometry, for various displacements.

Subroutine UFXORD transformed the coordinates in the mesh file by mapping the flat mesh onto the curved specimen geometry.

Subroutine FORCDT takes the equation for the deformed surface corresponding to the displacement increment and determines the location on this surface of the inside surface nodes. This is done by equating the linear distances from the crack plane to the same nodes in the file created by program NDISP with the distance measured from the crack plane along the curved, deformed surface.

The entire program input listing and data output listing are reproduced for increment 5 at 2a/W = 0.5.

```
                  SUBROUTINE UFXORD(XORD,NCRD,N)
                  DIMENSION XORD(NCRD),CRD(3)
C
C                 COORDINATE MODIFICATION FOR ALL NODES
C
                  THETA=XORD(1)*3.1415927/180.
                  R=XORD(2)
                  XORD(1)=R*SIN(THETA)
                  XORD(2)=R*COS(THETA)

                  RETURN
                  END
```

```
       SYMBOLIC REFERENCE MAP (R=1)

ENTRY POINTS
    3  UFXORD

VARIABLES     SN  TYPE          RELOCATION
   24  CRD        REAL       *UNDEF                      0  N          INTEGER   *UNUSED    F.P.
    0  NCRD       INTEGER              F.P.             23  R          REAL
   22  THETA      REAL                                   0  XORD       REAL        ARRAY    F.P.

EXTERNALS           TYPE    ARGS
       COS        REAL       1 LIBRARY                      SIN        REAL        1 LIBRARY

STATISTICS
  PROGRAM LENGTH                 27B       23
        600008 CM USED
```

```
      SUBROUTINE FORCDT(U,V,A,DP,DU,TIME,DTIME,NDEG,NODE,
     +UG,XORD,NCRD,IACFLG,INC)
      DIMENSION U(NDEG),V(NDEG),DP(NDEG),DU(NDEG),UG(NDEG),
     +XORD(NCRD),P(10)

C     FOLLOWING GIVES COEFFICIENTS OF 10TH DEGREE FIT TO
C     DEFORMED SURFACE FOR INCREMENT 5.
C
      P(1)=.51601652E+02
      P(2)=.61775848E-03
      P(3)=-.98130649E-02
      P(4)=.14185403E-06
      P(5)=.25177180E-05
      P(6)=-.48487337E-06
      P(7)=.29790184E-07
      P(8)=-.96199935E-09
      P(9)=.15719796E-10
      P(10)=-.10534460E-12
      DS=.25
      DEFANG=.2514
      XPIV=34.5
      YPIV=-5.5
C
C     TEST FOR PIN-HOLE NODE NOT ON I.D.
C     PIN-HOLE NODES NOT ON I.D. BUT CONTAINED IN LIST "NIDPH"
C     WILL HAVE DEFORMED CO-ORDS CALCULATED FROM A STRAIGHT
C     FORWARD ROTATION OF "DEFANG" DEGREES.
C
      ZMIN=-3.51
      ZMAX=3.51
      IF(XORD(3).LT.ZMIN.OR.XORD(3).GT.ZMAX) GO TO 10
      R=SQRT(XORD(1)**2+XORD(2)**2)
      RMIN=51.5
      IF(R.LT.RMIN) GO TO 10
C
C     FOLLOWING TO "GO TO 500" IS ONLY APPLIED TO
C     PIN-HOLE NODES NOT ON THE SPECIMEN I.D.
C
      DX=XORD(1)-XPIV
      DY=XORD(2)-YPIV
      R=SQRT((ABS(DX))**2+(ABS(DY))**2)
      PIVANG=ATAN2(DY,DX)
      ANG1=PIVANG-DEFANG*3.1415927/180.
C
C     X2,Y2 ARE DEFORMED COORDINATES
C     UP= PREVIOUS INCREMENT'S TOTAL DISPLACEMENT
C     U(1) = TOTAL X DISPLACEMENT FOR THIS INCREMENT
C     DU(1) = INCREMENTAL X DISPLACEMENT FOR THIS INCREMENT
C     SIMILARLY U(2),DU(2) ARE Y DISPLACEMENTS
C
      X2=R*COS(ANG1)+XPIV
      Y2=R*SIN(ANG1)+YPIV
      UP=U(1)
      U(1)=X2-XORD(1)
      DU(1)=U(1)-UP
      UP=U(2)
      U(2)=Y2-XORD(2)
```

```
      DU(2)=U(2)-UP
      GO TO 500
   10 CONTINUE
C
C     READ FLAT SPECIMEN DISPLACEMENT DATA FROM DISPNOD_PT_ FILE
C
C
C     N1 = I.D. NODE NO.
C     XI1,XT1 ARE RESPECTIVELY INCREMENTAL AND TOTAL "X" DISPLACEMENTS
C     FROM FLAT ANALYSIS.
C     XT1 ALSO EQUALS DISTANCE MEASURED CIRCUMFERENTIALLY FROM
C     Y-AXIS TO DEFORMED NODE.
C
      READ(24,*) N1,XI1,XT1
      IF(NODE.NE.N1) GO TO 900
      DELTAX=.0001
      X2=0.
      Y2=0.
      S=0.
      IF(S.GE.XT1) GO TO 200
      DO 100 I=1,5000
      X10=(I-1)*.01
      DO 90 II=1,100
      X1=X10+(II-1)*DELTAX
      X2=X10+II*DELTAX
      Y1=P(1)+P(2)*X1
      Y2=P(1)+P(2)*X2
      DO 50 J=3,10
      Y1=Y1+P(J)*X1**(J-1)
      Y2=Y2+P(J)*X2**(J-1)
   50 CONTINUE
      XL=ABS(X2-X1)
      YL=ABS(Y2-Y1)
      DELTAS=SQRT(XL**2+YL**2)
      S=S+DELTAS
      IF(S.GE.XT1)GO TO 300
   90 CONTINUE
  100 CONTINUE
      GO TO 300
  200 CONTINUE
      Y2=P(1)
  300 CONTINUE
      UP=U(1)
      U(1)=X2-XORD(1)
      DU(1)=U(1)-UP
      UP=U(2)
      U(2)=Y2-XORD(2)
      DU(2)=U(2)-UP
  500 CONTINUE
      WRITE(6,599) NODE,X2,Y2,XORD(1),XORD(2),U(1),U(2),DU(1),DU(2),S,
     +XT1
  599 FORMAT(5X,I5,10(2X,F8.4))
      GO TO 1000
  900 CONTINUE
      WRITE(6,999) NODE,N1
  999 FORMAT(1H0,*--ERROR--*,2X,I5,* .NE. *,I5//)
 1000 CONTINUE
```

```
      SUBROUTINE IMPD(N,DD,TD,XORD,F,V,A,NDEG,NCRD)
      DIMENSION DD(NDEG),TD(NDEG),XORD(NCRD),F(NDEG),V(NDEG),A(NDEG)
C
C     CTNZ=Z CO-ORD OF CRACK TIP NODES
C
      CTNZ=0.-.01
      IF(XORD(3).LT.CTNZ) GO TO 100
      XMIN=.01
      IF(XORD(1).GE.XMIN) GO TO 100
      N2=726
      IF(N.EQ.N2) GO TO 20
      READ(22,*) F1
      REWIND 22
      F(1)=F(1)+F1
      N3=800
      IF(N.EQ.N3) GO TO 50
   20 CONTINUE
      WRITE(22,*) F(1)
      REWIND 22
      GO TO 100
   50 CONTINUE
      WRITE(6,99) F(1)
   99 FORMAT(1H0,*REACTION FORCE OVER LIGAMENT =*,F10.3,* N*)
  100 CONTINUE
      RETURN
      END
```

```
     SYMBOLIC REFERENCE MAP (R=1)

ENTRY POINTS
    3  IMPD

VARIABLES      SN  TYPE          RELOCATION
    0  A           REAL          ARRAY    F.P.          61  CTNZ      REAL
    0  DD          REAL          ARRAY    F.P.           0  F         REAL       ARRAY     F.P.
   64  F1          REAL                                  0  N         INTEGER              F.P.
    0  NCRD        INTEGER                F.P.           0  NDEG      INTEGER              F.P.
   63  N2          INTEGER                              65  N3        INTEGER
    0  TD          REAL          ARRAY    F.P.           0  V         REAL       ARRAY     F.P.
   62  XMIN        REAL                                  0  XORD      REAL       ARRAY     F.P.

FILE NAMES         MODE
    TAPE22         FREE                 TAPE6      FMT

STATEMENT LABELS
   23  20                         30  50                                50  99        FMT
   32  100

STATISTICS
  PROGRAM LENGTH                 66B        54
        60000B CM USED
```

M A R C - C D C

C A R D   I N P U T   D A T A

P A G E   1

```
     5    10    15    20    25    30    35    40    45    50    55    60    65    70    75    80
--------------------------------------------------------------------------------
TITLE,CURVED PRESSURE TUBE SPECIMEN KSUBI CALCULATIONS
SIZING,40000,138,800,457,0,21,
INPUT TAPE,1,
MESH PLOT,1,
ALL POINTS
LOAD COR
TAPES,22,1000,
TAPES,24,2000,
ELSTO
VECSTO
ECS,45,
FORCDT,182,
RESTART
J-INT,237,2,3,
END
NEW
CONNECTIVITY
138,1,
COORDINATES
3,800,1,
UFXORD
1 TO 800 BY 1
DEFINE    NODE SET XLIG
726,727,728,729,730,731,732,733,734,735,736,737,738,739,740,CONTINUE
741,742,743,744,745,746,747,748,749,750,751,752,753,754,755,CONTINUE
756,757,758,759,760,761,762,763,764,765,766,768,769,771,772,CONTINUE
774,775,797,798,799,800,
DEFINE    NCDE SET ZEDGE
42,47,50,55,58,63,66,71,74,77,80,83,88,91,96,CONTINUE
99,104,107,112,115,118,121,124,129,132,137,140,145,148,411,CONTINUE
412,413,414,415,416,417,418,419,420,421,447,451,458,462,469,CONTINUE
473,480,484,488,492,496,
DEFINE    NCDE SET NIDPH
1,2,3,4,5,8,13,16,21,24,29,30,31,32,35,CONTINUE
38,41,42,43,44,45,46,49,54,57,62,65,70,71,72,CONTINUE
73,83,84,85,86,87,112,113,114,124,125,126,127,128,153,CONTINUE
154,155,165,166,167,168,169,194,195,196,206,207,208,209,210,CONTINUE
235,236,237,247,248,249,250,251,276,277,278,288,289,290,291,CONTINUE
292,295,300,303,308,311,316,317,318,319,322,325,328,329,330,CONTINUE
340,344,345,355,359,360,370,371,381,385,386,396,400,401,411,CONTINUE
412,422,426,430,431,441,442,443,444,445,446,447,481,482,483,CONTINUE
484,497,498,499,500,501,502,530,531,532,542,543,544,545,546,CONTINUE
547,575,576,577,587,588,589,590,591,592,620,621,622,632,633,CONTINUE
634,635,636,637,665,666,667,677,678,679,680,681,682,710,711,CONTINUE
712,713,726,727,728,729,730,731,732,766,767,777,781,785,789,CONTINUE
--------------------------------------------------------------------------------
     5    10    15    20    25    30    35    40    45    50    55    60    65    70    75    80
```

```
    5   10   15   20   25   30   35   40   45   50   55   60   65   70   75   80
--------------------------------------------------------------------------------
793,797,
FORCOT
NIDPH
UDUMP
112,138,726,800,
PROPERTY
1,
95000,.38,,,,800,
1 TO 138
WORK HARD
2,
1666.67,0,
0,.03
PRINT CHOICE
1,6,1,
133,138,
5,70,292,328,447,447,480,480,726,775,797,800,
14,
BOUNDARY CONDITIONS
3,
0,
1,
XLIG AND NIDPH
0,
2,
NIDPH
0,
3,
ZEDGE
J-INTEGRAL
2,
0,0,.001
766,768,769,771,772,774,775,
0,0,.00075
767,770,773,776,777,778,779,780,781,782,783,784,785,786,787,CONTINUE
788,789,790,791,792,793,794,795,796,797,798,799,800,
2,
0,0,.001
441,448,452,459,463,470,474,481,485,489,493,497,503,506,512,CONTINUE
515,521,524,530,533,536,539,542,548,551,557,560,566,569,575,CONTINUE
578,581,584,587,593,596,602,605,611,614,620,623,626,629,632,CONTINUE
638,641,647,650,656,659,665,668,671,674,677,683,686,692,695,CONTINUE
701,704,710,714,718,722,726,733,737,744,748,755,759,766,767,CONTINUE
768,769,770,771,772,773,774,775,776,777,778,779,780,781,782,CONTINUE
783,784,785,786,787,788,789,790,791,792,793,794,795,796,797,CONTINUE
798,799,800,
0,0,.0005
442,453,464,475,498,507,516,525,543,552,561,570,588,597,606,CONTINUE
615,633,642,651,660,678,687,696,705,727,738,749,760,
2,
--------------------------------------------------------------------------------
    5   10   15   20   25   30   35   40   45   50   55   60   65   70   75   80
```

```
     5   10   15   20   25   30   35   40   45   50   55   60   65   70   75   80
--------------------------------------------------------------------------------
0,0,.001
441,442,443,448,449,452,453,454,459,460,463,464,465,470,471,CONTINUE
474,475,476,481,482,485,486,489,490,493,494,497,498,499,503,CONTINUE
504,506,507,508,512,513,515,516,517,521,522,524,525,526,530,CONTINUE
531,533,534,536,537,539,540,542,543,544,548,549,551,552,553,CONTINUE
557,558,560,561,562,566,567,569,570,571,575,576,578,579,581,CONTINUE
582,584,585,587,588,589,593,594,596,597,598,602,603,605,606,CONTINUE
607,611,612,614,615,616,620,621,623,624,626,627,629,630,632,CONTINUE
633,634,638,639,641,642,643,647,648,650,651,652,656,657,659,CONTINUE
660,661,665,666,668,669,671,672,674,675,677,678,679,683,684,CONTINUE
686,687,688,692,693,695,696,697,701,702,704,705,706,710,711,CONTINUE
714,715,718,719,722,723,726,727,728,733,734,737,738,739,744,CONTINUE
745,748,749,750,755,756,759,760,761,766,767,768,769,770,771,CONTINUE
772,773,774,775,776,777,778,779,780,781,782,783,784,785,786,CONTINUE
787,788,789,790,791,792,793,794,795,796,797,798,799,800,
0,0,.0005
444,455,466,477,500,509,518,527,545,554,563,572,590,599,608,CONTINUE
617,635,644,653,662,680,689,698,707,729,740,751,762,
CONTROL
20,3,0,0,
.1,
RESTART
3,,4,
OPTIMIZE,1,
150,,,,300,
END OPTION
AUTO LOAD
1,
CONTINUE
PLOT TYPE
1,
0,1000,0,
SECTIONING
1,
70,79,88,97,106,115,122,125,128,131,134,137,
SCALING
1,
10,10,
CONTOURS
11,2,5,5,1,4,,,1,
0,800,
SLICE
1,
5,
70,79,88,97,106,115,122,125,128,131,134,137,
TITLE
X-DIR. STRESS/MID-WALL/.2514DEG
CONTINUE
END PLOT
1,
--------------------------------------------------------------------------------
     5   10   15   20   25   30   35   40   45   50   55   60   65   70   75   80
```

STRAIN ENERGY DIFFERENCE FOR J-INTEGRAL ESTIMATION -

EVALUATION NUMBER	STRAIN ENERGY DIFFERENCE
1	.9993E-01
2	.9458E-01
3	-.3082E-02

	TRESCA INTENSITY	MISES INTENSITY	MEAN NORMAL INTENSITY	PRINCIPAL VALUES MINIMUM	INTERMEDIATE	MAXIMUM	PHYSICAL COMPONENTS 1	2	3	4	5	6
ELEMENT 133 POINT 14												
STRESS	9.091E+02	8.208E+02	1.368E+03	9.908E+02	1.213E+03	1.900E+03	1.895E+03	1.213E+03	9.962E+02	5.202E+00	-1.085E+01	6.648E+01
STRAIN	3.329E-02	2.097E-02	3.456E-03	-9.779E-03	-3.362E-03	2.351E-02	2.323E-02	-3.384E-03	-9.474E-03	3.674E-04	-7.333E-04	6.101E-03
PLAS.ST	2.010E-02	1.247E-02	-9.252E-18	-7.764E-03	-4.571E-03	1.233E-02	1.212E-02	-4.586E-03	-7.530E-03	2.162E-04	-4.182E-04	4.170E-03
ELEMENT 134 POINT 14												
STRESS	9.013E+02	8.201E+02	1.312E+03	9.448E+02	1.144E+03	1.846E+03	1.842E+03	1.131E+03	9.624E+02	1.487E+01	-4.878E+01	6.177E+01
STRAIN	3.243E-02	2.051E-02	3.313E-03	-9.433E-03	-3.629E-03	2.300E-02	2.275E-02	-4.134E-03	-8.680E-03	8.520E-04	-3.218E-03	5.566E-03
PLAS.ST	1.936E-02	1.205E-02	-9.252E-18	-7.432E-03	-4.499E-03	1.193E-02	1.174E-02	-4.820E-03	-6.922E-03	4.199E-04	-1.801E-03	3.771E-03
ELEMENT 135 POINT 14												
STRESS	8.612E+02	8.237E+02	1.062E+03	7.479E+02	8.291E+02	1.609E+03	1.604E+03	8.077E+02	7.748E+02	5.354E+01	-3.476E+01	4.206E+01
STRAIN	3.461E-02	2.246E-02	2.683E-03	-9.854E-03	-6.853E-03	2.476E-02	2.444E-02	-8.293E-03	-8.101E-03	4.288E-03	-2.688E-03	4.951E-03
PLAS.ST	2.221E-02	1.418E-02	-3.701E-17	-8.068E-03	-6.069E-03	1.414E-02	1.389E-02	-7.282E-03	-6.611E-03	2.733E-03	-1.678E-03	3.729E-03
ELEMENT 136 POINT 14												
STRESS	9.035E+02	8.019E+02	1.244E+03	8.512E+02	1.127E+03	1.755E+03	1.743E+03	8.512E+02	1.139E+03	-1.018E+00	1.166E+00	8.390E+01
STRAIN	1.507E-02	9.963E-03	3.144E-03	-3.425E-03	1.208E-03	1.165E-02	1.145E-02	-3.425E-03	1.402E-03	-2.680E-05	2.791E-05	2.822E-03
PLAS.ST	1.949E-03	1.150E-03	2.602E-18	-8.568E-04	-2.358E-04	1.093E-03	1.064E-03	-8.568E-04	-2.074E-04	2.768E-06	-5.948E-06	3.841E-04
ELEMENT 137 POINT 14												
STRESS	9.185E+02	8.028E+02	1.180E+03	7.570E+02	1.108E+03	1.676E+03	1.665E+03	7.717E+02	1.104E+03	5.268E-01	-7.064E+01	7.820E+01
STRAIN	1.624E-02	1.036E-02	2.982E-03	-4.504E-03	1.714E-03	1.173E-02	1.153E-02	-4.252E-03	1.662E-03	1.415E-05	-2.465E-03	2.827E-03
PLAS.ST	2.896E-03	1.687E-03	3.469E-18	-1.338E-03	-2.200E-04	1.558E-03	1.514E-03	-1.299E-03	-2.149E-04	-1.155E-06	-4.124E-04	5.550E-04
ELEMENT 138 POINT 14												
STRESS	9.330E+02	8.081E+02	9.950E+02	5.334E+02	9.853E+02	1.466E+03	1.458E+03	5.336E+02	9.934E+02	1.240E+01	5.770E+00	6.208E+01
STRAIN	2.198E-02	1.318E-02	2.514E-03	-8.423E-03	2.411E-03	1.355E-02	1.332E-02	-8.417E-03	2.643E-03	6.786E-04	2.499E-04	3.180E-03
PLAS.ST	8.428E-03	4.866E-03	1.446E-18	-4.232E-03	3.529E-05	4.196E-03	4.076E-03	-4.228E-03	1.524E-04	3.185E-04	8.226E-05	1.376E-03

N O D A L   P O I N T   D A T A

I N C R E M E N T A L   D I S P L A C E M E N T S

5	3.44000E-02	-3.84445E-03	-1.70838E-03	6	2.49181E-02	-5.11577E-03	1.37692E-03
7	2.97474E-02	-4.65917E-03	1.60481E-04	8	3.48787E-02	-4.28712E-03	-1.72093E-03
9	2.48463E-02	-5.44583E-03	1.39324E-03	10	2.71913E-02	-5.15841E-03	1.05513E-03
11	3.01883E-02	-5.04746E-03	1.49702E-04	12	3.41094E-02	-5.78142E-03	-8.21907E-04
13	3.53227E-02	-4.69520E-03	-1.72918E-03	14	2.48318E-02	-5.97546E-03	1.40885E-03
15	3.06076E-02	-5.37058E-03	1.38537E-04	16	3.57668E-02	-5.10192E-03	-1.73846E-03
17	2.48440E-02	-6.55817E-03	1.43629E-03	18	2.75127E-02	-6.13386E-03	1.06715E-03
19	3.10810E-02	-5.75891E-03	1.29250E-04	20	3.54355E-02	-6.23278E-03	-8.73065E-04
21	3.62122E-02	-5.50744E-03	-1.75396E-03	22	2.48592E-02	-7.29225E-03	1.45902E-03
23	3.16609E-02	-6.25137E-03	1.23975E-04	24	3.66599E-02	-5.91184E-03	-1.77514E-03
25	2.49076E-02	-8.02349E-03	1.48941E-03	26	2.81060E-02	-7.46447E-03	1.10602E-03
27	3.23212E-02	-6.91403E-03	1.23157E-04	28	3.67656E-02	-6.82622E-03	-9.26723E-04
29	3.71078E-02	-6.31491E-03	-1.80483E-03	30	2.19000E-02	5.71726E-04	-2.84591E-03
31	2.69000E-02	-4.78690E-04	-1.90800E-03	32	3.47000E-02	-3.59107E-03	-1.25576E-05
33	2.24331E-02	-3.48106E-04	-2.85946E-03	34	2.74250E-02	-1.13486E-03	-1.84979E-03
35	3.56056E-02	-4.44692E-03	-6.84079E-05	36	2.28688E-02	-1.16137E-03	-2.82725E-03
37	2.81265E-02	-1.92323E-03	-1.87031E-03	38	3.64818E-02	-5.26952E-03	-1.74271E-04
39	2.32924E-02	-1.96614E-03	-2.62183E-03	40	2.88279E-02	-2.92007E-03	-2.04932E-03
41	3.73620E-02	-6.08943E-03	-1.45343E-04	42	1.90000E-02	5.63795E-03	0.
43	2.08000E-02	5.79453E-03	-4.45045E-04	44	2.30000E-02	5.54973E-03	-5.97421E-04
45	2.66000E-02	3.84453E-03	-9.48213E-04	46	3.55000E-02	-3.06957E-03	-2.66007E-03
47	1.92624E-02	5.43404E-03	0.	48	2.31700E-02	5.02136E-03	-6.01371E-04
49	3.58695E-02	-3.40153E-03	-2.54452E-03	50	1.95127E-02	5.23899E-03	0.
51	2.13041E-02	5.04477E-03	-4.38051E-04	52	2.32832E-02	4.57548E-03	-6.26231E-04
53	2.76344E-02	2.67211E-03	-9.71589E-04	54	3.63050E-02	-3.81514E-03	-2.43087E-03
55	1.97897E-02	5.03163E-03	0.	56	2.34530E-02	4.11468E-03	-6.46490E-04
57	3.67407E-02	-4.22737E-03	-2.28359E-03	58	2.00645E-02	4.83926E-03	0.
59	2.17305E-02	4.41153E-03	-4.11818E-04	60	2.35668E-02	3.72249E-03	-6.79249E-04
61	2.83245E-02	2.02010E-03	-1.04891E-03	62	3.71771E-02	-4.63887E-03	-2.15607E-03
63	2.03098E-02	4.63480E-03	0.	64	2.36711E-02	3.28479E-03	-6.91572E-04
65	3.76149E-02	-5.05027E-03	-2.36764E-03	66	2.05389E-02	4.44272E-03	0.
67	2.20859E-02	3.93203E-03	-3.78194E-04	68	2.37163E-02	2.93273E-03	-6.90838E-04
69	2.89178E-02	1.74338E-03	-1.59661E-03	70	3.80528E-02	-5.46029E-03	-2.80545E-03

T O T A L   D I S P L A C E M E N T S

5	.17266	-1.87796E-02	-7.50556E-03	6	.12646	-2.71781E-02	7.24251E-03
7	.14988	-2.43001E-02	1.13971E-03	8	.17471	-2.11630E-02	-7.59895E-03
9	.12609	-2.91346E-02	7.31391E-03	10	.13725	-2.74582E-02	5.40708E-03
11	.15179	-2.61512E-02	1.11168E-03	12	.17050	-2.86501E-02	-3.57736E-03
13	.17694	-2.32028E-02	-7.71118E-03	14	.12615	-3.19483E-02	7.38906E-03
15	.15377	-2.78047E-02	1.05217E-03	16	.17916	-2.52357E-02	-7.84478E-03
17	.12631	-3.49491E-02	7.50681E-03	18	.13922	-3.24018E-02	5.45836E-03
19	.15599	-2.97942E-02	9.95660E-04	20	.17638	-3.12467E-02	-3.83589E-03
21	.18140	-2.72626E-02	-7.99083E-03	22	.12656	-3.85531E-02	7.59783E-03
23	.15865	-3.22028E-02	9.57284E-04	24	.18364	-2.92839E-02	-8.10784E-03
25	.12692	-4.20893E-02	7.73703E-03	26	.14221	-3.89147E-02	5.58473E-03
27	.16166	-3.53566E-02	9.12882E-04	28	.18242	-3.45660E-02	-4.13189E-03
29	.18589	-3.12985E-02	-8.26373E-03	30	.11439	-3.55276E-03	-1.15963E-02
31	.13777	-6.39654E-03	-8.20042E-03	32	.17409	-1.75269E-02	-4.21321E-04
33	.11649	-8.37824E-03	-1.16733E-02	34	.14078	-1.00995E-02	-8.05654E-03
35	.17835	-2.19569E-02	-4.31179E-04	36	.11865	-1.28004E-02	-1.14998E-02
37	.14429	-1.41614E-02	-8.13926E-03	38	.18275	-2.60688E-02	-9.62641E-04
39	.12086	-1.69680E-02	-1.06343E-02	40	.14790	-1.90596E-02	-8.84859E-03
41	.18716	-3.01671E-02	-1.17618E-03	42	.10239	1.73186E-02	0.
43	.11048	1.82880E-02	-2.06142E-03	44	.12181	1.91137E-02	-3.33615E-03
45	.13889	1.32664E-02	-6.57202E-03	46	.17750	-1.45519E-02	-7.88083E-03
47	.10350	1.61045E-02	0.	48	.12312	1.62994E-02	-3.45136E-03
49	.17966	-1.67193E-02	-7.38619E-03	50	.10462	1.48543E-02	0.
51	.11326	1.47067E-02	-1.95990E-03	52	.12416	1.38657E-02	-3.62840E-03

[illegible]	[illegible]	[illegible]	[illegible]				
43	.12048	[illegible]	-1.17618E-03	44	.14790	[illegible]	[illegible]
45	.13889	1.82080E-02	-2.06142E-03	46	.10230	[illegible]	[illegible]
47	[illegible]	1.32664E-02	-6.57202E-03	48	[illegible]	[illegible]	[illegible]
49	[illegible]	[illegible]	[illegible]	50	[illegible]	[illegible]	[illegible]
51	.11326	[illegible]	[illegible]	52	[illegible]	[illegible]	[illegible]
53	.14359	7.44327E-03	-6.74689E-03	54	[illegible]	[illegible]	[illegible]
55	.10585	1.35662E-02	0.	56	.12526	1.16186E-02	-3.71196E-03
57	.18403	-2.08474E-02	-6.67225E-03	58	.10709	1.23102E-02	0.
59	.11572	1.14002E-02	-1.87424E-03	60	.12611	9.68770E-03	-3.83922E-03
61	.14709	3.75174E-03	-7.22985E-03	62	.18622	-2.29043E-02	-6.46312E-03
63	.10827	1.09813E-02	0.	64	.12696	7.55583E-03	-3.91992E-03
65	.18842	-2.49608E-02	-7.26343E-03	66	.10938	9.71387E-03	0.
67	.11781	8.56305E-03	-1.71488E-03	68	.12757	5.76200E-03	-3.99545E-03
69	.15016	1.54607E-03	-9.12793E-03	70	.19061	-2.70103E-02	-8.80956E-03

TOTAL EQUIVALENT NODAL FORCES (DISTRIBUTED PLUS POINT LOADS)

5	0.	0.	0.	6	0.	0.	0.
7	0.	0.	0.	8	0.	0.	0.
9	0.	0.	0.	10	0.	0.	0.
11	0.	0.	0.	12	0.	0.	0.
13	0.	0.	0.	14	0.	0.	0.
15	0.	0.	0.	16	0.	0.	0.
17	0.	0.	0.	18	0.	0.	0.
19	0.	0.	0.	20	0.	0.	0.
21	0.	0.	0.	22	0.	0.	0.
23	0.	0.	0.	24	0.	0.	0.
25	0.	0.	0.	26	0.	0.	0.
27	0.	0.	0.	28	0.	0.	0.
29	0.	0.	0.	30	0.	0.	0.
31	0.	0.	0.	32	0.	0.	0.
33	0.	0.	0.	34	0.	0.	0.
35	0.	0.	0.	36	0.	0.	0.
37	0.	0.	0.	38	0.	0.	0.
39	0.	0.	0.	40	0.	0.	0.
41	0.	0.	0.	42	0.	0.	0.
43	0.	0.	0.	44	0.	0.	0.
45	0.	0.	0.	46	0.	0.	0.
47	0.	0.	0.	48	0.	0.	0.
49	0.	0.	0.	50	0.	0.	0.
51	0.	0.	0.	52	0.	0.	0.
53	0.	0.	0.	54	0.	0.	0.
55	0.	0.	0.	56	0.	0.	0.
57	0.	0.	0.	58	0.	0.	0.
59	0.	0.	0.	60	0.	0.	0.
61	0.	0.	0.	62	0.	0.	0.
63	0.	0.	0.	64	0.	0.	0.
65	0.	0.	0.	66	0.	0.	0.
67	0.	0.	0.	68	0.	0.	0.
69	0.	0.	0.	70	0.	0.	0.

REACTION FORCES AT FIXED BOUNDARY CONDITIONS, RESIDUAL LOAD CORRECTION ELSEWHERE

5	359.93	61.408	3.7426	6	1.67620E-09	-8.62997E-10	2.40107E-10
7	.37374	-.36387	-.49196	8	323.59	-1456.7	-3.3583
9	-5.22505E-09	5.38421E-10	-4.77485E-12	10	4.82260E-10	1.92813E-09	7.09406E-11
11	-2.1764	2.3457	2.1563	12	2.1414	-2.3453	-2.5129
13	177.64	290.64	7.0923	14	4.12382E-09	1.19223E-09	-1.23691E-10
15	.02456	-.69524	-.47130	16	711.89	-1099.1	-3.0836
17	2.79397E-09	-4.00178E-11	1.17552E-10	18	-1.26624E-09	4.91127E-11	-4.36557E-11
19	-2.3067	3.0169	2.1335	20	2.4010	-3.1375	-2.4629
21	22[illegible].16	254.56	7.1316	22	3.03623E-09	6.23913E-10	6.54836E-11

19	-2.3087	3.0169	2.1335	20	2.4010	-3.1375	-2.4829
21	229.16	254.56	7.1316	22	3.03623E-09	6.23913E-10	6.54836E-11
23	.30405	-.53608	-.50733	24	475.50	-1104.8	-3.5463
25	4.38945E-10	2.11912E-10	-1.28011E-10	26	8.29004E-10	-7.55563E-10	-1.00044E-10
27	-.42741	.91781	1.0418	28	.31912	-.79250	-1.1954
29	95.788	-370.56	3.6555	30	93.232	353.37	9.86233E-12
31	-29.399	-237.61	-2.0926	32	1605.4	1094.2	-12.449
33	1.44291E-09	-6.73026E-11	1.66892E-10	34	1.8640	-2.0790	-5.2724
35	404.48	-766.38	-32.670	36	-2.06705E-09	-1.10958E-10	4.54747E-11
37	1.9883	-2.3962	-5.6873	38	274.76	-879.03	-36.279
39	-7.70001E-10	-1.28352E-10	-5.79803E-12	40	.50954	-.99176	-2.0410
41	-815.30	-1500.8	-12.577	42	50.724	94.222	324.45
43	-92.634	163.28	-1.25056E-10	44	-237.26	-90.363	2.5090
45	-182.83	2066.0	-1.8044	46	856.86	-590.19	9.5968
47	-5.04185E-10	1.39516E-09	460.02	48	3.2579	-2.2929	-1.0728
49	1802.6	-2130.2	9.7898	50	6.44832E-10	-7.33507E-10	492.61
51	-9.71340E-10	-1.04501E-09	5.54792E-11	52	-6.2608	4.4380	4.3983
53	15.438	-12.658	-1.9992	54	1003.4	-806.17	23.468
55	1.70320E-09	3.96540E-10	507.17	56	3.2171	-3.0511	-.37994
57	1961.2	-1947.5	11.520	58	1.51113E-09	1.25328E-09	475.77
59	-5.94810E-10	1.34605E-10	1.65528E-10	60	-4.5993	5.4971	3.4982
61	11.300	-14.983	-.62487	62	1136.1	-739.48	24.214
63	2.76395E-09	1.17871E-09	504.21	64	1.9001	-3.3214	3.12257E-02
65	1541.2	-1813.6	9.4904	66	-7.23048E-10	4.46562E-10	231.25
67	2.72848E-11	-8.54925E-11	-5.91172E-11	68	-.79583	.77378	1.6163
69	-1.6493	-1.2973	-2.2762	70	759.78	-589.09	7.7607

I N C R E M E N T A L   D I S P L A C E M E N T S

292	3.55000E-02	-3.06957E-03	-7.14691E-04	293	1.39446E-02	1.44053E-02	9.83578E-03
294	2.09262E-02	8.03474E-03	-1.99561E-05	295	3.58695E-02	-3.40153E-03	-8.96824E-04
296	1.40255E-02	1.42221E-02	9.85077E-03	297	1.77863E-02	1.02787E-02	4.01406E-03
298	2.09811E-02	7.62304E-03	-2.52531E-05	299	2.62676E-02	4.56422E-03	-1.46156E-03
300	3.63050E-02	-3.81514E-03	-1.08168E-03	301	1.41413E-02	1.40075E-02	9.87452E-03
302	2.11479E-02	7.13526E-03	-4.45758E-05	303	3.67407E-02	-4.22737E-03	-1.28811E-03
304	1.42817E-02	1.37659E-02	9.87391E-03	305	1.80946E-02	9.63114E-03	3.95620E-03
306	2.12559E-02	6.72838E-03	-5.28046E-05	307	2.71298E-02	3.96840E-03	-1.47395E-03
308	3.71771E-02	-4.63887E-03	-1.47871E-03	309	1.43940E-02	1.34949E-02	9.87483E-03
310	2.13747E-02	6.25972E-03	-7.03605E-05	311	3.76149E-02	-5.05027E-03	-1.23244E-03
312	1.45063E-02	1.32083E-02	9.86088E-03	313	1.83798E-02	9.08004E-03	3.82857E-03
314	2.14475E-02	5.85946E-03	-1.00431E-04	315	2.79511E-02	3.70947E-03	-1.01898E-03
316	3.80528E-02	-5.46029E-03	-7.84873E-04	317	2.05000E-02	3.02185E-03	7.70570E-03
318	2.60000E-02	7.86174E-04	2.21357E-03	319	3.47000E-02	-3.59107E-03	-3.61496E-03
320	2.07143E-02	2.14157E-03	7.74030E-03	321	2.64821E-02	3.81221E-05	2.10558E-03
322	3.56056E-02	-4.44692E-03	-3.59310E-03	323	2.09632E-02	1.23813E-03	7.77029E-03
324	2.71681E-02	-8.41938E-04	2.07251E-03	325	3.64818E-02	-5.26952E-03	-3.54653E-03
326	2.12355E-02	3.04948E-04	7.64843E-03	327	2.78677E-02	-1.93194E-03	2.21322E-03
328	3.73620E-02	-6.08943E-03	-3.64789E-03				

T O T A L   D I S P L A C E M E N T S

292	.17750	-1.45519E-02	-9.80897E-03	293	7.79679E-02	5.88519E-02	4.54771E-02
294	.11173	3.15892E-02	1.95100E-03	295	.17966	-1.67193E-02	-1.05487E-02
296	7.81082E-02	5.78831E-02	4.54165E-02	297	9.55503E-02	4.06947E-02	1.98504E-02
298	.11262	2.91561E-02	1.97829E-03	299	.13716	1.60765E-02	-4.84009E-03
300	.18185	-1.87868E-02	-1.11800E-02	301	7.85448E-02	5.66457E-02	4.54913E-02
302	.11364	2.68218E-02	1.91149E-03	303	.18403	-2.08474E-02	-1.18302E-02
304	7.91023E-02	5.52714E-02	4.54979E-02	305	9.73777E-02	3.73378E-02	1.95731E-02
306	.11442	2.48379E-02	1.89833E-03	307	.14119	1.27393E-02	-4.77107E-03
308	.18622	-2.29043E-02	-1.23949E-02	309	7.96408E-02	5.37369E-02	4.55346E-02
[illegible]	[illegible]	[illegible]	[illegible]	[illegible]	[illegible]	[illegible]	[illegible]

[illegible]	[illegible]	[illegible]	[illegible]	[illegible]	[illegible]	[illegible]	[illegible]
306	.11442	2.48379E-02	1.89833E-03	307	.14119	1.27393E-02	-4.77107E-03
308	.18622	-2.29043E-02	-1.23949E-02	309	7.96408E-02	5.37369E-02	4.55346E-02
310	.11527	2.26004E-02	1.83358E-03	311	.18842	-2.49608E-02	-1.17714E-02
312	8.02044E-02	5.21528E-02	4.54524E-02	313	9.90437E-02	3.42673E-02	1.90842E-02
314	.11590	2.06516E-02	1.82137E-03	315	.14487	1.09836E-02	-3.17027E-03
316	.19061	-2.70103E-02	-1.04416E-02	317	.10729	8.79870E-03	3.57441E-02
318	.13387	-9.43111E-04	1.04565E-02	319	.17409	-1.75269E-02	-1.58463E-02
320	.10804	4.18543E-03	3.59256E-02	321	.13668	-4.68463E-03	1.00391E-02
322	.17835	-2.19569E-02	-1.61728E-02	323	.10935	-5.87272E-04	3.60679E-02
324	.14010	-8.89623E-03	9.90260E-03	325	.18275	-2.60688E-02	-1.61430E-02
326	.11087	-5.20771E-03	3.56092E-02	327	.14372	-1.41371E-02	1.04344E-02
328	.18716	-3.01671E-02	-1.65690E-02				

TOTAL EQUIVALENT NODAL FORCES (DISTRIBUTED PLUS POINT LOADS)

292	0.	0.	0.	293	0.	0.	0.
294	0.	0.	0.	295	0.	0.	0.
296	0.	0.	0.	297	0.	0.	0.
298	0.	0.	0.	299	0.	0.	0.
300	0.	0.	0.	301	0.	0.	0.
302	0.	0.	0.	303	0.	0.	0.
304	0.	0.	0.	305	0.	0.	0.
306	0.	0.	0.	307	0.	0.	0.
308	0.	0.	0.	309	0.	0.	0.
310	0.	0.	0.	311	0.	0.	0.
312	0.	0.	0.	313	0.	0.	0.
314	0.	0.	0.	315	0.	0.	0.
316	0.	0.	0.	317	0.	0.	0.
318	0.	0.	0.	319	0.	0.	0.
320	0.	0.	0.	321	0.	0.	0.
322	0.	0.	0.	323	0.	0.	0.
324	0.	0.	0.	325	0.	0.	0.
326	0.	0.	0.	327	0.	0.	0.
328	0.	0.	0.				

REACTION FORCES AT FIXED BOUNDARY CONDITIONS, RESIDUAL LOAD CORRECTION ELSEWHERE

292	1148.8	-633.92	-2.3975	293	5.78530E-09	3.90719E-09	7.48287E-10
294	2.9486	-2.0221	.53409	295	2050.5	-2416.4	-5.6298
296	-4.53088E-09	-2.29898E-09	-7.23048E-10	297	-1.22600E-09	1.81535E-09	-1.81899E-10
298	-6.9287	5.7960	-.40740	299	13.516	-11.425	-1.1347
300	1160.0	-934.27	-8.8171	301	1.25465E-09	2.69711E-09	2.46473E-10
302	4.2184	-4.9610	-1.4420	303	2189.0	-2224.8	-9.1251
304	-5.22596E-09	1.11140E-09	-2.13277E-10	305	-2.85354E-09	-9.80435E-10	-1.32786E-10
306	-9.1916	10.196	3.5759	307	5.3538	-12.775	-9.2662
308	1333.5	-837.81	-7.8705	309	2.93551E-09	2.38424E-09	2.14982E-10
310	1.6939	-3.8543	4.8175	311	1633.3	-2073.0	-18.326
312	-2.85945E-09	-3.32420E-10	-1.78261E-10	313	4.22517E-10	1.03910E-10	3.05590E-10
314	-2.9462	1.1341	-3.39698E-02	315	-19.707	18.812	12.129
316	785.62	-752.65	-1.5946	317	197.33	190.75	8.66365E-11
318	-182.90	-168.61	.91574	319	1920.8	1435.3	4.4738
320	1.29239E-09	-7.59428E-10	-9.32232E-11	321	.77754	-.78178	2.9949
322	387.15	-826.39	17.844	323	9.86802E-11	2.55568E-10	-2.13731E-10
324	.88953	-1.3266	3.4495	325	224.37	-944.41	21.703
326	-1.16989E-09	4.54747E-12	1.04720E-10	327	-2.33314E-02	-6.28086E-02	.97860
328	-1075.1	-1769.5	5.1963				

I N C R E M E N T A L   D I S P L A C E M E N T S

447 1.80000E-02 3.01822E-02 0.

T O T A L   D I S P L A C E M E N T S

447 9.80000E-02 .15162 0.

TOTAL EQUIVALENT NODAL FORCES (DISTRIBUTED PLUS POINT LOADS)

447 0. 0. 0.

REACTION FORCES AT FIXED BOUNDARY CONDITIONS, RESIDUAL LOAD CORRECTION ELSEWHERE

447 -5.3760 11.525 -116.02

I N C R E M E N T A L   D I S P L A C E M E N T S

480 1.92475E-02 3.11148E-02 0.

T O T A L   D I S P L A C E M E N T S

480 .10551 .15696 0.

TOTAL EQUIVALENT NODAL FORCES (DISTRIBUTED PLUS POINT LOADS)

480 0. 0. 0.

REACTION FORCES AT FIXED BOUNDARY CONDITIONS, RESIDUAL LOAD CORRECTION ELSEWHERE

480 -1.03668E-11 -9.87392E-10 -116.17

I N C R E M E N T A L   D I S P L A C E M E N T S

I N C R E M E N T A L   D I S P L A C E M E N T S

726	0.	3.01940E-02	-8.83580E-03	727	0.	3.01940E-02	-8.30482E-03
728	0.	3.01940E-02	-8.14494E-03	729	0.	3.01940E-02	-8.29717E-03
730	0.	3.01940E-02	-8.62344E-03	731	0.	3.01940E-02	-9.00652E-03
732	0.	3.01940E-02	-9.39588E-03	733	0.	2.96195E-02	-8.78334E-03
734	0.	2.98833E-02	-8.14826E-03	735	0.	3.00185E-02	-8.62999E-03
736	0.	3.00959E-02	-9.40192E-03	737	0.	2.89905E-02	-8.70698E-03
738	0.	2.92839E-02	-8.33487E-03	739	0.	2.95830E-02	-8.17467E-03
740	0.	2.97403E-02	-8.31835E-03	741	0.	2.98449E-02	-8.65480E-03
742	0.	2.99126E-02	-9.03047E-03	743	0.	3.00050E-02	-9.41349E-03
744	0.	2.82595E-02	-8.65963E-03	745	0.	2.92777E-02	-8.21977E-03
746	0.	2.96666E-02	-8.69175E-03	747	0.	2.99026E-02	-9.43919E-03
748	0.	2.75133E-02	-8.62520E-03	749	0.	2.83565E-02	-8.36588E-03
750	0.	2.89850E-02	-8.29069E-03	751	0.	2.92882E-02	-8.42712E-03
752	0.	2.94895E-02	-8.74118E-03	753	0.	2.96328E-02	-9.10023E-03
754	0.	2.98063E-02	-9.47821E-03	755	0.	2.67293E-02	-8.58589E-03
756	0.	2.87028E-02	-8.40443E-03	757	0.	2.93193E-02	-8.79983E-03
758	0.	2.97117E-02	-9.52940E-03	759	0.	2.60916E-02	-8.82643E-03
760	0.	2.75932E-02	-8.72862E-03	761	0.	2.84206E-02	-8.54522E-03
762	0.	2.88594E-02	-8.59819E-03	763	0.	2.91585E-02	-8.86552E-03
764	0.	2.93629E-02	-9.22227E-03	765	0.	2.96224E-02	-9.60281E-03
766	0.	3.01940E-02	-8.25140E-03	767	6.80000E-03	3.01973E-02	-7.58425E-03
768	0.	2.95838E-02	-8.36793E-03	769	0.	2.93343E-02	-8.45670E-03
770	6.81318E-03	2.95537E-02	-7.79734E-03	771	0.	2.90560E-02	-8.37745E-03
772	0.	2.81690E-02	-8.34783E-03	773	6.67527E-03	2.87682E-02	-7.92477E-03
774	0.	2.67956E-02	-8.55308E-03	775	0.	2.52479E-02	-7.89660E-03

T O T A L   D I S P L A C E M E N T S

726	0.	.15165	-4.61325E-02	727	0.	.15165	-4.31330E-02
728	0.	.15165	-4.24240E-02	729	0.	.15165	-4.36271E-02
730	0.	.15165	-4.57966E-02	731	0.	.15165	-4.81926E-02
732	0.	.15165	-5.05611E-02	733	0.	.14909	-4.60813E-02
734	0.	.15005	-4.24342E-02	735	0.	.15057	-4.58066E-02
736	0.	.15092	-5.05714E-02	737	0.	.14639	-4.59458E-02
738	0.	.14724	-4.31310E-02	739	0.	.14849	-4.25345E-02
740	0.	.14911	-4.37551E-02	741	0.	.14953	-4.59094E-02
742	0.	.14985	-4.82539E-02	743	0.	.15024	-5.06109E-02
744	0.	.14327	-4.57251E-02	745	0.	.14690	-4.27041E-02
746	0.	.14849	-4.60711E-02	747	0.	.14956	-5.07282E-02
748	0.	.14004	-4.54507E-02	749	0.	.14275	-4.31601E-02
750	0.	.14538	-4.29909E-02	751	0.	.14663	-4.42224E-02
752	0.	.14748	-4.62870E-02	753	0.	.14813	-4.85664E-02
754	0.	.14892	-5.09083E-02	755	0.	.13660	-4.48516E-02
756	0.	.14392	-4.34538E-02	757	0.	.14650	-4.65550E-02
758	0.	.14829	-5.11515E-02	759	0.	.13368	-4.52329E-02
760	0.	.13890	-4.43632E-02	761	0.	.14250	-4.40762E-02
762	0.	.14428	-4.49628E-02	763	0.	.14557	-4.68401E-02
764	0.	.14650	-4.91141E-02	765	0.	.14770	-5.15002E-02
766	0.	.15165	-4.78495E-02	767	2.46000E-02	.15166	-4.66399E-02
768	0.	.14929	-4.79700E-02	769	0.	.14760	-4.80291E-02
770	2.48589E-02	.14831	-4.71321E-02	771	0.	.14605	-4.78680E-02
772	0.	.14293	-4.76883E-02	773	2.46326E-02	.14429	-4.72550E-02
774	0.	.13773	-4.81791E-02	775	0.	.13112	-4.49406E-02

TOTAL EQUIVALENT NODAL FORCES (DISTRIBUTED PLUS POINT LOADS)

726	0.	0.	0.	727	0.	0.	0.
728	0.	0.	0.	729	0.	0.	0.
730	0.	0.	0.	731	0.	0.	0.
732	0.	0.	0.	733	0.	0.	0.
734	0.	0.	0.	735	0.	0.	0.
736	0.	0.	0.	737	0.	0.	0.
738	0.	0.	0.	739	0.	0.	0.
740	0.	0.	0.	741	0.	0.	0.
742	0.	0.	0.	743	0.	0.	0.
744	0.	0.	0.	745	0.	0.	0.
746	0.	0.	0.	747	0.	0.	0.
748	0.	0.	0.	749	0.	0.	0.
750	0.	0.	0.	751	0.	0.	0.
752	0.	0.	0.	753	0.	0.	0.
754	0.	0.	0.	755	0.	0.	0.
756	0.	0.	0.	757	0.	0.	0.
758	0.	0.	0.	759	0.	0.	0.
760	0.	0.	0.	761	0.	0.	0.
762	0.	0.	0.	763	0.	0.	0.
764	0.	0.	0.	765	0.	0.	0.
766	0.	0.	0.	767	0.	0.	0.
768	0.	0.	0.	769	0.	0.	0.
770	0.	0.	0.	771	0.	0.	0.
772	0.	0.	0.	773	0.	0.	0.
774	0.	0.	0.	775	0.	0.	0.

REACTION FORCES AT FIXED BOUNDARY CONDITIONS, RESIDUAL LOAD CORRECTION ELSEWHERE

726	423.17	-38.001	-.26011	727	-1264.4	-11.672	-3.00417E-11
728	515.88	-87.010	-2.41016E-11	729	-871.64	150.60	5.56213E-11
730	351.59	-160.06	-5.10738E-11	731	-721.10	203.37	-3.75806E-11
732	171.86	-80.585	2.09784E-10	733	-2279.6	-5.59301E-02	-7.20122E-02
734	-1906.9	-2.25668E-11	1.40972E-10	735	-1446.5	-2.98030E-10	-1.19371E-10
736	-593.13	1.82308E-09	-1.99819E-10	737	822.37	-5.39407E-02	.91975
738	-2432.5	5.55929E-11	-1.34150E-11	739	1051.5	-7.99105E-10	1.69393E-10
740	-1615.1	-4.48381E-10	-4.07283E-11	741	728.14	-5.47971E-11	-2.34422E-10
742	-1317.3	8.64929E-10	2.89901E-12	743	354.19	-8.97444E-10	1.30427E-10
744	-2231.2	2.54732E-02	-.84070	745	-1887.0	3.51065E-10	-3.81988E-11
746	-1423.3	1.31593E-09	6.77574E-11	747	-582.41	-4.86011E-10	2.93269E-10
748	749.21	.13785	.89982	749	-2289.3	1.50408E-10	-2.13731E-11
750	1012.1	-1.17222E-09	1.53705E-10	751	-1561.8	3.34921E-10	-1.69308E-10
752	722.45	-4.11819E-09	6.90648E-11	753	-1279.3	7.99446E-10	-9.76286E-11
754	345.64	-1.89493E-09	-7.32996E-11	755	-1950.7	-.60521	-.41697
756	-1765.6	2.42204E-09	6.36646E-12	757	-1387.2	1.04342E-09	6.32099E-11
758	-566.23	2.59007E-09	4.02487E-10	759	422.64	.22253	.29252
760	-1037.8	1.06237E-10	4.06999E-11	761	482.34	-7.83956E-10	3.86535E-11
762	-761.67	6.73750E-10	-1.00613E-11	763	357.74	-3.73674E-10	1.66665E-10
764	-618.09	3.90393E-10	1.07264E-10	765	172.76	-6.75429E-10	-9.11626E-11
766	207.20	18.571	2.8619	767	-52.522	14.293	-.89135
768	-626.08	.17872	-4.7739	769	428.44	.14749	5.8089
770	1.4904	-6.13027E-02	-3.4217	771	-612.27	-.26638	-4.8874
772	389.68	-.81125	5.7090	773	1.6379	-.24318	-2.6566
774	-534.10	1.4354	-4.5815	775	191.13	-2.2109	2.6713

I N C R E M E N T A L   D I S P L A C E M E N T S

797	0.	3.01940E-02	-8.90629E-03	798	0.	2.91114E-02	-8.67010E-03
799	0.	2.76487E-02	-8.64573E-03	800	0.	2.46212E-02	-8.47233E-03

```
                         T O T A L   D I S P L A C E M E N T S

   797  0.              .15165     -4.78974E-02          798  0.              .14703     -4.75346E-02
   799  0.              .14123     -4.72013E-02          800  0.              .12973     -4.52960E-02


           TOTAL EQUIVALENT NODAL FORCES (DISTRIBUTED PLUS POINT LOADS)

   797  0.             0.         0.                    798  0.             0.            0.
   799  0.             0.         0.                    800  0.             0.            0.


           REACTION FORCES AT FIXED BOUNDARY CONDITIONS, RESIDUAL LOAD CORRECTION ELSEWHERE

   797  -770.23       -36.944       .25054              798  -1461.2      -1.86170E-02  -1.1269
   799  -1376.5     -5.51618E-03  -1.0941               800  -550.61       -.42906       -.40307
 REACTION FORCE OVER LIGAMENT =-29820.673 N


                       E N D   O F   I N C R E M E N T   5
                        TIME =    4811.60


 RESTART DATA AT INCREMENT   5.   0   ON TAPE  8
                       PLOT TYPE 1 - PERSPECTIVE 3-D PLOT
                       VIEW-POINT COORDINATES                        0.000     1000.000        0.000
                       DIRECTION PLOTTED ALONG HORIZONTAL AXIS       0.000        0.000        0.000
                       NUMBER OF ELEMENT SECTIONS  1
       A LIST OF ELEMENTS GIVEN BELOW
          70   79   88   97  106  115  122  125  128  131  134  137
                       FRAME SIZE    10.000    10.000
                       CONTOUR PLOT OF VARIABLE    11  RANGE TYPE  2  NO.LEVELS    5  ON SLICE(3-D ONLY
                       CONTOURS WILL BE PLOTTED ON DEFORMED MESH
                                 FIRST CONTOUR LABELLED  1     INCREMENT FOR LABELLING  4
                       CONTOUR LEVELS RANGE FROM 0.         TO  .800E+03
                          1 SETS OF SLICES TO FOLLOW
                       SLICE
       A LIST OF ELEMENTS GIVEN BELOW
          70   79   88   97  106  115  122  125  128  131  134  137
                       X-DIR. STRESS/MID-WALL/.2514DEG


                       PLOT SIZE (INCHES) 10.00 10.00
```

APPENDIX F

Stress Contour Plots

Figures F.1 to F.15 show the development of the stresses perpendicular to the crack plane, which roughly correspond to the tube circumferential direction in the curved specimen. The values of displacements and rotations are analytical values and apply to one half of the grips only.

Figures F.1 to F.5 show the development of stresses near the crack tip for 2a/W = 0.5 as displacement increases.

Figures F.6 to F.15 show near tip and surrounding stress contours for the range of 2a/W values analysed at a constant half grip rotation of 0.3015°, corresponding to a displacement increase on the half specimen inside surface of 0.30 mm.

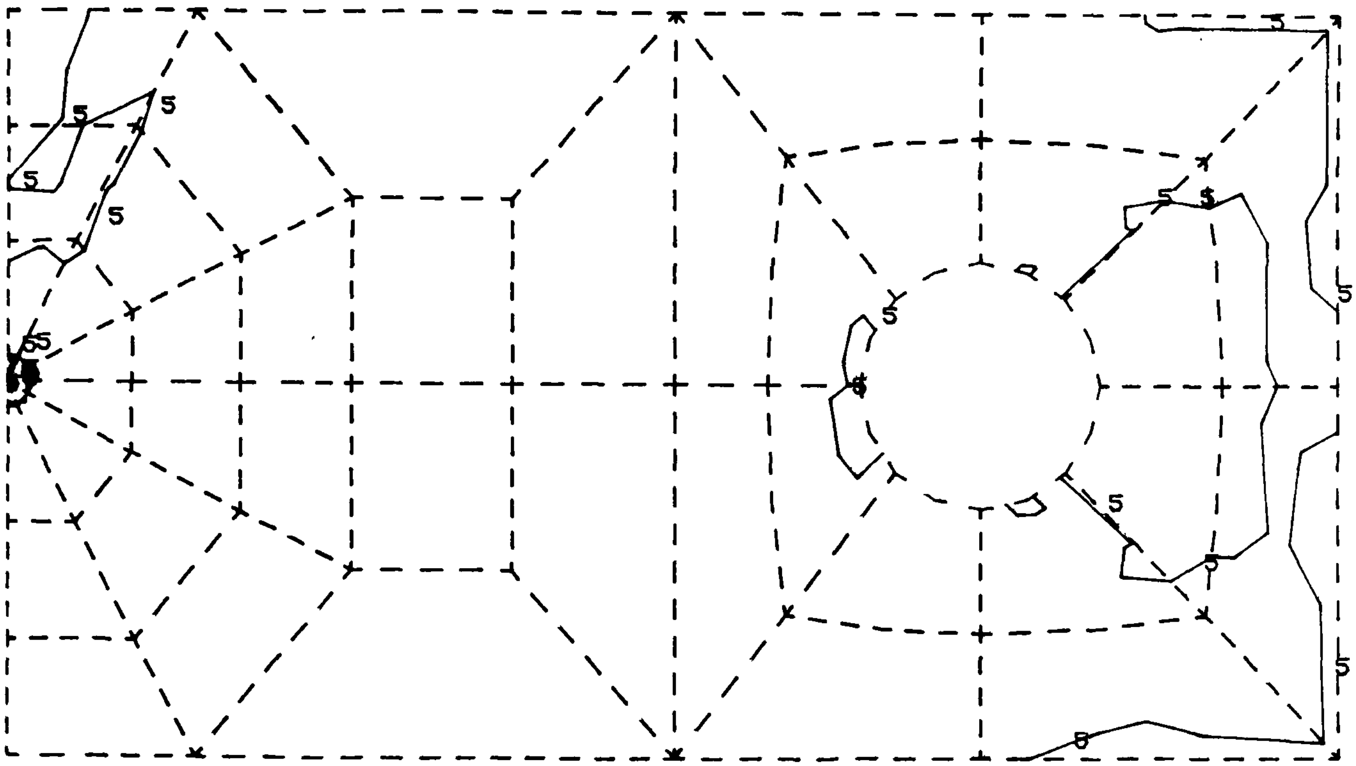

Contour	*Stress (MPa)*
5	*0*
6	*200*

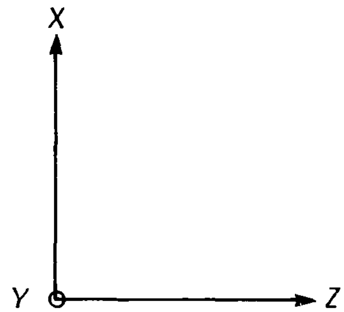

FIGURE F.1

MID-THICKNESS X-DIRECTION (TUBE CIRCUMFERENTIAL)
STRESS CONTOURS AFTER 1ST LOAD INCREMENT
FOR 2a/W = 0.5 (FULL MESH SHOWN)
DISPLACEMTNET = .05mm
MOTION = .0505°

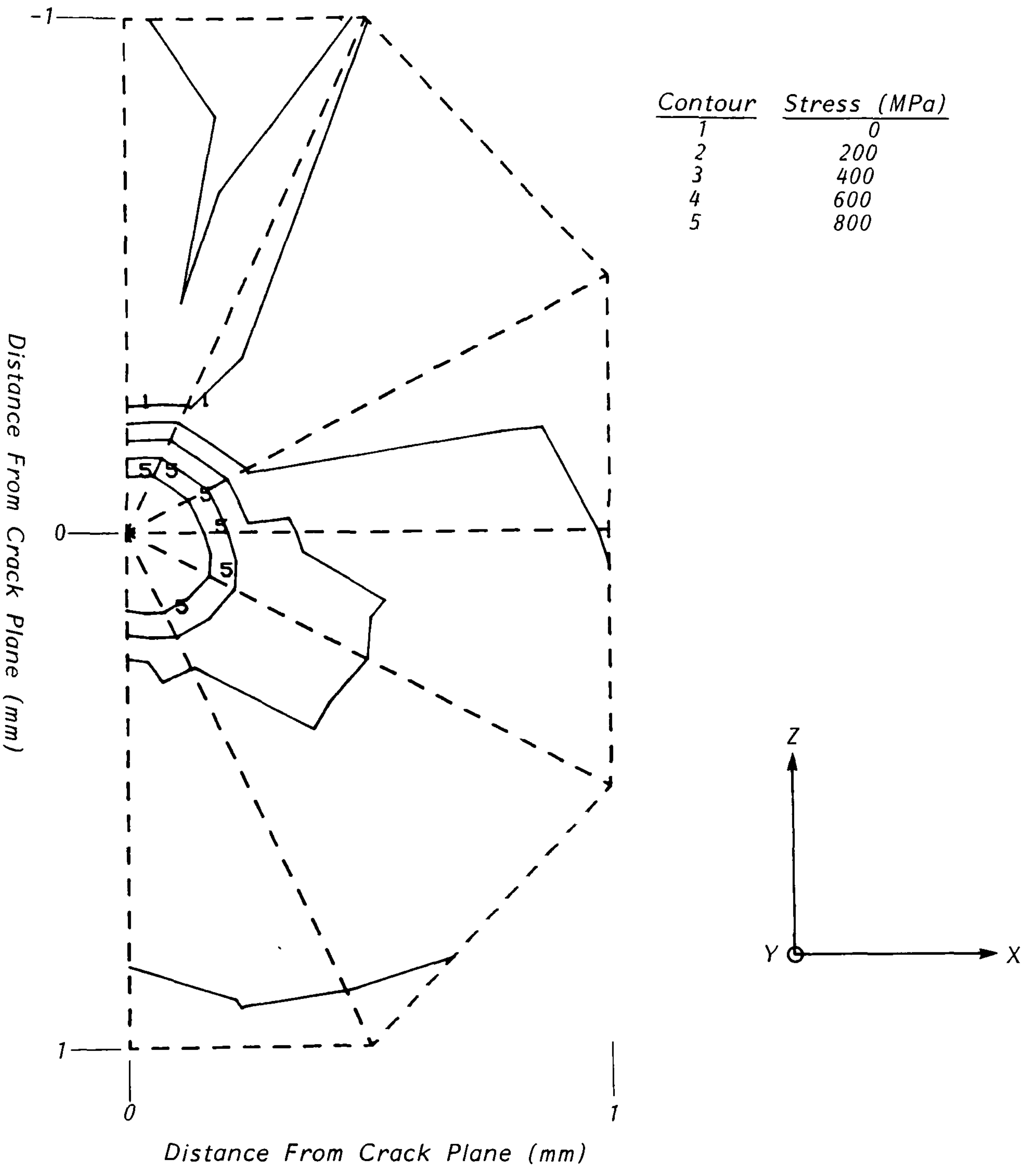

FIGURE F.2

MID-THICKNESS X-DIRECTION (TUBE CIRCUMFERENTIAL)
STRESS CONTOURS AFTER 1ST LOAD INCREMENT
FOR 2a/W = 0.5
(CRACK TIP ELEMENTS ONLY)
DISPLACEMENT = .05mm
MOTION = .0505°

172568 RD

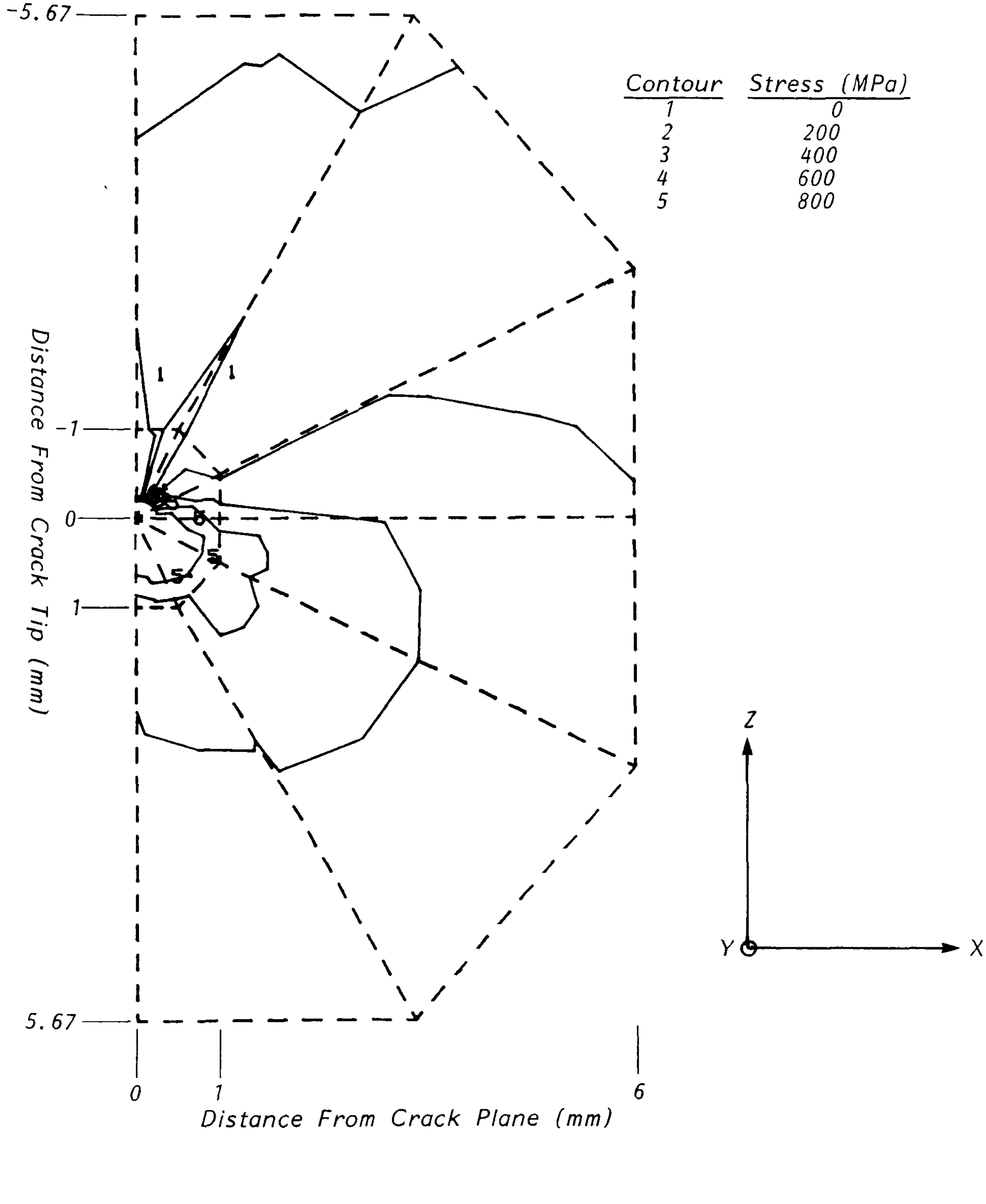

FIGURE F.3

MID-THICKNESS X-DIRECTION (TUBE CIRCUMFERENTIAL)
STRESS CONTOURS AFTER 3RD LOAD INCREMENT
FOR 2a/W = 0.5
ELEMENTS SURROUNDING CRACK TIP ELEMENTS ALSO SHOWN
DISPLACEMENT = .15mm
MOTION = .1510°

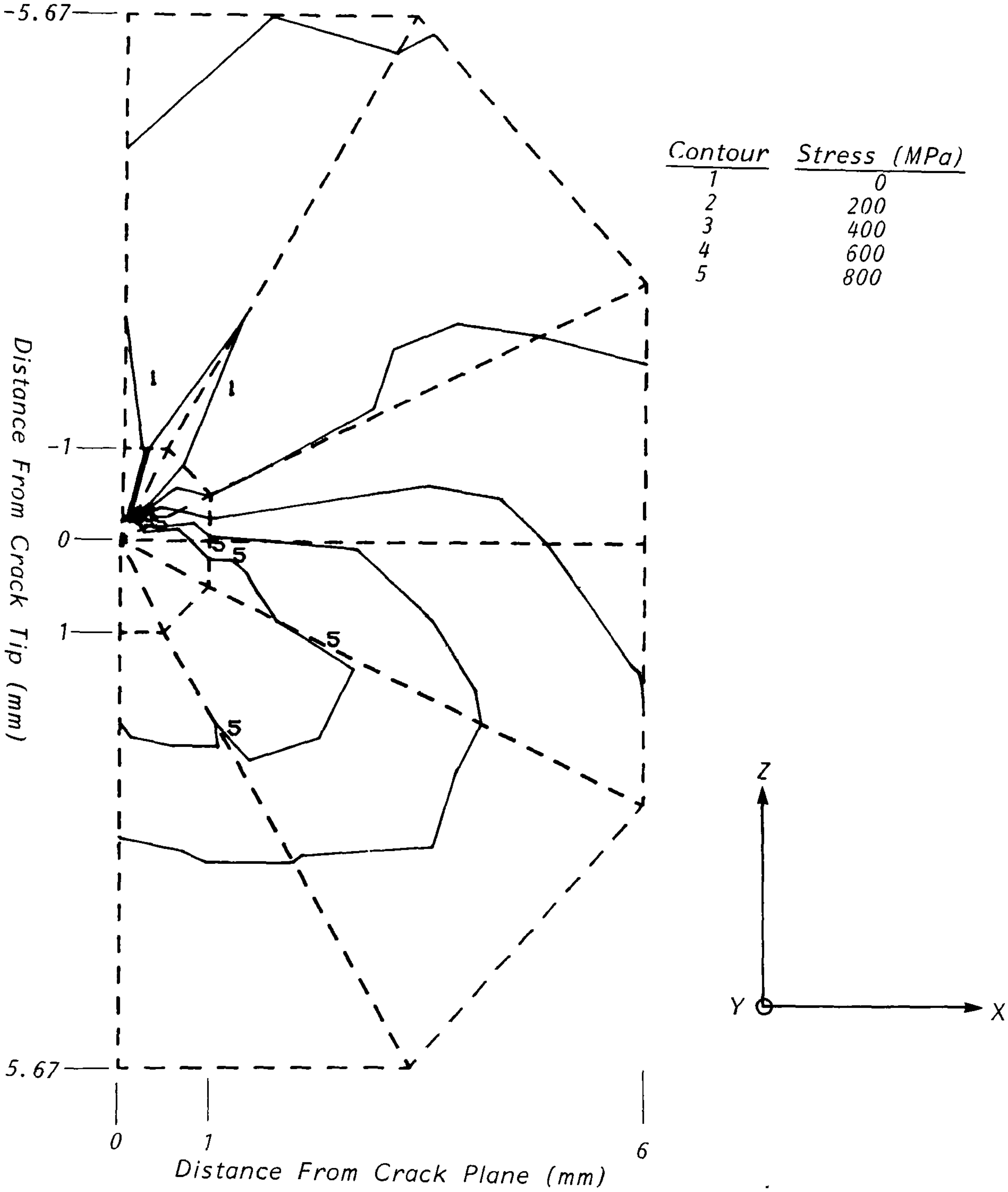

FIGURE F.4

MID-THICKNESS X-DIRECTION (TUBE CIRCUMFERENTIAL)
STRESS CONTOURS AFTER 5TH LOAD INCREMENT
FOR 2a/W = 0.5
(TWO ELEMENT ROWS NEAREST CRACK TIP SHOWN)
DISPLACEMENT = .25mm
MOTION = .2514°

172566 RD

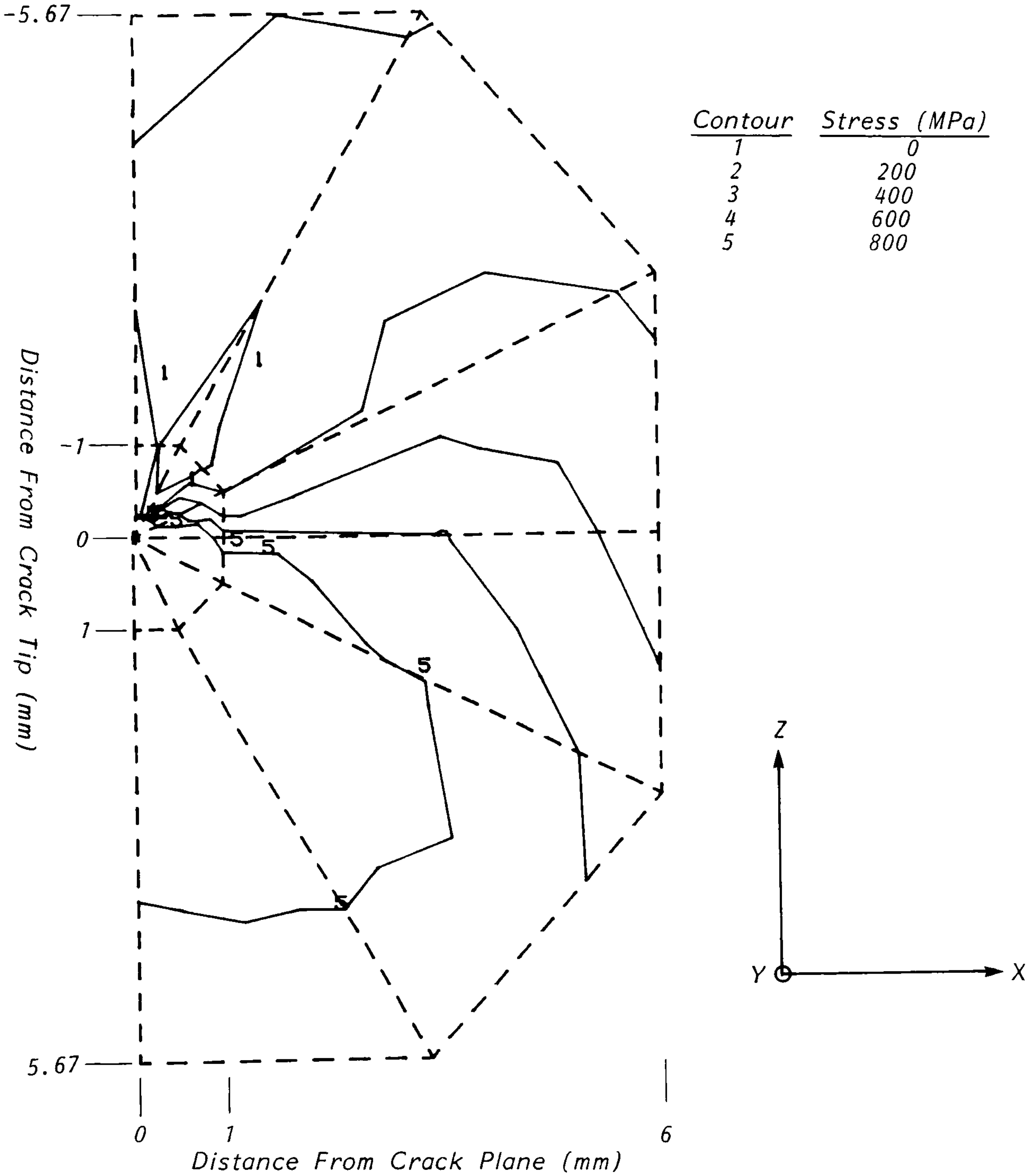

FIGURE F.5
MID-THICKNESS X-DIRECTION (TUBE CIRCUMFERENTIAL)
STRESS CONTOURS AFTER 7TH LOAD INCREMENT
FOR 2a/W = 0.5
(TWO ELEMENT ROWS NEAREST CRACK TIP SHOWN)
DISPLACEMENT = .35mm
MOTION = .3517°

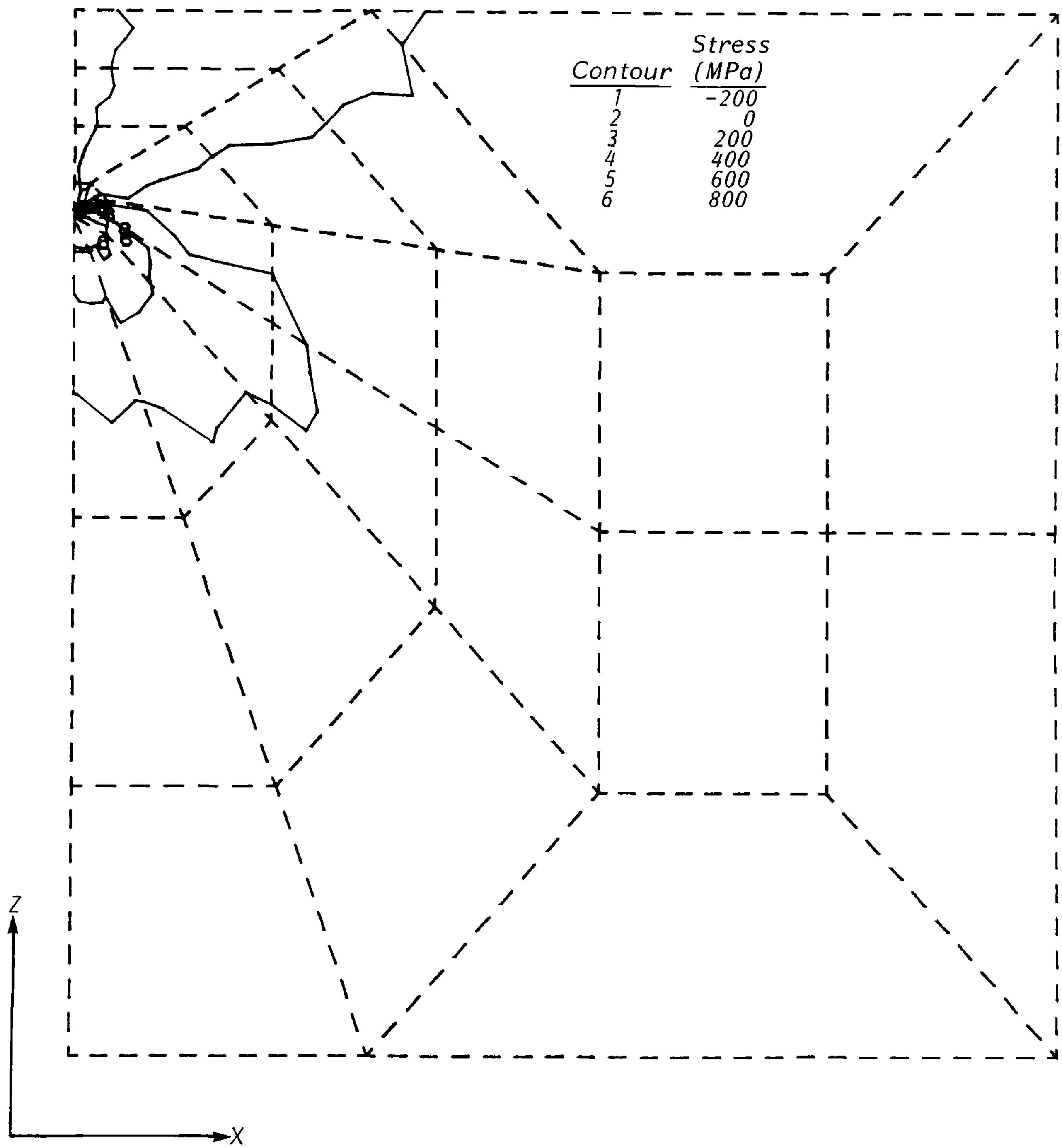

FIGURE F.6

MID-THICKNESS X-DIRECTION (TUBE CIRCUMFERENTIAL)
STRESS CONTOURS AFTER 6TH LOAD INCREMENT
FOR 2a/W = 0.2 (HALF OF MESH SHOWN)
DISPLACEMENT = 0.3mm
MOTION = .3015°

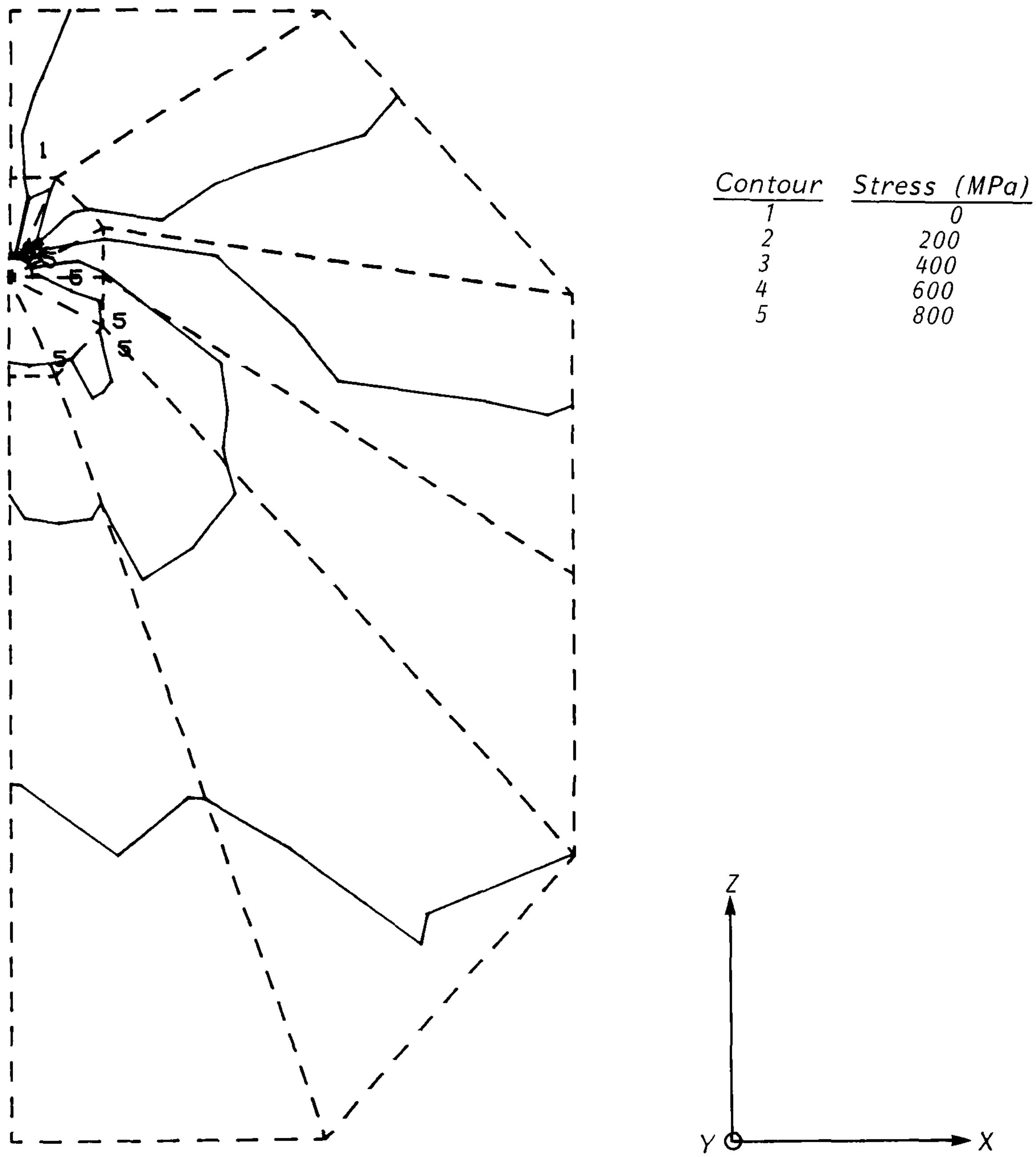

FIGURE F.7

ENLARGEMENT OF TWO ROWS OF ELEMENTS
NEAREST THE CRACK TIP FROM
FIGURE F.6 FOR LOAD INCREMENT
6 AT 2a/W = 0.2

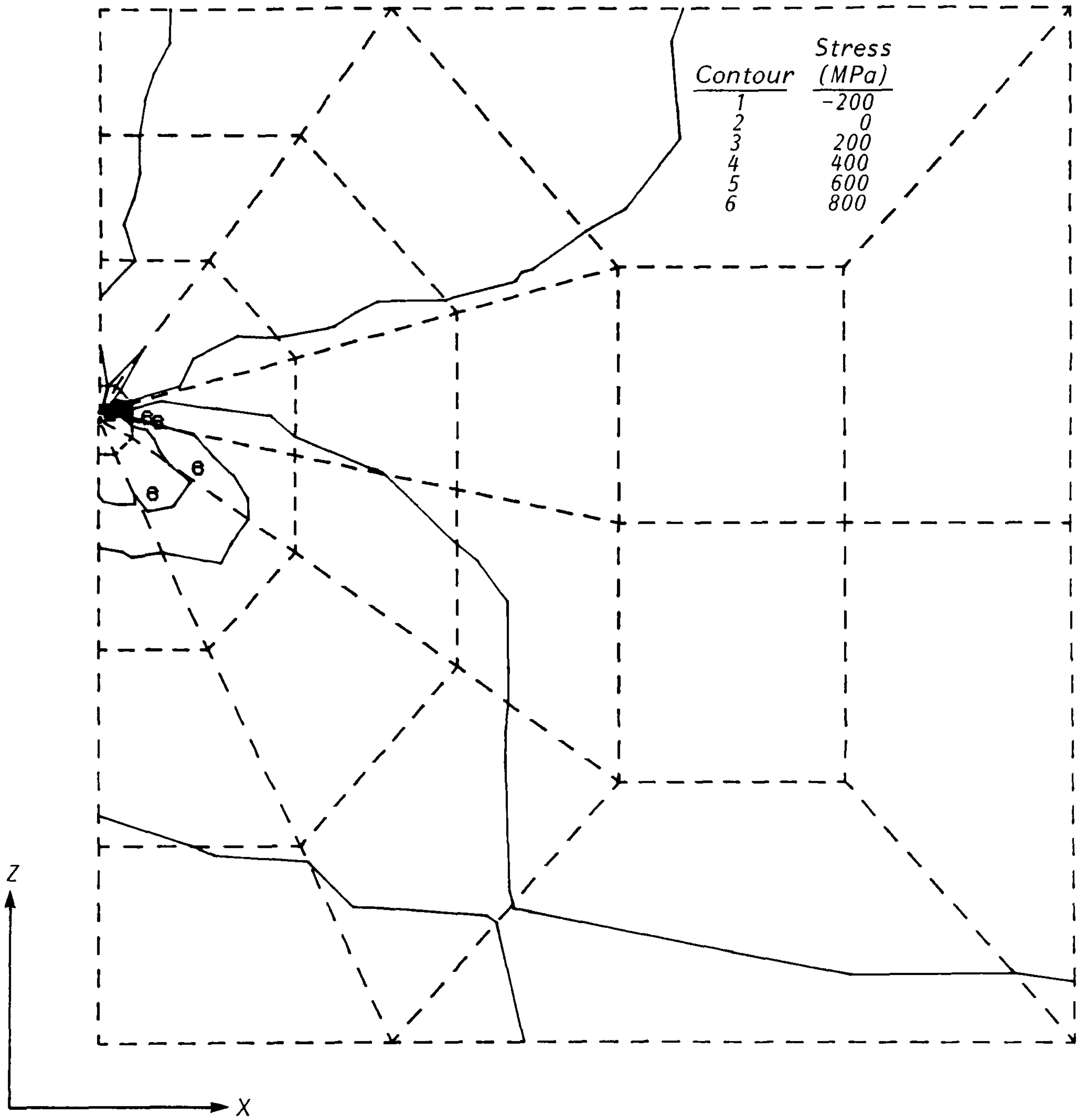

FIGURE F.8

MID-THICKNESS X-DIRECTION (TUBE CIRCUMFERENTIAL)
STRESS CONTOURS AFTER 6TH LOAD INCREMENT
FOR 2a/W = 0.4 (HALF OF MESH SHOWN)
DISPLACEMENT = 0.3mm
MOTION = 0.3015°

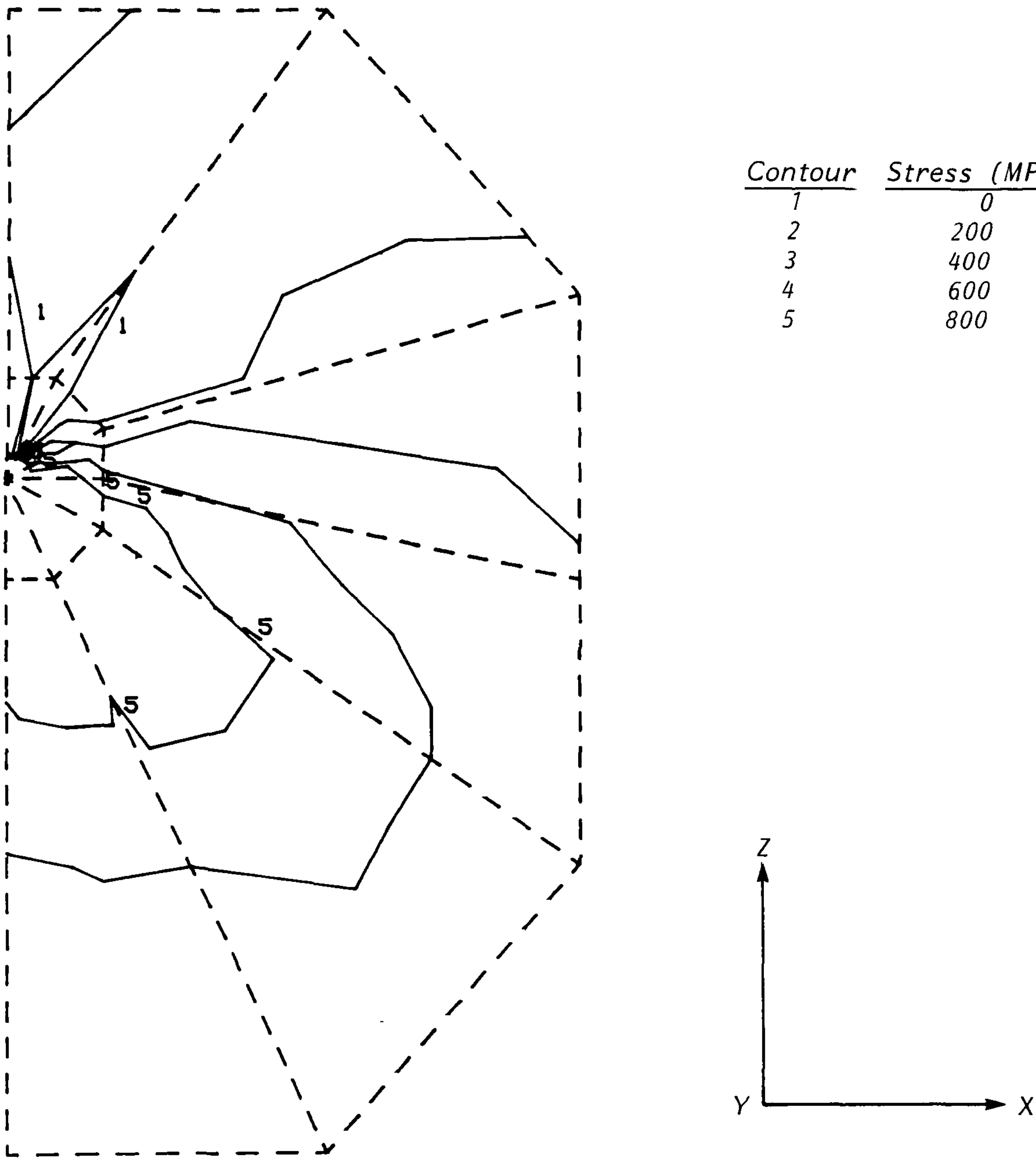

Contour	Stress (MPa)
1	0
2	200
3	400
4	600
5	800

FIGURE F.9

ENLARGEMENT OF TWO ROWS OF ELEMENTS NEAREST THE CRACK TIP FROM FIGURE F.8, FOR 2a/W = 0.4

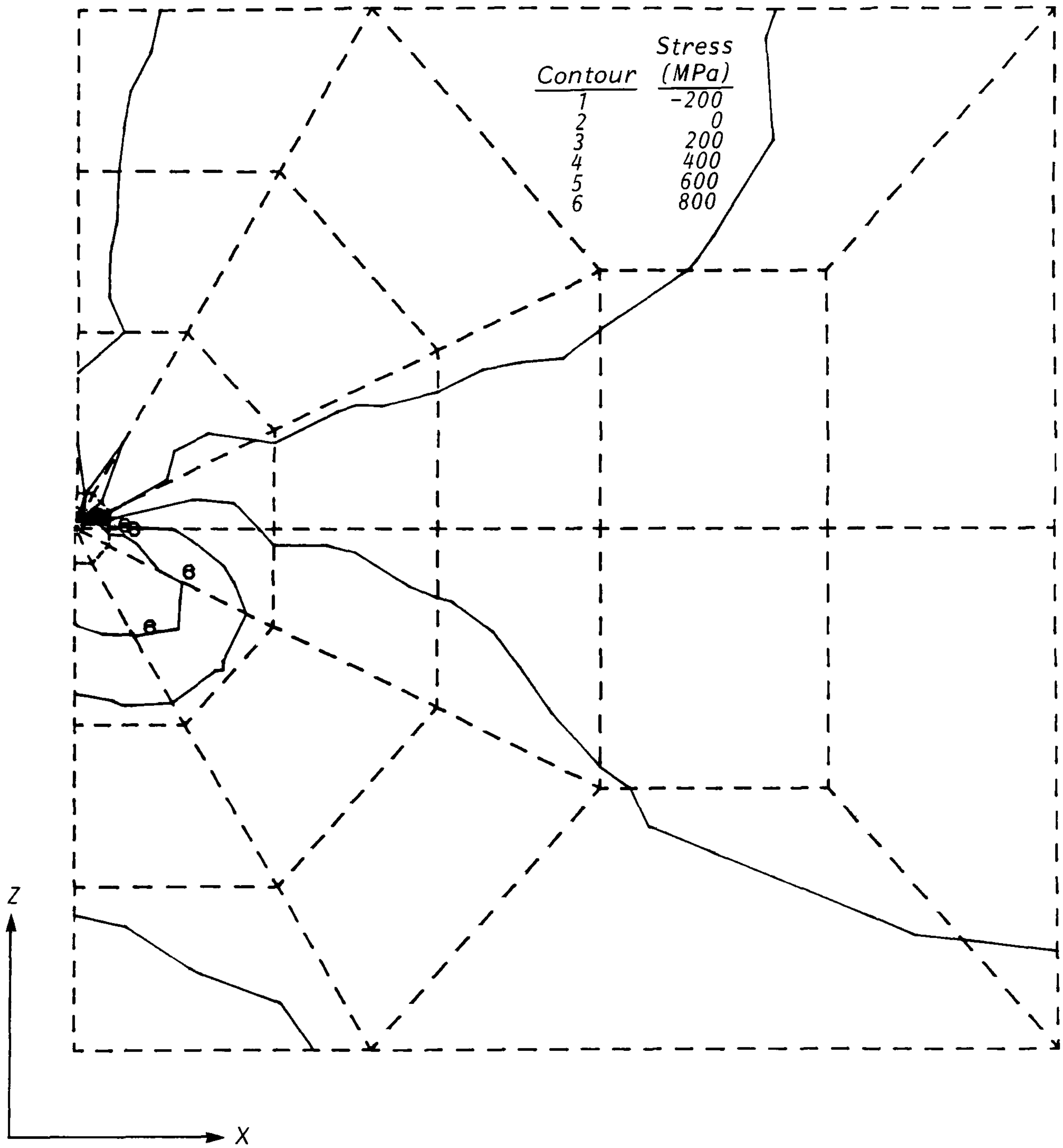

FIGURE F.10

MID-THICKNESS X-DIRECTION (TUBE CIRCUMFERENTIAL)
STRESS CONTOURS AFTER 6TH LOAD INCREMENT
FOR 2a/W = 0.5 (HALF OF MESH SHOWN)
DISPLACEMENT = 0.3mm
MOTION = 0.3015°

172561 RD

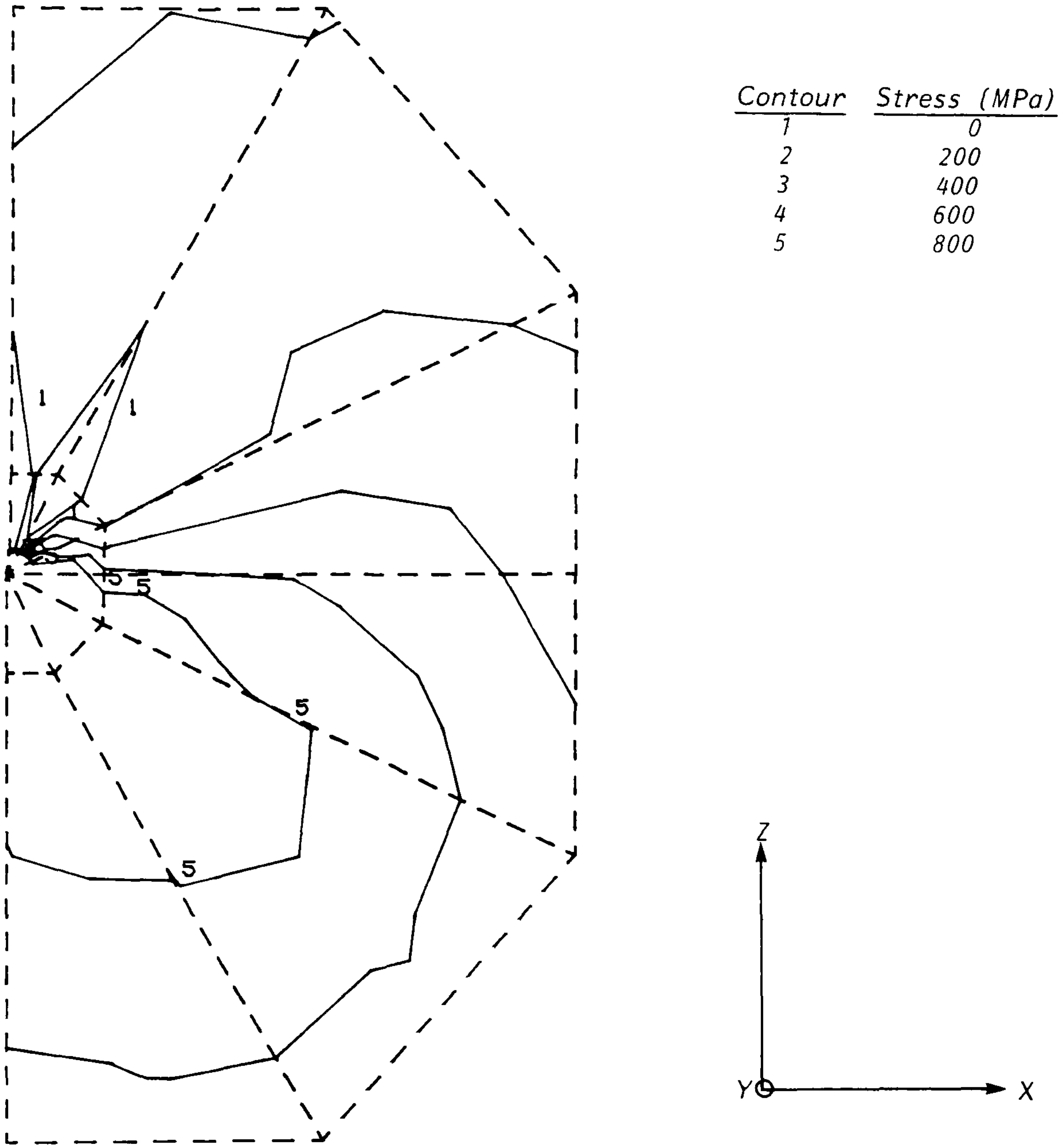

FIGURE F.11

ENLARGEMENT OF TWO ROWS OF ELEMENTS
NEAREST THE WORK TIP FROM
FIGURE F.10, FOR 2a/W = 0.5

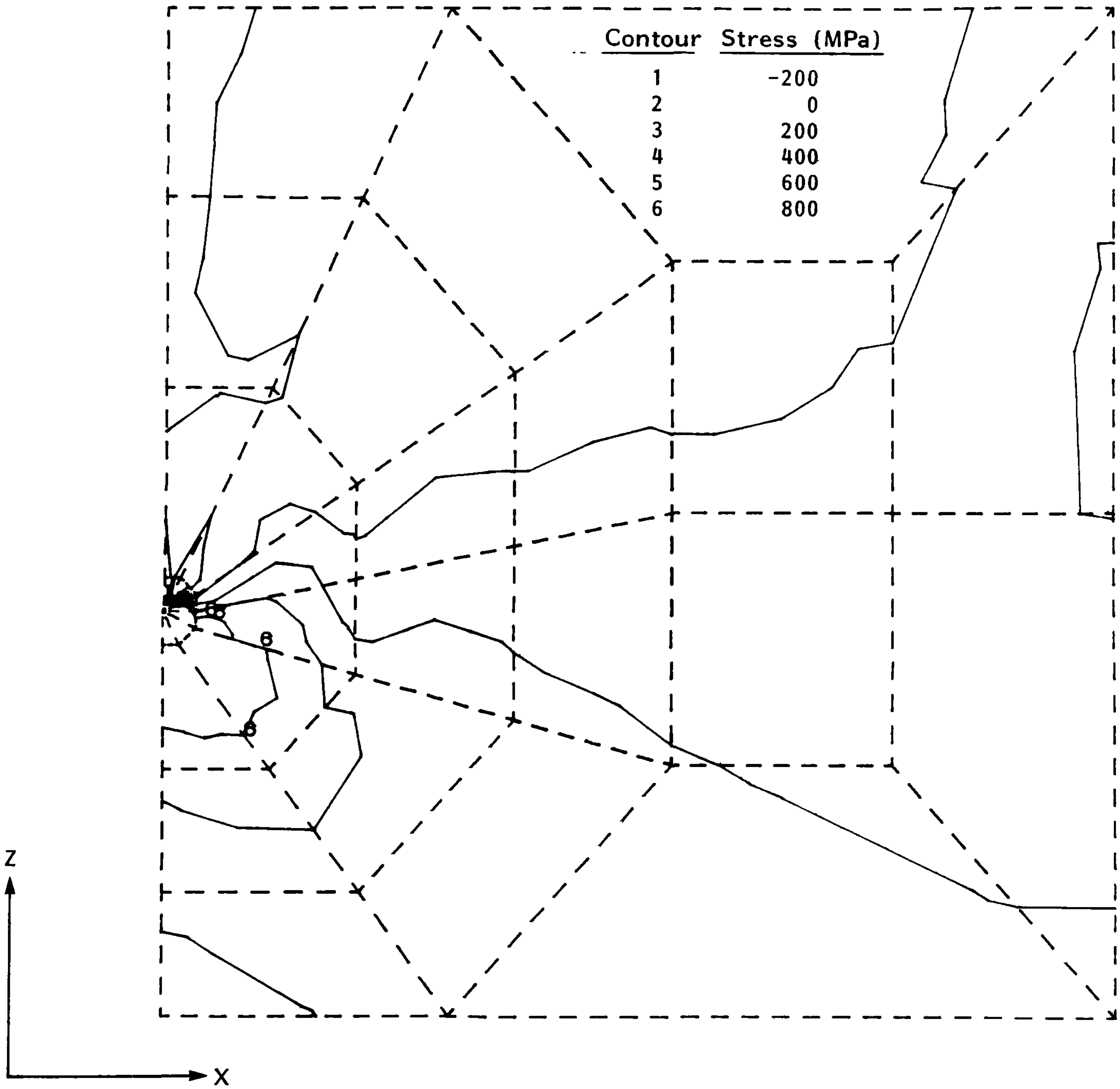

FIGURE F12

MID-THICKNESS X-DIRECTION (TUBE CIRCUMFERENTIAL) STRESS CONTOURS AFTER 6TH LOAD INCREMENT FOR 2a/W = 0.6 (HALF OF MESH SHOWN)
DISPLACEMENT = 0.3mm
MOTION = 0.3015°

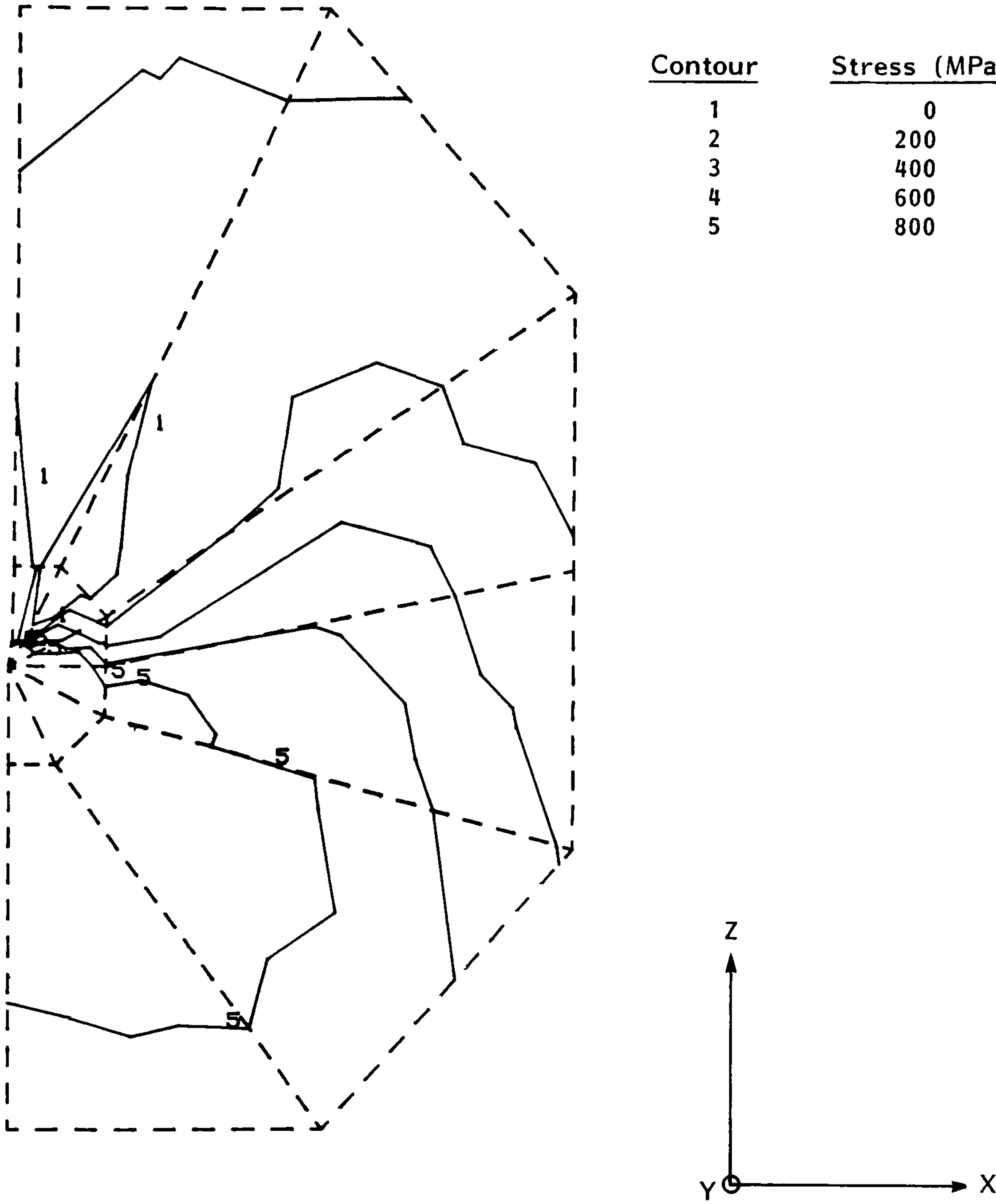

Contour	Stress (MPa)
1	0
2	200
3	400
4	600
5	800

FIGURE F.13

ENLARGEMENT OF TWO ROWS OF ELEMENTS NEAREST THE CRACK TIP FROM FIGURE F.12 FOR 2a/W = 0.6

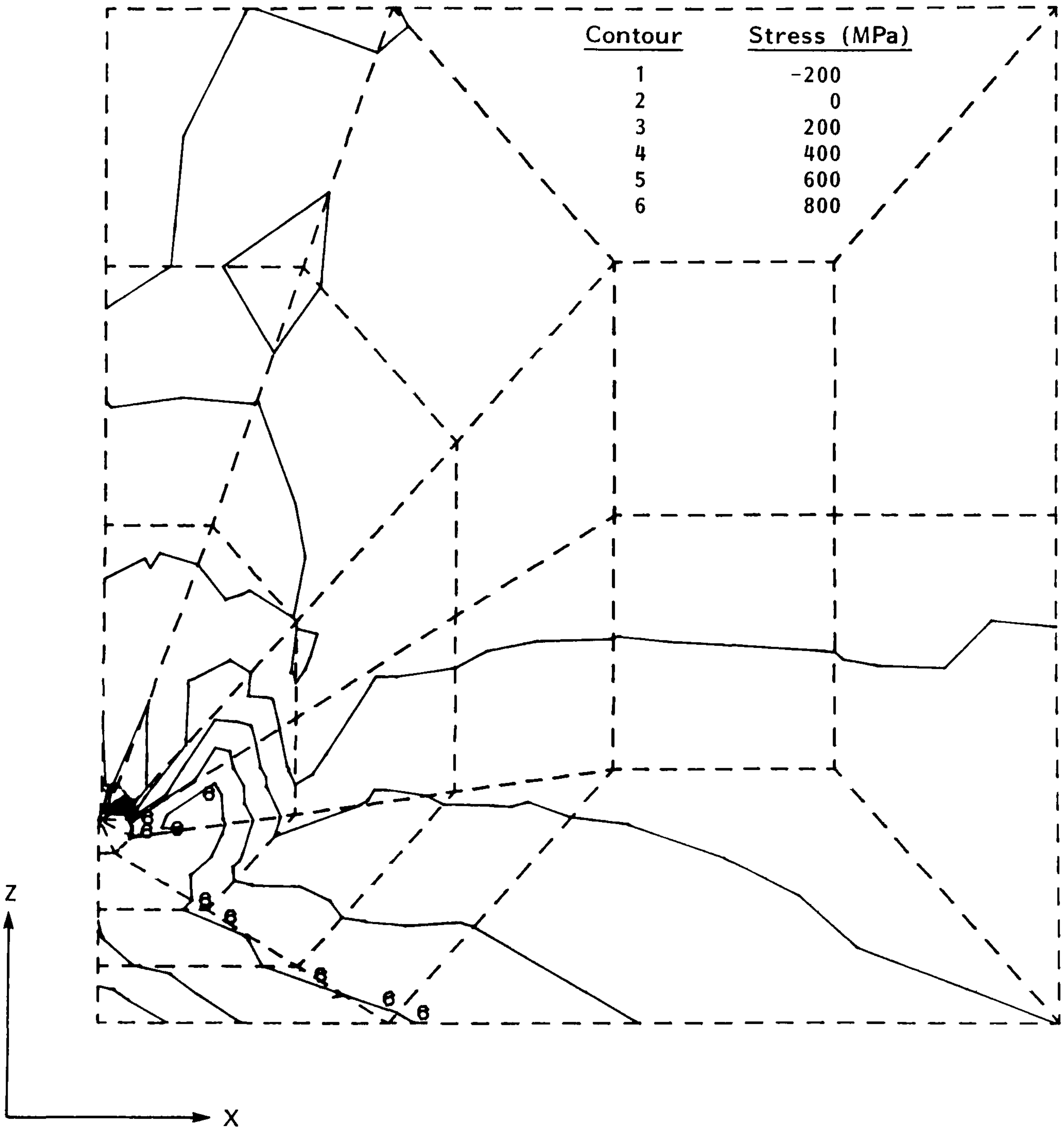

FIGURE F.14

MID-THICKNESS X-DIRECTION (TUBE CIRCUMFERENTIAL) STRESS CONTOURS AFTER LOAD INCREMENT 6 FOR 2a/W = 0.8. (HALF OF MESH SHOWN)
DISPLACEMENT = 0.3mm
ROTATION = 0.3015°

172556 RD

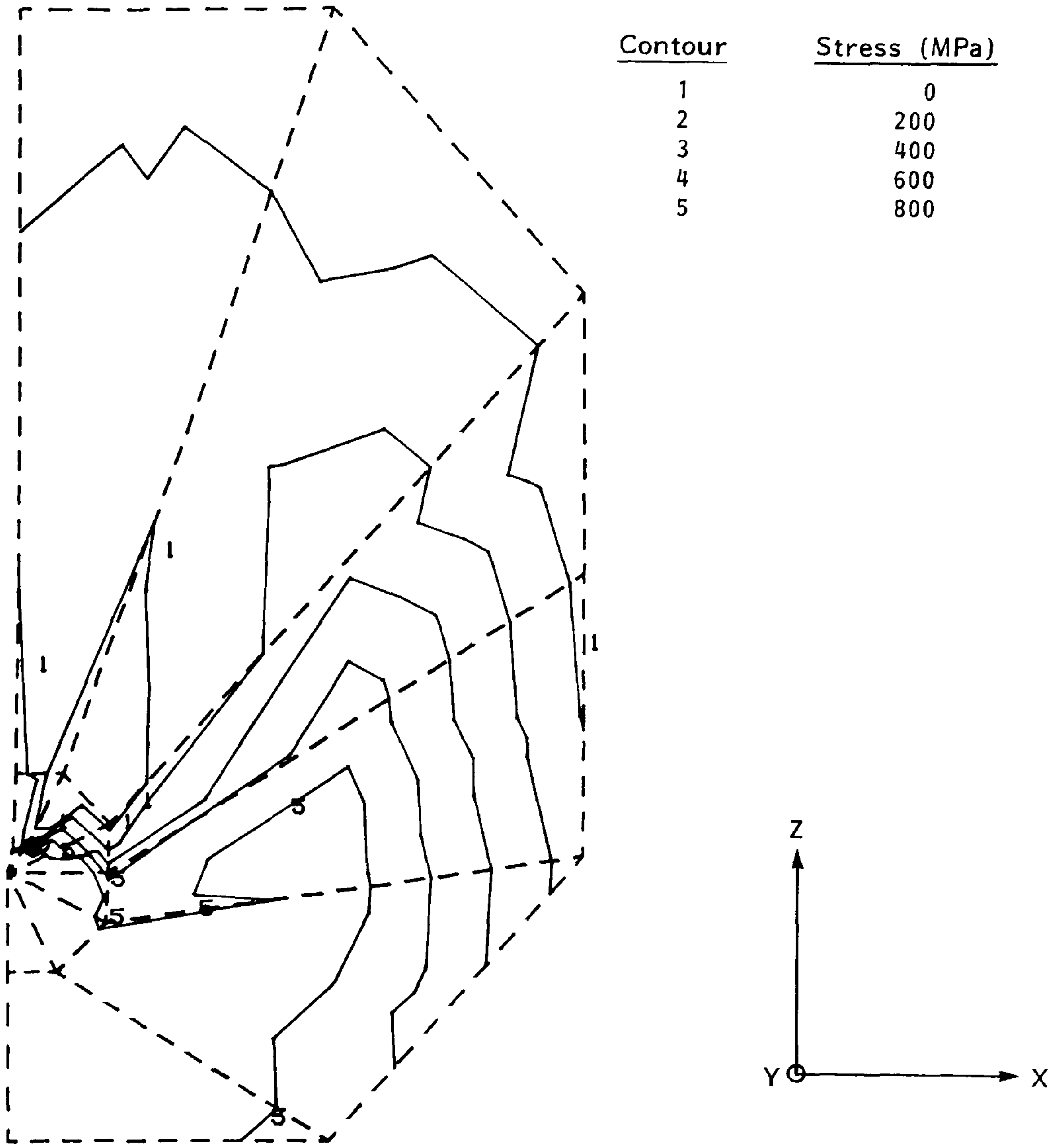

FIGURE F.15

ENLARGEMENT OF TWO ROWS OF ELEMENTS NEAREST THE CRACK TIP FROM FIGURE F.14 FOR 2a/W = 0.8